



universität  
wien

# DISSERTATION / DOCTORAL THESIS

Titel der Dissertation /Title of the Doctoral Thesis

„Path Indistinguishability in Photon Pair Emission“

verfasst von / submitted by

DI Armin Hochrainer Bakk. phil

angestrebter akademischer Grad / in partial fulfilment of the requirements for the degree of  
Doktor der Naturwissenschaften (Dr. rer. nat.)

Wien, 2020

Studienkennzahl lt. Studienblatt /  
degree programme code as it appears on the student  
record sheet:

A 796 605 411

Dissertationsgebiet lt. Studienblatt /  
field of study as it appears on the student record sheet:

Physik

Betreut von / Supervisor:

emer. o. Univ.-Prof. Dr. DDr. h.c. Anton Zeilinger



# Abstract

The connection between interference and the availability of path information is a feature of quantum mechanics that intrigues physicists for more than a century. In the early 1990s, a series of experiments demonstrated a peculiar aspect of this connection. It was shown that quantum interference occurs when different photon pair sources emit one or both photons into identical beams. In contrast to most nonclassical phenomena involving light, the above effect can be observed directly in the intensity at a single detector without the need for coincidence detection. This fact leads to the possibility of controlling single photon interference by manipulating another photon beam that is not detected.

In recent years, a growing field of research has evolved around this interference effect called “induced coherence without induced emission”, after its applications in imaging and spectroscopy have been demonstrated. This thesis focuses on fundamental aspects, with the goal of obtaining a deeper understanding of quantum complementarity in the resulting unusual situations. After providing an overview of past and current research related to the subject, we turn to the experimental observation of the phenomenon of induced coherence without induced emission in a multimode scenario. We demonstrate the formation of spatial interference fringes in one beam by controlling another, undetected, beam. The fringes are compared to their classical analogs and differences are analyzed, in particular concerning their wavelength dependence. Subsequently, an experiment is presented, in which induced coherence is used to measure correlations between two photons by detecting only one of them. We further demonstrate that it is possible to change the polarization of one light beam by changing the available path information in another beam. This scheme allows to control the degree of polarization without affecting the intensity. We perform a delayed-choice experiment illustrating the complementarity in a situation in which both photons are emitted into identical modes. The duality analyzed in this experiment goes beyond the often studied complementarity between wave and particle behavior and requires an abstraction of the concept of interference involving the entire photon pair emission process. Finally, a gedankenexperiment is presented, which demonstrates an inconsistency that arises if one assigns a definite origin to a photon pair in an experiment involving three indistinguishable sources. We conclude by stating several open questions that were stimulated by our results.



# Zusammenfassung

Der Zusammenhang zwischen Interferenz und der Verfügbarkeit von Pfadinformation ist ein Merkmal der Quantenmechanik, das Physiker seit mehr als einem Jahrhundert fasziniert. In den frühen neunziger Jahren wurde eine Reihe von Experimenten durchgeführt, die einen neuen Aspekt dieses Zusammenhangs aufzeigten. In diesen Experimenten wurde Quanteninterferenz in Situationen gezeigt, in welchen verschiedene Photonenpaarquellen ein oder beide Photonen in identische Strahlen emittierten. Im Gegensatz zu Quanteninterferenzexperimenten, in denen beide Photonen korreliert detektiert werden, kann die Interferenz in diesem Fall in der Intensität eines einzelnen Photonenstrahls beobachtet werden, obwohl Photonenpaare an dem Phänomen beteiligt sind. Dies erlaubt die Beobachtung von klassisch nicht erklärbaren Effekten mit einem einzelnen Detektor. Diese Beobachtung eröffnet die Möglichkeit, die Einzelphotoneninterferenz nur durch Manipulation eines anderen Photonenstrahls zu kontrollieren, welcher selbst nicht detektiert werden muss.

In den letzten Jahren hat sich ein wachsendes Forschungsgebiet um diesen als "induced coherence without induced emission" bezeichneten Interferenzeffekt etabliert, nachdem Anwendungen für Bildgebung und Spektroskopie demonstriert wurden. Die vorliegende Arbeit konzentriert sich auf grundlegende Aspekte des obigen Interferenzeffekts mit dem Ziel, unser Verständnis der Quantenkomplementarität in den daraus resultierenden ungewöhnlichen Situationen zu vertiefen. Nach einem kurzen Überblick über vergangene und aktuelle Forschung wenden wir uns experimentellen Beobachtungen des Phänomens der "induced coherence without induced emission" in einem Multimode-Szenario zu. Wir demonstrieren die Entstehung eines Interferenzmusters in einem Strahl, indem wir einen anderen Strahl kontrollieren, der nicht detektiert wird. Die Interferenzstreifen werden mit analogen Beobachtungen in klassischer Interferometrie verglichen und Unterschiede, insbesondere hinsichtlich ihrer Wellenlängenabhängigkeit, analysiert. Des weiteren wird ein Experiment vorgestellt, in dem nur eines von zwei Photonen eines Paares detektiert wird. Wir demonstrieren, dass das in einem einzelnen Photonenstrahl entstandene Interferenzmuster dazu verwendet werden kann, die Korrelationen zwischen beiden Photonen zu messen. Anschließend wird gezeigt, dass es möglich ist, die Polarisation eines Lichtstrahls zu ändern, indem lediglich die in einem anderen Strahl verfügbare Pfadinformation geändert wird. Dieses Schema ermöglicht es, den Polarisationsgrad eines Lichtstrahls zu kontrollieren, ohne dessen Intensität zu beeinflussen. Die Komplementarität in einer Situation, in der beide Photonen in identische Moden emittiert werden, wird in einem anderen Experiment untersucht. Wir führen ein Delayed-Choice-Experiment durch, das die Komplementarität zwischen Interferenz und Information über

den Ursprung eines Photonenpaares illustriert. Die in diesem Experiment analysierten komplementären Eigenschaften gehen über die häufig untersuchte Komplementarität zwischen Wellen- und Teilchenverhalten hinaus. Sie erfordern eine Abstraktion des Interferenzkonzepts, welche den gesamten Photonenpaar-Emissionsprozess miteinbezieht. Schließlich wird ein Gedankenexperiment vorgestellt, in dem die Emission von Photonenpaaren aus drei nicht unterscheidbaren Quellen betrachtet wird. In diesem wird gezeigt, dass die Zuschreibung einer bestimmten Quelle als Ursprung eines Photonenpaares inkonsistent ist. Zum Abschluss werden einige offene Fragen diskutiert, die durch unsere Ergebnisse angeregt wurden.

# Contents

<b>Abstract</b>	<b>3</b>
<b>Zusammenfassung</b>	<b>5</b>
<b>1 Introduction</b>	<b>11</b>
1.1 General Context	11
1.2 Scope of this Thesis	13
1.3 Overview	14
<b>2 Background</b>	<b>15</b>
2.1 Interference and Information	15
2.1.1 Feynman's "First Principles"	15
2.2 Complementarity	17
2.2.1 Delayed-Choice experiments	17
2.2.2 Partial Path Information and Partial Visibility	19
2.3 Spontaneous Parametric Down Conversion	21
2.3.1 Spatial Correlations Between Down-Converted Photons	21
2.4 Three Different Ways to Interfere a Photon Pair	24
2.4.1 Two-Photon Interference in Coincidence	24
2.4.2 The Zou, Wang, Mandel, (Ou) experiment	26
2.4.3 Frustrated Two-Photon Creation	29
2.4.4 Coherence Length Requirements in Two-Photon Interference Experiments	31
2.5 Quantum Imaging with Undetected Photons	35
2.5.1 Principle	35
2.5.2 Lens Systems and Spatial Modes	36
2.5.3 Quantitative Description	37
2.6 Other Applications of Induced Coherence	40
2.7 The Role of Stimulated Emission	40
2.7.1 Stimulated Emission as an Interference Effect	40
2.7.2 Significance in Laser Pumped Induced Coherence	41
2.8 Atoms and Mirrors	43
2.8.1 Spontaneous Emission in the Vicinity of Mirrors	43

2.8.2	Discussion about Physical Origin and Time-Dependence . . . . .	43
2.8.3	Can an Optical Experiment Clarify the Interpretation? . . . . .	44
<b>3</b>	<b>Interference Fringes in Induced Coherence Without Induced Emission</b>	<b>47</b>
3.1	Motivation . . . . .	47
3.1.1	Specific Questions and Experiments . . . . .	48
3.2	Experimental Setup . . . . .	49
3.3	Observation of Spatial Interference Fringes . . . . .	52
3.4	Wavelength Dependence . . . . .	54
3.4.1	Goal of the Experiment . . . . .	54
3.4.2	Analogy to Classical Interferometry . . . . .	54
3.4.3	Performed Measurements . . . . .	55
3.4.4	Results . . . . .	55
3.4.5	Quantum State in the Experiment . . . . .	58
3.4.6	Discussion . . . . .	60
3.5	Quantifying the Momentum Correlation Between Two Photons by Detecting One	63
3.5.1	Goal of the Experiment . . . . .	63
3.5.2	Momentum Correlation in Laser Pumped SPDC . . . . .	63
3.5.3	Fringe Visibility with Tuned Momentum Correlation . . . . .	63
3.5.4	Quantitative Description . . . . .	64
3.5.5	Performed Measurements . . . . .	66
3.5.6	Image Analysis . . . . .	67
3.5.7	Results . . . . .	67
3.5.8	Summary of the Method . . . . .	70
3.5.9	Discussion . . . . .	71
3.6	Conclusions . . . . .	72
<b>4</b>	<b>Controlling Partial Polarization by Path Distinguishability</b>	<b>73</b>
4.1	Motivation and Goal . . . . .	73
4.2	Degree of Polarization . . . . .	74
4.3	Experimental Setup . . . . .	74
4.4	Performed Measurements . . . . .	75
4.5	Results . . . . .	76
4.5.1	Degree of Polarization and Path Distinguishability . . . . .	76
4.5.2	Reconstructed Quantum States . . . . .	78
4.6	Theoretical Quantum States in the Experiment . . . . .	79
4.7	Discussion . . . . .	79
4.8	Conclusion . . . . .	80
<b>5</b>	<b>Delayed-Choice Frustration of Down-Conversion</b>	<b>81</b>
5.1	Motivation and Goal . . . . .	81
5.2	Outline of the Experiment . . . . .	82
5.3	Implementation . . . . .	84
5.3.1	Experimental Setup . . . . .	84
5.3.2	Distances and Switching Times . . . . .	85
5.3.3	Lens Systems . . . . .	85
5.4	Characterization and Calibration . . . . .	86
5.4.1	Reference Measurement . . . . .	86
5.5	Measurement During Destructive Interference . . . . .	88
5.5.1	Visibility and Stability . . . . .	88
5.6	Results . . . . .	90
5.6.1	Time Dependent Frustrated Down-Conversion . . . . .	90

5.6.2	Quantitative Predictions for Photon Arrival Times at the Inserted Detector	91
5.6.3	Experimental Constraints on Hypothetical Delay	91
5.7	Interpretation and Discussion	93
5.7.1	Complementarity in Frustrated Down-Conversion	93
5.7.2	Alternative Explanations of Our Results	95
5.8	Conclusion and Outlook	96
<b>6</b>	<b>Complementarity with Three Indistinguishable Sources</b>	<b>99</b>
6.1	Motivation	99
6.2	Duality Relations in Frustrated Down-Conversion with Two Sources	100
6.3	Indistinguishable Photon Pair Emission from Three Sources	101
6.4	Inconsistent Which-Path Information	101
6.5	Discussion	104
6.5.1	Analogy to Three Slit Interference	104
6.5.2	Remarks on Regarding Two Sources as One Combined Source	105
6.6	Conclusion	105
<b>7</b>	<b>Conclusions and Outlook</b>	<b>107</b>
7.1	Questions For Future Research	108
<b>A</b>	<b>Appendix</b>	<b>111</b>
A.1	Experimental Details on Interference Fringes in Induced Coherence Without Induced Emission	111
A.1.1	Initial Alignment of the Idler Beam Lens System	111
A.1.2	Phase-Shift of a Defocused 4f System	111
A.2	Experimental Details on Delayed-Choice Frustration of Down-Conversion	114
A.2.1	Auxiliary Alignment Imaging System for Obtaining High-Visibility Frustration of SPDC	114
A.2.2	Electronics and Detection	114
A.2.3	Electro Optical Modulator	115
A.2.4	Timing Resolution in the Experiment	117
	<b>References</b>	<b>118</b>
	<b>Acknowledgements</b>	<b>129</b>
	<b>Curriculum Vitae</b>	<b>131</b>
	<b>List of Publications</b>	<b>132</b>



# 1

## Introduction

### 1.1 General Context

Since its discovery more than a century ago, quantum physics has been very successful in describing the world around us. Today, it is the most accurate tool available to quantitatively understand a vast variety of natural phenomena and has defied numerous experimental tests. Despite its enormous success, the conceptual implications of quantum mechanics are at odds with long-standing philosophical ideas [1] and their interpretation remains controversial until today.

It is subjective to pinpoint a particular concept as the essence of quantum theory that makes it incompatible with classical physics. Famous quotations name entanglement as its “characteristic trait” [2], quantum interference of probabilities as the “only mystery” [3, Sec. 1.1], or quantum complementarity as the “bedrock” of quantum mechanics [4, pp. 284]. As discussed below, these phenomena are closely related to each other.

In the first demonstration of quantum entanglement [5, 6], non-classical polarization correlations between two photons have been observed. Since then, experimental tests of entanglement have been refined and extended to numerous other systems, which established that the observed correlations are not explicable under the classical assumptions that information cannot propagate faster than the speed of light and that the properties of individual particles exist independent of measurement. Quantum entanglement is now the cornerstone of many quantum information and quantum communication technologies.

On the other hand, the interference of light is well understood within classical physics. Many phenomena in optical interferometry, imaging, and related fields can accurately be described using the concepts of classical electromagnetic fields governed by Maxwell’s equations. While the occurrence of interference itself is not per se a “quantum phenomenon”, optical interference effects have been observed that are outside the scope of classical theory. With some notable exceptions (in particular the experiments mentioned below), these effects were almost exclusively demonstrated by correlating the detections of two or more photons [7]. The quantitative understanding of these phenomena requires an abstraction of the concept of interference in the sense

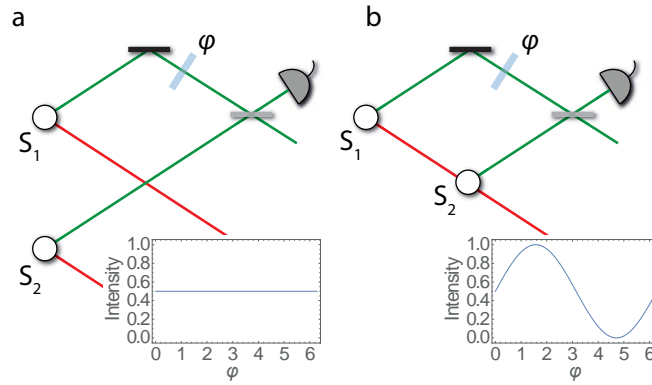


**Figure 1.1:** Principle of the interference effect demonstrated by Zou, Wang, and Mandel [13]. A photon pair can be created in one of two sources,  $S_1$  or  $S_2$ . One beam from each source is superposed on a beam splitter and subsequently detected. (a) No interference occurs if the second photon (red) carries path information about the first photon (green). (b) If the red beams are aligned, the two events of creating a photon pair at source 1 or at source 2 are indistinguishable and interference in the green beams is observed.

that interference does not take place between physical fields, but instead between probability amplitudes.

The principle of complementarity [8, 9] states that pairs of properties of quantum systems cannot be measured simultaneously with arbitrary precision. Nevertheless, only one of them is not sufficient to fully describe the system. When applied to the behavior of a quantum particle in a two-path interference experiment, the statement addresses the fact that one can either observe interference (wave-like behavior), or determine which of the paths were taken (particle, or “ball” like behavior). It is impossible to observe both properties simultaneously, as the experimental arrangements that correspond to the two measurements are mutually exclusive. The complementarity principle thus illustrates the close relationship between the availability of information and physical phenomena.

The polarization correlation in entanglement experiments with photons was shown to be explicable by quantum interference of photon pair emissions. This has intuitively been demonstrated by experiments in which entanglement was generated by interfering photon pairs from different origins [10–12]. It is possible to understand the correlations observed in a Bell-test experiment with polarized photons as a consequence of two photon interference and the erasure of polarization information.

Thus, quantum interference can be regarded as a way to reduce quantum entanglement to its simplest form. However, quantum interference of probability amplitudes (in our case corresponding to the emission of a photon pair in a particular set of modes) also leads to a variety of effects different than entanglement, some of which are outside of the scope of classical theory.

Of particular relevance for this thesis is a quantum interference phenomenon that occurs when photon pairs are created in two or more alternative ways that result in indistinguishable experimental outcomes. Although no coincidence detection is necessary to observe interference, this effect cannot be quantitatively described using classical theory. Its first experimental demonstration dates back to 1991 and used two photon pair sources [13, 14]. The two sources were arranged in a way that a photon pair could be emitted by either of them (Fig. 1.1). One beam from each source was superposed on a beam splitter and subsequently detected. As photons are always produced in pairs, every photon arriving at the detector is accompanied by a partner photon in either one of the two remaining beams (Fig. 1.1 a). This partner photon could in principle be detected, which would reveal the path taken by the first photon. In that sense, the

two possible origins of the photon are distinguishable. As a consequence, it is not possible to observe interference.

The striking idea in this experiment was to align the second beam of the first source to be identical to the second beam of the second source (Fig. 1.1 b). In this way, one of the photons is always emitted into the same beam, regardless of which source it initially came from. It, therefore, does not carry any information as to which source the photon pair originated from and thus no path information about the other, detected, photon. As a consequence, interference fringes can be observed by detecting that other photon behind a beam splitter. Remarkably, the aligned partner photon does not need to be actually detected for this effect to occur. The mere fact that the two ways of creating a photon pair are indistinguishable is sufficient to enable one of the photons to interfere. This demonstrates how complementarity arises not because a particular measurement is actually performed, but because information is or is not accessible in principle. The authors termed the effect “induced coherence without induced emission”.

A related experiment was performed a few years later [15], in which again a photon pair could be emitted in one of two alternative ways. Instead of aligning only one of the beams, both beams were overlapped to be indistinguishable. In this way, the experiment allowed for the creation of the entire photon pair in two indistinguishable ways. The total rate of emitted photon pairs was shown to exhibit interference, which could be observed with a single detector and without superposing the paths of a photon on a beam splitter. For certain phase settings, the interference results in the suppression of photon pair emissions from the system.

Although already demonstrated in the 1990s, these effects found use in several applications for imaging, spectroscopy and other fields only recently. Of particular relevance for this thesis is their use in a spatially multimode scenario for quantum imaging with undetected photons [16].

The investigation of the phenomena described above touches on several deep questions about the nature of light and the role of information in physics. In particular, the experiments demonstrate that the in principle (un)availability of information about a quantum system results in measurable physical effects. As such, the phenomenon is deeply connected with the notion of quantum complementarity.

## 1.2 Scope of this Thesis

In this thesis, I describe a series of experiments that aim to contribute to a deeper understanding of the above non-classical interference phenomena, with a particular focus on understanding quantum complementarity in these situations. The investigation of these effects stimulated many questions, both of fundamental nature and in view of possible novel applications. The following questions guided the work presented in this thesis:

- What is the role of spatial correlations and of different wavelengths in multimode induced coherence without induced emission and in quantum imaging with undetected photons?
- What information about the properties of a photon pair can be accessed using measurements on only one photon? Can the resulting possibilities lead to novel applications?
- Can the effect of induced coherence without induced emission be used to “remotely” control other degrees of freedom of single photons than their ability to interfere?
- Can we gain a deeper understanding of the effect of suppressed photon pair emission by analyzing its time-dependent aspects?
- What can we learn about complementarity by investigating the effect of quantum interference of photon pairs emitted by more than two indistinguishable sources?

## 1.3 Overview

In Chapter 2, I review some core concepts and previous key experiments that led to the advancement of the field and made our experiments possible. The chapter aims to clarify the connection between the mentioned non-classical interference phenomena as well as their relation to fundamental concepts. It also touches upon the discussion about quantum and classical aspects of these effects and several applications with the focus on quantum imaging with undetected photons. Moreover, the cavity quantum electrodynamics problem of suppressed spontaneous emission is briefly presented, which bears strong analogies to the suppression of photon pair emission by interference.

In Chapter 3, I describe two experiments that aim to gain a deeper understanding of spatially multimode induced coherence without induced emission. In the first experiment, we show that interference fringes can be produced and controlled without interacting with the light beam that is interfering. Instead, we control them by performing manipulations in an auxiliary photon beam that is not itself interfering and remains undetected. We investigate the formation of these fringes and show how they provide insights about the role of different wavelengths involved in the process.

The second experiment demonstrates that the visibility of the interference fringes observed by detecting only one of the photons depends on the correlation between two photons. An analysis of the interference pattern allows us to quantify the momentum correlation between two photons although we detect only one of them. This experiment shows that information stored in correlations can in principle be accessed by intensity measurements using only one detector.

In an experiment described in Chapter 4, we investigate the question to what extent other properties of a photon can be controlled by manipulating an auxiliary photon. In particular, we show that by changing how much path information is carried by the auxiliary photon, it is possible to control the degree of polarization of another photon. This experiment demonstrates a situation in which the origin of partial polarization cannot be explained using the classical theory of light.

In Chapter 5, I present an experiment in which we analyze the time-dependent aspect of the related phenomenon of “frustrated down conversion”, in which both photon beams are aligned to be indistinguishable and interference is observed in the total rate of emitted photon pairs. We address a question that arose shortly after the first demonstration of this phenomenon, namely whether photons are emitted at all from the individual processes during suppressed photon pair emission by interference. To this end, we investigate the phenomenon on short time-scales. We draw analogies to the related phenomenon of suppressed spontaneous emission of an excited atom in the vicinity of a mirror, for which a similar question has been asked. Our experiment can be regarded as a delayed-choice experiment, which illustrates the complementarity between interference and “which-source” information in this phenomenon.

Chapter 6 investigates a slightly different situation, in which the complementarity in suppressed down-conversion has counterintuitive implications. To this end, we analyze the phenomenon of frustrated down conversion in a slightly generalized scenario involving three sources of photon pairs. We show that in this case, the assignment of a definite origin to a photon pair is inconsistent.

In the last chapter, I summarize the conclusions from the presented experiments and mention several open questions that were stimulated by the obtained results.

# 2

## Background

### 2.1 Interference and Information

Information plays a central role in quantum mechanics. In the famous example of a double-slit experiment (Fig. 2.1), the observation of interference is only possible, if the path of an individual particle cannot be determined. If the experiment is constructed in a way that it is in principle possible to obtain complete path-information, no interference is observed.

This principle does not only hold for interference experiments with light but governs all physical phenomena that have been experimentally tested to date. Consistent with the formalism of quantum theory, interference can be seen as a direct consequence of the non-availability of information to in principle distinguish different alternatives.

#### 2.1.1 Feynman's "First Principles"

Arguably, one of the most striking features of quantum mechanics is the concept of interfering probability amplitudes, which forces us to reconsider the fundamental notion of probability. This concept was summarized by Richard Feynman in his famous lecture series as "First principles of quantum mechanics" [3], as outlined below.

In order to compute the outcome of an experiment, macroscopic "events" are identified as a first step. In the example of a double-slit experiment (Fig. 2.1), such an event would be for instance "the particle leaves the source and arrives at the detector at a specific location". Each possible event is not just assigned a probability  $P$  to occur, but a complex probability amplitude  $\phi$ . The probability for the event to occur is given by the squared modulus of the corresponding probability amplitude,

$$P = |\phi|^2. \quad (2.1)$$

The situation becomes more interesting if an event can happen in several alternative ways. In this case, the probability depends on whether the alternatives are distinguishable or not. According to classical reasoning, if an event can happen in one way with probability  $P_1$ , and alternatively in a different way with probability  $P_2$ , then the probability of the event occurring

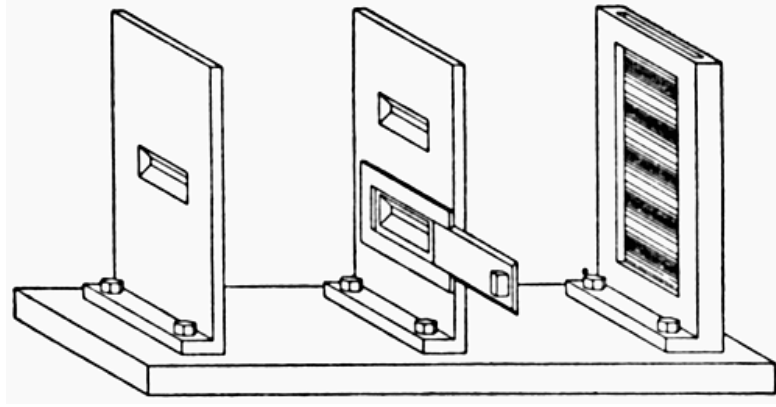


**Figure 2.1:** Double slit experiment. A quantum particle enters the apparatus from the left through the single hole in the first plate. After passing through the double slit in the middle plate, it is recorded on a screen (rightmost plate). The experimenter can choose whether or not to allow the particle to pass through both slits or through only one of them. If both slits are open, no information about the traveled path can be obtained and interference is observed. Path information can be obtained e.g. by blocking one of the slits, such that the other path can be inferred for each detected particle, in which case the interference is lost. Picture taken from [9].

is given by the sum  $P_1 + P_2$ . In quantum mechanics, this premise does not hold in general. Depending on whether the two alternatives are in principle distinguishable or indistinguishable, the total probability is computed in different ways.

In the case of indistinguishable alternatives, the probability for the event to occur is given by the squared modulus of the sum of probability amplitudes corresponding to the individual alternatives,

$$P = |\phi_1 + \phi_2|^2. \quad (2.2)$$

Equation 2.2 gives rise to interference, which can dramatically change the result compared to a classical calculation.

If, instead, the experiment “is capable of determining whether one or another alternative is actually taken” [3], then the probability for the event is given by the sum of the individual probabilities  $P_1$  and  $P_2$ , as in classical physics,

$$P = P_1 + P_2 = |\phi_1|^2 + |\phi_2|^2. \quad (2.3)$$

In order to appreciate the precise meaning of distinguishability and indistinguishability, it is important to stress that the difference between the two situations is the “capability” or the potential to find out, in which of the alternative ways the event occurred. Indistinguishability does not merely mean that the experimenter lacks the technical equipment or purposefully closes his/her eyes on the result, but instead that the experimental arrangement renders it in principle impossible to conduct any measurement that distinguishes between the alternatives. On the other hand, probability amplitudes of in principle distinguishable events add like in Eq. 2.3 and no interference is observed. In other words, interference *necessarily* occurs as soon as two or more alternatives for an event are indistinguishable. In this sense, the presence or absence of in principle distinguishing information in an experiment plays a crucial role in quantum physics.

The above statements have profound consequences. The concept of interference that has been known for light since the early days of physics, is generalized to a fundamental principle that affects all physical phenomena for which probabilities are calculated. Interference cannot only occur for light [17] or massive particles [18], but for *any* physical event that can occur in indistinguishable ways. Such events can even involve more complicated processes like particle emission or absorption.

Numerous interference experiments have been performed using a vast variety of different systems (e.g. neutrons [19], atoms [20–22], large molecules [23], etc.), illustrating the generality of this concept. In Sec 2.4, three experiments are described, which demonstrate its versatility by interfering photon pair emission processes in different ways.

## 2.2 Complementarity

In the example of an interferometer, it follows from the above arguments that the indistinguishability of the paths constitutes the experimental condition for observing interference. This condition implies that the path taken by an individual particle cannot be determined if interference is observed. As soon as the experiment is set up in a way that the paths are in principle distinguishable, the mere possibility of measuring the path of an individual quantum particle inevitably eliminates the possibility of interference. Thus, the observation of interference and the knowledge about which path a particle took are mutually exclusive<sup>1</sup>.

In general, quantum systems possess distinct properties that cannot be measured simultaneously but can only be revealed by mutually exclusive experiments. Nevertheless, a single one of the measurable properties is not sufficient to completely describe the system and its evolution. The properties are said to be complementary to each other [8, 9, 24], as both of them are needed for a complete description of the system and yet, the measurement of one precludes the definiteness of the other.

A consequence of this concept is that a quantum system in an interferometer does not a priori behave as wave or as particle, depending on the experimental setup it is confronted with. Instead, it can only be described using both aspects. This is illustrated by experiments, in which the choice of which aspect to measure is delayed to a time when the particle already traveled through the setup, or in some variants, even at a time the particle has already been detected. The idea of such “delayed-choice” experiments is briefly outlined below. For a comprehensive review of delayed choice experiments, see e.g. [25].

### 2.2.1 Delayed-Choice experiments

#### 2.2.1.1 Historical Note on Delayed-Choice Experiments

The famous Heisenberg microscope [26] was introduced as an illustration of the quantum mechanical uncertainty principle. The resolution of a microscope operating at a given wavelength is limited by the opening angle of the lens. A large opening angle allows to determine for instance an electron’s position accurately, however it allows a detected photon to enter the microscope in a large set of possible angles. According to Heisenberg, this corresponds to an uncertainty in the electron’s momentum due to the recoil the electron receives after the photon has been scattered. The observer can decide whether to detect the precise position or whether to detect the precise momentum of the electron by choosing to detect the photon in the image plane or in the focal plane of the microscope. Inevitably, he/she is confronted with an uncertainty in the other property.

The above decision can in principle be made at a time after the photon already had been scattered off the electron and has already entered the microscope [27, 28]. Therefore, the uncertainty about the property that is not measured must be introduced at a more fundamental level than merely by the physical interaction with the system of interest. The disturbance of the position instead comes from the act of “noticing”<sup>2</sup> [29] the momentum of the electron.

Thus, the electron per se possesses both properties, position and momentum, with the restriction that they can never be accessed simultaneously. Mutually exclusive experimental situations

<sup>1</sup>Note that partial path information can be obtained together with partial interference visibility, see Sec. 2.2.2

<sup>2</sup>German: *Kenntnisnahme*

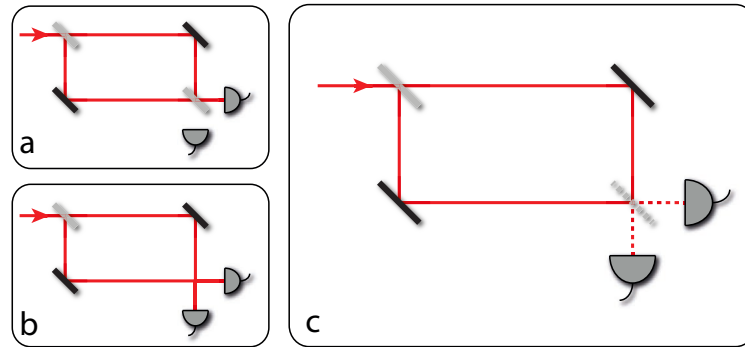


**Figure 2.2:** Illustration of Wheeler’s version of the delayed choice experiment. A single photon travels through a Mach-Zehnder interferometer. By varying the relative lengths of the two paths, interference can be observed (a). If the second beam splitter is removed, the apparatus is used to measure, which of the two paths a photon takes (b). The observer can choose whether or not to insert the final beam splitter at a time when the photon is already inside the interferometer (c). The result is the same as if this choice is made before the photon is sent in. This shows that a photon does not a priori decide whether it behaves as a particle or as a wave.

would produce knowledge about different properties of the system. Therefore, the complete description of the electron needs to account for both of the two complementary measurements [8,9].

The idea of delaying the choice of which property to measure was further refined by Wheeler [30], who considered a single photon in a Mach-Zehnder interferometer (Fig. 2.2). At a time after the photon passed through the first beam splitter, the observer decides, whether or not to introduce the second beam splitter. The two cases correspond to measurements of the path of a photon (without final beam splitter) and to the observation of interference with the final beam splitter in place. The experiment thus allows to experimentally access the “wave” (interference) or the “particle” (path knowledge) character of the photon depending on the choice of the observer.

### 2.2.1.2 Interpretation of Delayed-Choice experiments

The idea of a delayed-choice experiment has been realized in a variety of different systems (e.g. [31–36]).

These experiments show that a realistic<sup>3</sup> interpretation of wave and particle behavior along the lines of “the photon has a real property of being a wave, or a particle, which is fixed at a time before the photon enters the experimental apparatus” is challenged to say the least. In order to reproduce the experimental results, such an interpretation would have to invoke an influence of the experimenter’s choice on the photon back in time<sup>4</sup>.

All of the performed experiments are consistent with the quantum mechanical description of the systems in question. Problems in the interpretation of the results can come from attributing real values to properties that have not yet been measured. Instead, the situation can be interpreted as the measurement itself creating the physical reality. In Wheeler’s words:

“One can observe one feature of nature, or the complementary feature of nature, but not both features simultaneously.[...] It is wrong to attribute a tangibility to

<sup>3</sup>i.e. assuming that properties exist independent of their measurement.

<sup>4</sup>Recently these results have been revisited in the light of possible loopholes that would allow an understanding of the experimental results in terms of causal hidden variable theories (see [37,38]).

the photon in all its travel from the point of entry to its last instant of flight. A phenomenon is not yet a phenomenon until it has been brought to a close by an irreversible act of amplification such as the blackening of a grain of silver bromide emulsion or the triggering of a photodetector.” [30, pp. 184f].

### 2.2.1.3 Delayed-Choice Scenarios Beyond Wave-Particle Duality

While the majority of delayed-choice experiments highlights the complementarity between interference and path information about individual particles, the idea can be extended to demonstrate the complementarity of other quantum properties. In delayed choice quantum eraser experiments [36, 39, 40] for instance, the choice of which property to measure is made on a different system than the one under consideration. This allows seeing the behavior corresponding to that choice at a time when the particle in question already has been detected.

The complementarity between separability and entanglement of the polarization properties of a photon pair has been demonstrated in delayed-choice entanglement swapping [41, 42]. In this experiment, two pairs of entangled photons are produced independently. If a certain correlation measurement<sup>5</sup> is performed on one photon of each pair, the other two photons exhibit correlations that cannot be explained classically, i.e. they are entangled. If, however, one chooses to perform simple polarization measurements on one photon of each pair, the remaining two photons are in a product state, i.e. both of them individually possess definite polarization properties that are compatible with a local realistic description.

The experiment shows that polarization correlations between two photons can correspond to an entangled state or a product state, depending on the choice of measurement on a second pair of photons. Remarkably, it does not matter, which photon pair is detected first for this to occur. The decision whether to measure entanglement of two photons or whether to measure their product state behavior can be delayed to a time after the two photons in question have already been detected. As such, the experiment demonstrates a different aspect of complementarity. The two particles are neither definitely in a product state nor are they definitely entangled before all photons involved in the process have been detected.

In Chapters 5 and 6, we explore the complementarity in a different system, in which the mere existence of a photon as a measurement-independent property is challenged.

## 2.2.2 Partial Path Information and Partial Visibility

Full knowledge about which path a particle took renders the observation of interference impossible and vice-versa. However, it is possible to obtain partial which-path information about a system and at the same time observe partial interference. It is possible to relate the two concepts quantitatively.

The analysis of the double slit experiment in the case of partial path information [43, 44], showed that a surprisingly high interference visibility<sup>6</sup> can be obtained even when a considerable amount of path information is available. The situation was later analyzed by Greenberger and Yasin [45], who gave the following instructive example.

Consider an initially balanced interferometer, which is modified by placing an absorber in one of the two paths that absorbs 99% of particles. The interferometric visibility in this interferometer can be as high as 20%. This is due to the fact that the absorber acts on the amplitude, and not on the probability of passing through it (see Fig. 2.3).

In case no path information is available via any auxiliary system, the quantum state of a particle in an interferometer can be written as a pure state,

$$|\psi\rangle = a|1\rangle + e^{i\varphi}b|2\rangle, \quad (2.4)$$

<sup>5</sup>which projects two photons into one of four Bell states

<sup>6</sup>The visibility is defined as  $(R_{max} - R_{min})/(R_{max} + R_{min})$ , where  $R_{max}(R_{min})$  stands for the maximum (minimum) count rate upon varying the interferometric phase.

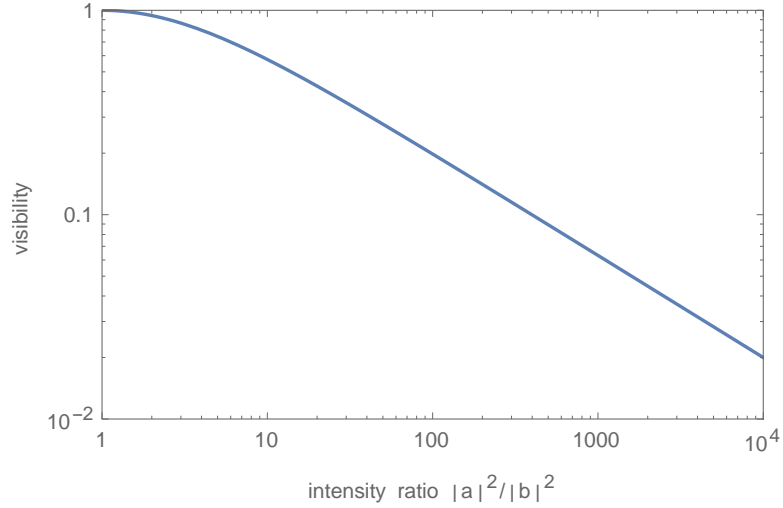


**Figure 2.3:** Visibility in an interferometer with unbalanced intensities. In an interferometer in which the two interfering beams have unequal intensities, the maximum visibility given by Eq. 2.6 drops very slowly. A ratio of 99:1 still results in almost 20% visibility.

where  $a$  and  $e^{i\varphi}b$  are the probability amplitudes for a particle traveling via path 1 or path 2. Here,  $a$  and  $b$  are real numbers<sup>7</sup> and the relative phase between the two amplitudes is denoted by  $\varphi$ . The corresponding intensity observed at the detector is given by,

$$I = |a + e^{i\varphi}b|^2 = a^2 + b^2 + 2ab \cos \varphi, \quad (2.5)$$

with the probabilities  $a^2$  and  $b^2$  for a particle passing through paths 1 and 2, respectively. The interferometric visibility is given by

$$V = \frac{I_{max} - I_{min}}{I_{max} + I_{min}} = \frac{2ab}{a^2 + b^2}. \quad (2.6)$$

Path information is introduced as the possibility of correctly predicting the outcome of a which-path measurement with a higher probability than pure chance. A quantitative “particle measure” can be defined as [45]

$$\mathcal{P} = \frac{a^2 - b^2}{a^2 + b^2}. \quad (2.7)$$

For a balanced interferometer (both paths equally likely),  $\mathcal{P}^2 = 0$ , whereas the other extreme case, in which one path is completely blocked results in  $\mathcal{P}^2 = 1$ .

The above analysis is generalized to partially coherent scenarios, i.e. including mixed states. It follows [45] that

$$V^2 + \mathcal{P}^2 \leq 1, \quad (2.8)$$

where the equality holds for the pure state case.

This analysis was later extended [46–48], noting that two fundamentally different ways exist to introduce path information. First, the imbalance of probabilities (as considered above), and second, distinguishability of the path with the help of an auxiliary system, which would allow to predict in advance, which path a photon takes<sup>8</sup>. Jaeger et al. [47] considered a source of correlated photons in which the detection of one photon can reveal the path of the other photon (see also the experiment described in Sec. 2.4.1). Further analysis of the scenario of a single photon in an interferometer was performed by Englert [48], showing that the complementarity between path information and interference has its origin in the quantum mechanical description of the detector used to distinguish the paths.

<sup>7</sup>fulfilling the conditions  $0 \leq a \leq 1$ ,  $0 \leq b \leq 1$ , and  $a + b = 1$

<sup>8</sup>Resulting in “mixedness” of the state.

## 2.3 Spontaneous Parametric Down Conversion

The most common way to produce photon pairs in today's laboratories is via the process of spontaneous parametric down-conversion (SPDC) [7, 49]. In the standard scenario, a nonlinear<sup>9</sup> crystal is illuminated by a laser beam. A photon from this laser beam can be converted into two photons of lower energy, i.e. of longer wavelength. For historical reasons, the resulting two down-converted photons are called “signal” and “idler”, a convention that is adopted throughout this thesis.

Spontaneous parametric down-conversion is a parametric process. This means that the state of the crystal is identical before and after the conversion of a laser photon into a photon pair [50, Sec. 1.2. ]. After the interaction, no measurement other than detecting the involved photons themselves can reveal whether SPDC has happened or not. If an experiment allows for different ways of creating down-converted photon pairs by e.g. illuminating two or more crystals coherently, these different ways are indistinguishable apart from information that is carried by the involved photons themselves. This allows to conveniently create photon pairs in superposition of different origins, or in superposition of momenta, frequencies, or polarizations.

Photon pairs produced in an SPDC process in general exhibit correlations both in frequency [51–54] and in momentum [55, 56] due to fundamental conservation laws. In the following, we discuss the “spatial” correlation between the transverse momenta of signal and idler photons, which are particularly relevant in the context of this thesis.

### 2.3.1 Spatial Correlations Between Down-Converted Photons

Already in the case of SPDC in a single nonlinear crystal, a photon pair can be produced with different momenta of signal and idler photons. In general, momentum conservation during the SPDC process only requires that the momenta of signal and idler photons add up to the momentum of the pump photon. This leads to the condition<sup>10</sup>,

$$\mathbf{q}_P = \mathbf{q}_S + \mathbf{q}_I, \quad (2.9)$$

where  $\mathbf{q}_P, \mathbf{q}_S, \mathbf{q}_I$  denote the transverse components of the wave vectors of pump, signal, and idler photons, respectively.

The momentum correlation between two photons has been measured in a variety of different ways. In the simplest case, detectors are placed in both beams that emerge from the source in a way that a pair of photons is detected only when each of the photons carries a particular momentum. This can be done, for example by placing lenses followed by small apertures in front of the detectors as indicated in Fig. 2.4. In this way, a photon can be detected behind the respective aperture only when it carries a transverse momentum that corresponds to the position of the aperture. The rate of coincident detections at a particular pair of aperture positions corresponds to the sampling of the joint probability distribution  $P(\mathbf{q}_S, \mathbf{q}_I)$  of the transverse momenta of a photon pair. In the case of perfect correlation, coincidence detection happens only for exactly one relative transverse position of the apertures<sup>11</sup>.

Suppose one chooses a fixed position of the aperture in the signal beam, corresponding to a particular momentum of the signal photon. A scan of the aperture in front of the idler detector then determines the conditional probability distribution

$$P(\mathbf{q}_I|\mathbf{q}_S) = \frac{P(\mathbf{q}_S, \mathbf{q}_I)}{P(\mathbf{q}_S)}, \quad (2.10)$$

<sup>9</sup>Nonlinear in the sense that the electric polarization of the material depends on the electric field in a nonlinear way.

<sup>10</sup>Throughout, we assume paraxial beams and the detection plane perpendicular to the optical axis. Moreover, we assume that a transverse phase mismatch [57] is negligible.

<sup>11</sup>which is implied by Eq. 2.9

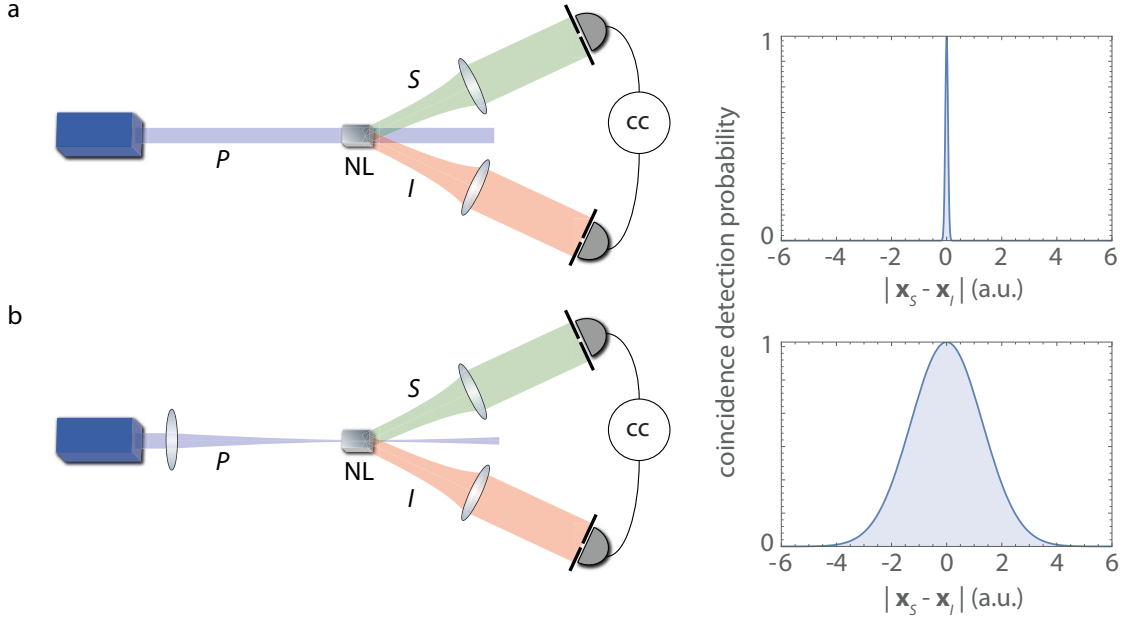


**Figure 2.4:** Illustration of a standard method to measure the momentum correlation between two photons produced by SPDC. Two detectors are placed in the signal and idler beams respectively in a way that only photons with a particular value of transverse momentum are detected. This can be achieved by placing lenses at focal distance to crystal and detector in both beams. In the case of a large pump focus (a), the beam approaches a plane wave and the transverse momentum of a pump photon is defined up to a small uncertainty. Eq. 2.9 can be fulfilled only for a narrow range of  $\mathbf{q}_S + \mathbf{q}_I$ , resulting in a sharp correlation. The sharper the correlation, the sharper the dependence of the coincident detection rate on the relative positions of the two apertures (denoted as  $|\mathbf{x}_S - \mathbf{x}_I|$ ). A narrow pump focus (b) corresponds to a high uncertainty in the momenta of the pump photons and correspondingly to a weaker correlation.

of detecting an idler photon with transverse momentum  $\mathbf{q}_I$ , given its partner signal photon is detected with  $\mathbf{q}_S$ . The variance of this distribution  $\sigma^2(\mathbf{q}_I|\mathbf{q}_S)$ , i.e. the uncertainty of the momentum of one of the two photons given the other photon is measured with a particular momentum, is a measure for the correlation strength.

In the case of zero uncertainty in the transverse momentum of a pump photon (i.e. an idealized “plane wave pump”), the detection of a signal photon at a precise momentum allows to infer the precise momentum of the partner idler photon, corresponding to perfect correlation ( $P(\mathbf{q}_I|\mathbf{q}_S) \propto \delta(\mathbf{q}_I + \mathbf{q}_S)$ ). A large value of  $\sigma^2(\mathbf{q}_I|\mathbf{q}_S)$ , on the other hand, corresponds to weakly correlated photon pairs. In order to measure  $\sigma^2(\mathbf{q}_I|\mathbf{q}_S)$ , usually both photons need to be detected.

It has been shown [55] that if the pump photon is in a superposition of different plane-wave modes, the angular spectrum [58, Sec. 3.10] of the pump beam is “transferred” to the correlation between signal and idler photons (Fig. 2.5), i.e. the distribution of pump momenta can be accessed in the momentum correlation,  $P(\mathbf{q}_S + \mathbf{q}_I) \propto P(\mathbf{q}_P)$ . This also occurs when the pump is a focused laser beam. A larger uncertainty in the transverse momentum of the pump photons leads to a weaker correlation between signal and idler photons, as with an uncertain  $\mathbf{q}_P$ , Eq. 2.9 can be fulfilled for a larger range of  $\mathbf{q}_I$  given  $\mathbf{q}_S$ . Intuitively, a narrow focus contains many plane wave modes with non-zero intensity, which leads to a wide range of possible momenta of the idler photon, given the signal photon is detected with a precise momentum (Fig. 2.4b).

Measurements of the momentum correlation have been performed using a variety of different implementations of this idea. These include the scanning of two slits [59], the use of spatial-light modulators [60], or arrays of optical fibers [61]. A particularly interesting modification of this technique used a single EMCCD camera to detect both beams [62]. Using statistical techniques,

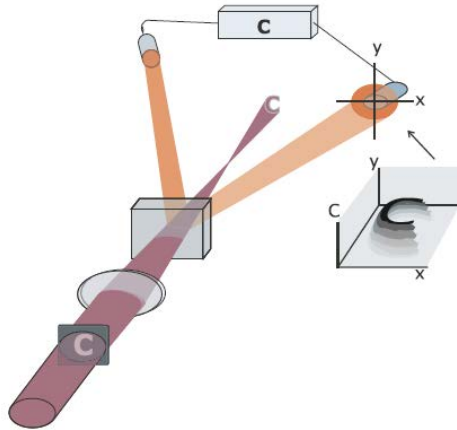


**Figure 2.5:** Illustration of how the angular spectrum of a pump photon is transferred to a down-converted photon pair [55]. A modulation of the angular spectrum (illustrated by a mask in front of a lens) of the pump beam can be reconstructed in the correlation between signal and idler photons, although none of the individual beams carries this information. The momentum distribution of the pump photon determines the distribution of the sum of signal and idler momenta. Picture taken from [56].

it was possible to determine the relative distances between the points a signal and an idler photon arrived on the camera, corresponding to the different respective momenta. All of these methods rely on the coincident detection of both photons of the pair, either directly, or by finding the most likely coincidence in the output of an EMCCD camera, which is an image produced by several photon pairs.

Of particular interest are measurements of the momentum correlation in conjunction with transverse correlations in the near field of the source [56, 63]. The product of the respective uncertainties can be used to demonstrate an analogous situation to the EPR-Paradox [1] with light (e.g. [59, 62, 64–66]).

The spatial correlation of photon pairs emitted by SPDC also led to applications, such as ghost imaging [67, 68] and ghost diffraction [69, 70], and quantum imaging with undetected photons [16].

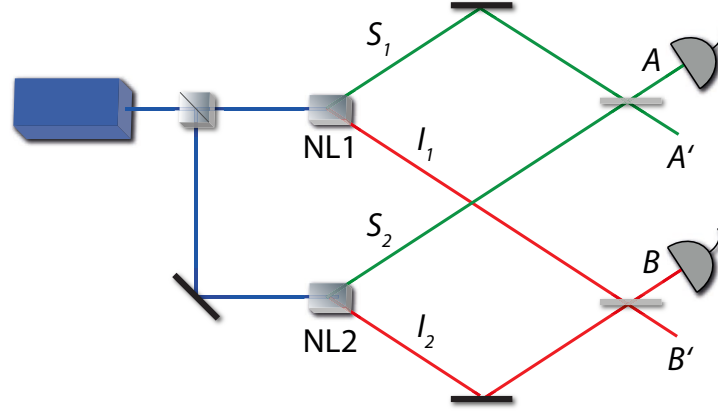


**Figure 2.6:** Schematic of a two-photon interference experiment. A photon pair can be created in either of the two sources. The two possible paths of a signal (idler) photon are superposed by a beam splitter and subsequently detected. Interference is observed in the coincidence rate but not in the individual detectors.

## 2.4 Three Different Ways to Interfere a Photon Pair

In the following, three experimental schemes are discussed with the aim to illustrate the generality of the concept of interference and indistinguishability. All of these experiments were performed with photon pairs generated by SPDC, however they could be generalized to other particles. Nevertheless, already in these examples, the richness of possible ways to interfere probability amplitudes of photon pair emissions can be demonstrated.

### 2.4.1 Two-Photon Interference in Coincidence

Consider the experiment depicted in Fig. 2.6, which is an idealization of the experiments reported in [71–75]. Further analysis of this scheme can be found in [76, 77].

Photon pairs are created by SPDC in either of two sources at a rate that only one photon pair at a time is present in the setup. Either the photon pair is emitted into beams  $S_1$  and  $I_1$ , or it is emitted into beams  $S_2$  and  $I_2$ . Beams  $S_1$  and  $S_2$  are superposed on a beam splitter and subsequently detected. Similarly, beams  $I_1$  and  $I_2$  are detected after a second beam splitter. In this experiment, neither of the two individual detectors records interference [75]. However, the rate of coincident photon detection in both detectors is modulated by an interferometric phase, as shown below.

Formally, we can write the quantum state of the photon pair emitted in a superposition of either source as

$$|\psi\rangle = \frac{1}{\sqrt{2}} (|S_1, I_1\rangle + e^{i\varphi} |S_2, I_2\rangle), \quad (2.11)$$

where  $|S_j, I_j\rangle$  denotes a photon pair in beams  $S_j$  and  $I_j$  and  $\varphi$  is an arbitrary interferometric phase. Note that  $\varphi$  can be tuned by varying the optical path lengths of any of the four photon paths or the pump beams.

Paths  $S_1$  and  $S_2$  are superposed by a 50:50 beam splitter, which results in the transformations

$$|S_1\rangle \rightarrow \frac{1}{\sqrt{2}} (|A\rangle + i|A'\rangle), |S_2\rangle \rightarrow \frac{1}{\sqrt{2}} (i|A\rangle + |A'\rangle), \quad (2.12)$$

and likewise paths  $I_1$  and  $I_2$ ,

$$|I_1\rangle \rightarrow \frac{1}{\sqrt{2}}(|B\rangle + i|B'\rangle), |I_2\rangle \rightarrow \frac{1}{\sqrt{2}}(i|B\rangle + |B'\rangle). \quad (2.13)$$

Accordingly, the quantum state Eq. 2.11 evolves to

$$|\psi\rangle = \frac{1}{2\sqrt{2}}[(1 - e^{i\varphi})(|AB\rangle + |A'B'\rangle) + i(1 + e^{i\varphi})(|AB'\rangle + |A'B\rangle)] \quad (2.14)$$

The probability of photon detection at detector  $A$  can be calculated using Born's rule disregarding ("tracing out") the two possible paths for the idler photon,  $B$  and  $B'$ ,

$$P_A = |\langle AB|\psi\rangle|^2 + |\langle AB'|\psi\rangle|^2 = \frac{1}{8}(2 - 2\cos\varphi) + \frac{1}{8}(2 + 2\cos\varphi) = \frac{1}{2}. \quad (2.15)$$

The probabilities of the two possible ways of detecting a signal photon ( $|\langle AB|\psi\rangle|^2$  and  $|\langle AB'|\psi\rangle|^2$ ) add incoherently<sup>12</sup>, due to the orthogonality (i.e. full distinguishability) of the corresponding idler modes. The probability of photon detection is constant, i.e. no interference is observed. An analogous relation holds for the detection probability of the idler photon at detector  $B$ .

The absence of interference in the individual detectors can be understood as a consequence of the possibility to retrieve path information via the other photon. Suppose the detector for the idler photon is removed and we detect only a signal photon. The detected photon could have arrived at the detector either via path  $S_1$  or via path  $S_2$ . Because the signal photon impinges on the detector behind the beam splitter, its detection does not reveal which of the two paths it has taken. However, this information could in principle be obtained from a measurement on the idler photon. Consider for example a situation in which the two output paths  $B$  and  $B'$  of the beam splitter of the partner idler photon are superposed with the help of a third beam splitter. In this case, the path taken by the signal photon from source to detector is correlated with the hypothetical detection of an idler photon in one of the two outputs of the third beam splitter. This hypothetical possibility is sufficient to eliminate the possibility to observe interference.

The probability of a *coincident* detection at both detectors  $A$  and  $B$  follows from Eq. 2.14 (cf. [77]),

$$P_{AB} = |\langle AB|\psi\rangle|^2 = \left|\frac{1}{2\sqrt{2}}(1 - e^{i\varphi})\right|^2 = \frac{1}{4}(1 - \cos\varphi). \quad (2.16)$$

The dependence on  $\varphi$  shows that interference occurs in this case.

These results can be understood in terms of indistinguishability as follows. Consider the correlated detection of a photon pair in both detectors  $A$  and  $B$ . This event can occur either by the signal photon traveling via path  $S_1$  and the idler photon via path  $I_1$ , or it can occur by the two photons taking paths  $S_2$  and  $I_2$ . After both photons have been detected behind the respective beam splitters, no subsequent manipulation or measurement can be performed on either of them. Therefore, the two possible sets of photon paths are indistinguishable and consequently, the probability of a coincident photon detection is given by the squared modulus of the probability amplitudes corresponding to the two alternatives.

It is interesting to identify the erasure of path information in this experiment. Information about the origin of a photon pair is initially present in both signal and idler photon. The information carried by the signal photon is "erased" by detecting the signal photon after the beam splitter. In the same way, information stored in the path of the idler photon is erased by detecting the idler photon after the beam splitter. Only if both photons of a pair have been detected, no path information remains about the origin of the photon pair and interference is observed.

---

<sup>12</sup>The probabilities are summed instead of their amplitudes

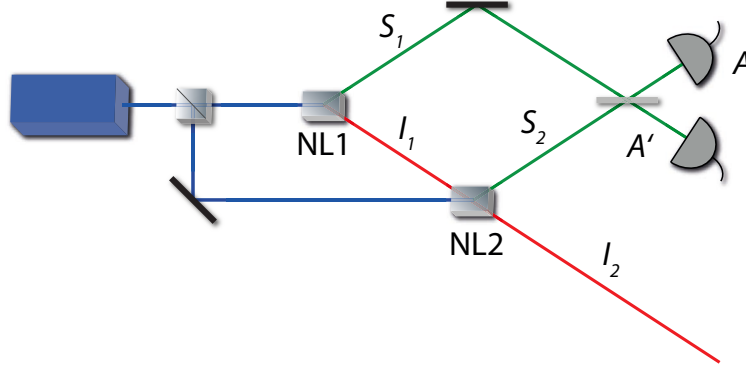


**Figure 2.7:** Two-photon interference setup with aligned idler beams (“Zou, Wang, Mandel interference”). A photon pair can be created in either of the two sources. The two signal beams are superposed on a beam splitter and subsequently detected. The two idler beams are aligned to be indistinguishable and not detected. Interference is observed in the detection rate of the signal beam, without the need of coincidence detection.

#### 2.4.2 The Zou, Wang, Mandel, (Ou) experiment

An interesting modification of the two-photon interference experiment (Fig. 2.7) was demonstrated by Zou, Wang, and Mandel (ZWM) in 1991 [13, 14], following a suggestion by Z.Y. Ou. In this experiment, the two possible paths of the signal photon are again superposed on a beam splitter and subsequently detected. The idler photon’s paths, however, are not superposed. Instead, the idler beam emerging from the first source travels through the second source and is aligned to be indistinguishable from the idler beam emerging from there.

Once the idler beams are aligned, interference between the two signal beams is observed. If the idler beam is blocked between the crystals, no interference occurs. The interferometric visibility<sup>13</sup> was shown to be proportional to the amplitude transmission of a filter placed in the idler beam between the two crystals [13].

In a scenario, in which the idler beams are not aligned (or the beam is blocked between the two crystals), a photon pair is again created in a superposition of its origin being either at NL1 or at NL2, as in the two-photon interference experiment discussed in the previous section,

$$|\psi\rangle = \frac{1}{\sqrt{2}} (|S_1, I_1\rangle + e^{i\varphi} |S_2, I_2\rangle). \quad (2.17)$$

In the case of perfect alignment of the idler modes and unit transmission between the two crystals, the two idler modes are identical. This is represented by the replacement  $|I_1\rangle \rightarrow e^{i\varphi_I} |I_2\rangle := e^{i\varphi_I} |I\rangle$ . In this case, a photon pair is produced in the state

$$|\psi\rangle = \frac{1}{\sqrt{2}} (|S_1, I\rangle + e^{i(\varphi - \varphi_I)} |S_2, I\rangle) = \frac{1}{\sqrt{2}} (|S_1\rangle + e^{i(\varphi - \varphi_I)} |S_2\rangle) |I\rangle. \quad (2.18)$$

As can be seen from Eq. 2.18, the signal photon is in a superposition of paths  $S_1$  and  $S_2$ , which leads to first order interference after the beam splitter. Using Eq. 2.12, we obtain

$$|\psi\rangle = \frac{1}{2} [(1 + e^{i\varphi'}) |A\rangle + i(1 - e^{i\varphi'}) |A'\rangle] |I\rangle, \quad (2.19)$$

where  $\varphi' = \varphi - \varphi_I + \pi/2$ .

<sup>13</sup>The visibility is defined as  $V = \frac{I_{max} - I_{min}}{I_{max} + I_{min}}$ , where  $I_{max(min)}$  represents the maximum (minimum) count rate at the detector as the interferometric phase is varied.

The detection probability after the beam splitter is given by

$$P_A = |\langle A, I | \psi \rangle|^2 = \frac{1}{2} (1 + \cos \varphi'). \quad (2.20)$$

In the case of a filter with amplitude transmission  $T$  present in the idler beam between the two crystals, only the transmitted part of  $|I_1\rangle$  is identical to  $|I\rangle$ . This can be written as  $|I_1\rangle \rightarrow T e^{i\varphi_I} |I\rangle + \sqrt{1 - T^2} |I_l\rangle$ , where  $|I_l\rangle$  subsumes the possible states of “lost” or absorbed idler photons<sup>14</sup>. The photon pair is in the state

$$|\psi\rangle = \frac{1}{\sqrt{2}} (T |S_1\rangle + e^{i\varphi'} |S_2\rangle) |I\rangle + \sqrt{1 - T^2} |S_1, I_l\rangle. \quad (2.21)$$

A detector placed after the beam splitter detects the signal photon with probability (cf. [13])

$$P_A = |\langle A | \psi \rangle|^2 = \frac{1}{2} (1 + T \cos \varphi'), \quad (2.22)$$

which is the equation for an interference fringe with visibility  $T$ .

This experiment contains several remarkable aspects. The effect is observed in direct first order intensity measurements. No coincidence or heralded detection is necessary. In fact, the idler beam does not need to be detected at all. Moreover, ZWM used a weak pump laser, such that the probability of two pairs being created simultaneously was negligible. Therefore, the effect cannot be attributed to induced emission at the second source, but to the indistinguishability of photon pair origins<sup>15</sup>. In this way, the experiment seems to demonstrate that what can be known “in principle” does have physical manifestations that can be measured, in line with the discussion about interference of in principle indistinguishable events. This point has been further illustrated by demonstrating that the interference can also be controlled by introducing path information in various different ways [78–80].

The experiment has been termed an instance of a “quantum eraser” [40], as interference is “regained” after the path information present in the idler photons is eliminated (e.g. [81]). Compared to quantum eraser experiments based on two-photon interference, there is, however, an important difference. In typical quantum eraser experiments, an entangled quantum state is prepared (cf. Eq. 2.11) and one subsystem (sometimes referred to as “path-marker”) is measured. Given a particular outcome of this measurement, interference is observed in the other subsystem. In other words, interference occurs in the coincident detection rate of both subsystems. Typically, one half of the prepared systems are discarded as a consequence of correlating the respective outcomes (compare Eq. 2.16, where  $P_{AB} \leq 1/2$ ).

If the idler beams are overlapped as in the experiment described here, no coincidence detection is necessary. That is, every single signal photon obeys the same interference law and no photon needs to be discarded in order to observe interference. This is due to the fact that instead of preparing the state including a path-marker and subsequently erasing it in a probabilistic fashion, here the path information is never generated in the first place.

As a consequence, interference can be observed in first order in intensity, i.e. with a single detector in the signal beam, whereas for a typical quantum eraser, interference is observed in second order in intensity, i.e. in the correlation between photon detections in two detectors. The difference can be seen by comparing Eqs. 2.16 and 2.20.

It is possible to analyze the erasure of information as follows. The information about the origin of an individual photon pair carried by a signal photon is erased by detecting it behind the beam splitter. Unlike the scheme in Sec. 2.4.1, path information in the idler beam does not need to be erased by another beam splitter. Instead, the idler photon is already emitted in a way that no

<sup>14</sup>Strictly speaking, absorbed photons can occupy a range of different modes. However, all of them are fully distinguishable and thus orthogonal to  $|I\rangle$ .

<sup>15</sup>This point was challenged in an ongoing discussion about the “quantumness” of the effect, which is briefly discussed in Sec. 2.7.

path information is created. Even when it remains undetected, no which source information can be obtained and consequently, interference between the two possible origins of a signal photon can be observed.

As the information about the transmission in the idler beam is observed in the signal beam, the question arises, how the information travels from filter to detector. This question has been addressed by measuring the time it takes for a change of the filter in the idler beam to affect the interference visibility in the signal beam [82]. The characteristic length scale was found to be the sum of the idler path between filter and NL2 and the signal path between NL2 and the detector.

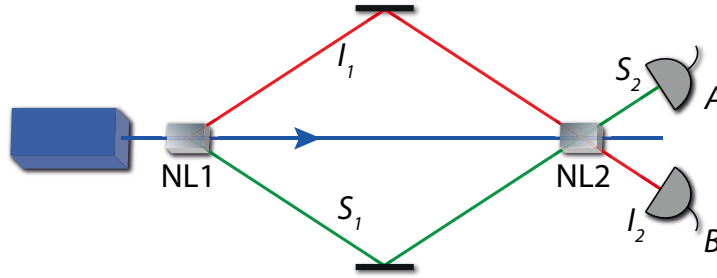


**Figure 2.8:** Two-photon interference with both signal and idler beams aligned (“frustrated two-photon creation via interference”). A photon pair can be emitted by either of the two crystals NL1 and NL2. Both signal and idler beams are aligned to be indistinguishable. Interference of the two possible ways of creating a photon pair is observed in either detector. No beam splitter or coincidence detection is used. The rate of produced photons itself depends on the interferometric phase. This phase is given as a combination of pump, signal, and idler phase shifts as  $\varphi = \varphi_P - \varphi_S - \varphi_I$ .

### 2.4.3 Frustrated Two-Photon Creation

The idea of making photon paths indistinguishable can be extended by aligning not only the two idler beams, but also the two signal beams to be indistinguishable, as sketched in Fig. 2.8. An experiment of this kind was performed 1995 in Anton Zeilinger’s group [15].

We again start with the quantum state representing a photon pair in a superposition of two origins,

$$|\psi\rangle = \frac{1}{\sqrt{2}} (|S_1, I_1\rangle + e^{i\varphi} |S_2, I_2\rangle). \quad (2.23)$$

No beam splitter is employed in this experiment. The alignment of the beams is represented by the replacements  $|I_1\rangle \rightarrow e^{i\varphi_I} |I_2\rangle := e^{i\varphi_I} |I\rangle$ , and  $|S_1\rangle \rightarrow e^{i\varphi_S} |S_2\rangle := e^{i\varphi_S} |S\rangle$  in Eq. 2.23.

Applying the same arguments as before, we can write the resulting quantum state as [15]

$$|\psi\rangle = \frac{1}{\sqrt{2}} (|S, I\rangle + e^{i\varphi'} |S, I\rangle) = \frac{1}{\sqrt{2}} (1 + e^{i\varphi'}) |S, I\rangle, \quad (2.24)$$

where here,  $\varphi' = \varphi - \varphi_S - \varphi_I$ , and  $|S, I\rangle$  represents a photon pair emitted by the two-crystal system.

The probability of photon pair emission is given by

$$P_A = P_B = \frac{1}{2} (1 + \cos \varphi'). \quad (2.25)$$

Interference is observed at each of the individual detectors simultaneously.

This scenario is again somewhat different from the previously described experiments. In order to observe interference in the case of both beams being aligned, clearly, no coincidence detection is necessary. However, in contrast to the ZWM experiment, the detection of a signal photon is not even required to be performed behind a beam splitter which would eliminate which-path information. The emission probability of the photon pairs itself is subject to interference. As such, this experiment could be regarded as the most fundamental form of two-photon interference, as no path information that would need to be erased is created with either photon.

The two possible SPDC emissions constitute two indistinguishable alternatives by which an individual photon pair can be created. No experiment can be performed on either photon emitted

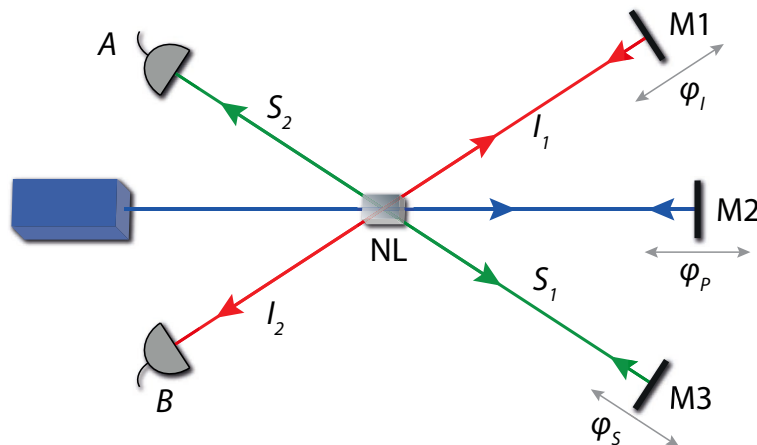


**Figure 2.9:** Experimental setup to observe “frustrated two-photon creation via interference” as implemented in [15]. A single nonlinear crystal is illuminated by a laser beam from both sides (via M2). Photon pairs can be created in either direction. Using mirrors M1 and M3, the two possible photon pair paths are overlapped to be indistinguishable. At the detector side, no information about the original direction of the photon pairs can be recovered in principle, and interference is observed.

from the setup that could determine its origin. Consequently, the probability of detecting a photon pair in this experiment is obtained by adding the probability amplitudes corresponding to these two processes. This leads to interference in the total rate of emitted photon pairs.

Path information does not need to be erased neither in the signal nor in the idler beam<sup>16</sup>, as both photons are already emitted in an indistinguishable way.

Instead of employing two non-linear crystals, this system was originally implemented experimentally by pumping one crystal from both sides (see Fig. 2.9) [15]. This allows for the generation of photon pairs in either of two opposite directions. The alignment was performed using mirrors for signal, idler, and pump beams. The interferometric phase was tuned by moving either of the three mirrors. The observation that at mirror positions corresponding to destructive interference, no photon pairs are emitted from the system led to the term “frustrated two-photon creation”, a reference to the phenomenon of “frustrated total internal reflection”.

A thorough theoretical description of this experiment can be found in [84] (see also [15, 85]).

<sup>16</sup>An interesting modification of this experiment in which path information is initially created and subsequently “quantum erased” was performed in [83].

### 2.4.4 Coherence Length Requirements in Two-Photon Interference Experiments

One of the most challenging tasks in the construction of interference experiments of the above kind is the alignment of the different path lengths. Therefore, the involved coherence requirements are briefly motivated below. Their understanding is not only crucial from an operational perspective, i.e. if one attempts to build a similar experiment, it also allows fundamental insights about the nature of the interference effects we are confronted with. In particular, a comparison between the coherence length requirements for the experiments described in the previous section illustrates the similarities and differences between these phenomena.

In a classical two-path interferometer with light, the interferometric phase is given by the relative phase of the electric field amplitudes of the two interfering beams. This phase can be tuned by extending one optical path length with respect to the other. Given the light is not strictly monochromatic, different frequency components acquire different phase shifts using this procedure, which results in a reduced visibility of the interference fringes for large path length differences. Nevertheless, interference is observed as long as the path length difference is small. The coherence length (defined via the reciprocal frequency bandwidth) is a characteristic length scale up to which the two path lengths can differ before the uncertainty of the relative phase becomes too large for an interference fringe to be observable.

Understanding interference in terms of the absence of information (Sec. 2.1.1), the physical meaning of this concept needs to be adapted. Even for a single photon in an interferometer, interference is observed as long as the path length difference does not exceed the coherence length. In order to be consistent in the interpretation, the coherence length must, therefore, account for an “unsharpness of timing information”, in the sense that information about the path of a single photon can be obtained in principle as soon as the two paths differ by more than the coherence length. Instead of caused by phase uncertainty, the absence of interference can thus be explained as caused by path information that is in principle available. The equivalence of these two interpretations has been shown theoretically in [86].

The observations in the three cases described in the previous section are somewhat different in the sense that interference is observed either in coincidences, after a beam splitter, or directly in the rate of down-converted photons. Nevertheless, as shown below, the path length requirements in all three cases can be deduced from the same simple arguments, indicating a common origin of the physical phenomena underlying these experiments.

In the described experiments, two coherence lengths are involved: the coherence length of the pump laser and that of the down-converted photons. We assume that they are equal to the uncertainty of knowing the emission time of a particular photon.

This leads to two requirements which need to be met in order for the pair emission from NL1 to be indistinguishable from a pair emission from NL2 and thus to see interference in any of the above experiments:

1. The arrival time difference between a signal and an idler photon must be indistinguishable for a photon pair emitted by NL1 compared to a pair emitted by NL2. That is, it must be smaller than the timing uncertainty  $\Delta l_{SPDC}$  of the down-converted photons.
2. The arrival time of a photon pair as a whole must not be different for NL1 than for NL2. That is, if we sent a laser pulse at a specific time into the setup, the time it takes from the emission of the pulse until photons are detected must be the same for both NL1 and NL2, up to the timing uncertainty of the laser pulse  $\Delta l_{Laser}$ .

These two conditions determine the alignment conditions for all experiments presented above, see Fig. 2.10. The path lengths of signal and idler beams from the  $j$ th source are denoted by  $S_j$  and  $I_j$ .

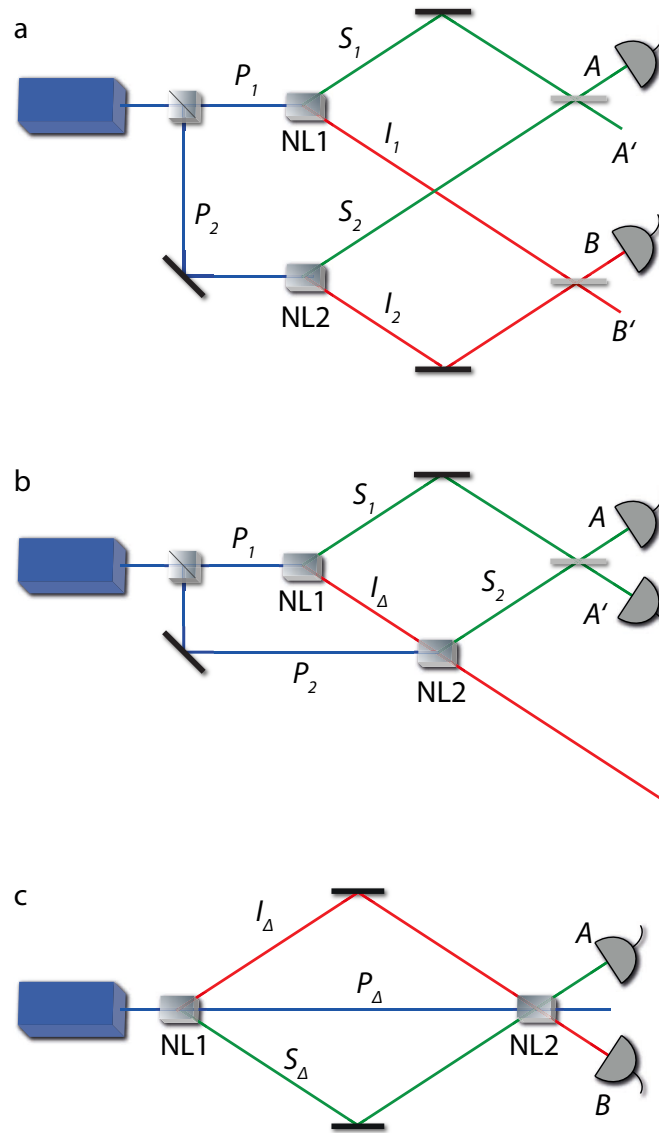


**Figure 2.10:** Comparison of the coherence length requirements in the three experiments. In (a), both signal (green) and idler (red) beams are superposed on beam splitters and interference is observed in the coincident detection rate. In (b), the signal beams are superposed on a beam splitter, while the idler beams are aligned to be indistinguishable. Interference is observed between the two signal beams. In (c), both signal and idler beams are aligned to be indistinguishable and interference is observed in the total rate of detected photons. In all three cases, a condition for interference is that the path lengths are adjusted in a way that the potential detection of the two photons does not allow to infer, from which source a photon pair has been emitted. In all three cases, this argument allows to deduce quantitative coherence length requirements. The fact that this is possible illustrates the common origin of these experiments on a fundamental level, although the interference manifests in different observations. The labels refer to the respective optical path lengths, see text.

#### 2.4.4.1 Two-Photon Interference in Coincidence

This case refers to Fig. 2.10a. Suppose a photon pair is emitted by NL1. The time difference between the detection of a signal and the detection of an idler photon is  $\Delta t_{NL1} = (S_1 - I_1)/c$ . Similarly, for a photon pair emitted by NL2, the arrival time difference is  $\Delta t_{NL2} = (S_2 - I_2)/c$ . Condition (1) requires that the difference  $|\Delta t_{NL1} - \Delta t_{NL2}|$  is small enough that no path information can be obtained in principle by precisely measuring arrival photon times. This is ensured via the arrival time uncertainty of the down-converted photons, if

$$|(S_1 - I_1) - (S_2 - I_2)| < \Delta l_{SPDC}. \quad (2.26)$$

The second condition concerns the arrival time of an entire photon pair from the two sources NL1 and NL2. The time delay between a laser pulse entering the setup through the first beam splitter and the detection of a signal photon from NL1 reads  $P_1 + S_1$ . If the signal photon is emitted by NL2, it arrives after the time  $P_2 + S_2$ . The difference results in the condition

$$|(P_1 + S_1) - (P_2 + S_2)| < \Delta l_{Laser}. \quad (2.27)$$

The same argument can be given for the idler photons, which leads to

$$|(P_1 + I_1) - (P_2 + I_2)| < \Delta l_{Laser}. \quad (2.28)$$

#### 2.4.4.2 Zou, Wang, Mandel, (Ou) Interference

The same conditions apply in the experiment depicted in Fig. 2.10b. However, the idler photon is not detected in this case. In order to identify, which information could in principle be recovered by measuring the idler, one can imagine a hypothetical detector for the idler photon just after NL2. Due to the geometry of the setup, the path lengths of the two idler beams between source and detector are related by  $I_1 = I_2 + I_\Delta$ , where  $I_\Delta$  denotes the optical path length of the idler beam between the two sources NL1 and NL2. Thus, the condition for interference (Eq. 2.26) reads

$$|S_1 - (S_2 + I_\Delta)| < \Delta l_{SPDC}. \quad (2.29)$$

The condition for the pump beam path differences remains the same, Eq. 2.27. It can be expressed in terms of the idler path length as

$$|(P_1 + I_\Delta) - P_2| < \Delta l_{Laser}. \quad (2.30)$$

#### 2.4.4.3 Frustrated Two-Photon Creation

If both signal and idler beams are aligned (Fig. 2.10c), we can further simplify Eq. 2.29. In analogy to the previous section, we denote the relative path lengths between the two sources of signal and idler beams respectively as  $S_\Delta = S_1 - S_2$ , and  $I_\Delta = I_1 - I_2$ .

The path length difference of the two pump beams is written as  $P_\Delta = P_2 - P_1$ . Note the different sign convention here, which is motivated by the fact that the path length of  $P_2$  is longer than  $P_1$ , whereas the down-converted beams from NL1 travel a longer path than that of NL2 (see Fig. 2.10).

In this case, Eq. 2.26 results in the simple condition

$$|S_\Delta - I_\Delta| < \Delta l_{SPDC}. \quad (2.31)$$

The second condition involving the pump laser can be written as,

$$|S_\Delta - P_\Delta| < \Delta l_{Laser}, \quad (2.32)$$

or

$$|I_{\Delta} - P_{\Delta}| < \Delta l_{\text{Laser}}, \quad (2.33)$$

Note that these conditions do not require the distance between the two SPDC processes to be smaller than the pump coherence length. A large<sup>17</sup> distance between the two crystals is possible, as long as it affects both the path length of the pump beam as well as the down-converted beams. This has been demonstrated using a pump laser with a shorter coherence length than the optical path of the pump beam between the two crystal passes [87]. A systematic theoretical account of these effects is provided in [88] for the case of the experimental arrangement of Fig. 2.10c, see also [15, 84].

---

<sup>17</sup>It would be interesting to explore whether any fundamental limits for this distance exist.

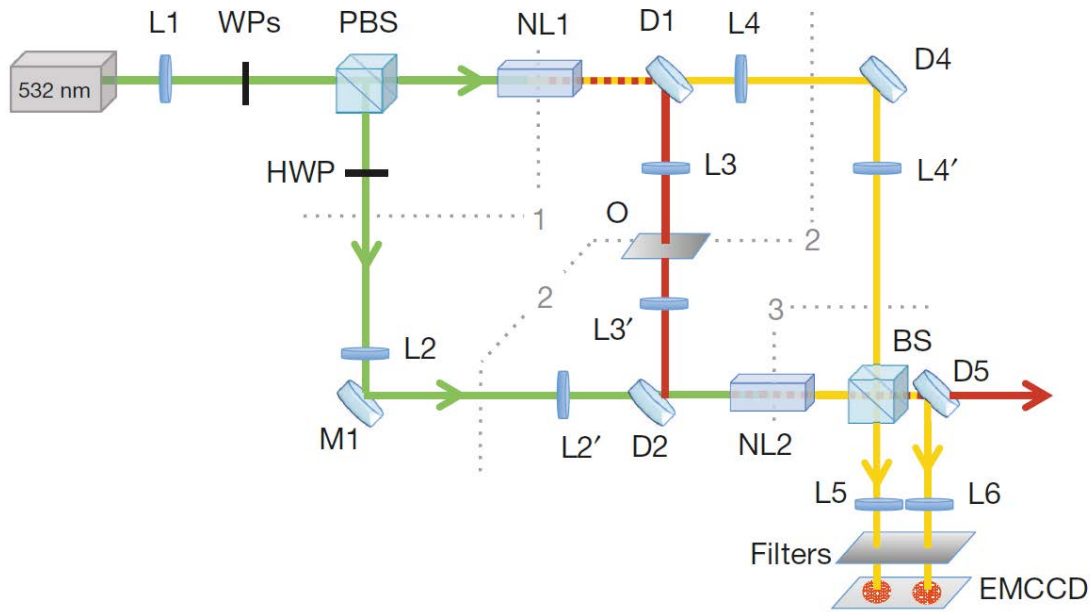


**Figure 2.11:** Experimental setup of quantum imaging with undetected photons. Two nonlinear crystals NL1 and NL2 are illuminated coherently by a laser (green) and emit photon pairs. The two signal beams (yellow) are superposed on a beam splitter (BS) and subsequently detected. The idler beams (red) remain undetected but are aligned to be indistinguishable. Plane wave components at the two crystals are mapped to points on the object O and to points on an EMCCD camera using lens systems L3/L3', L4/L4', and L5/L6. Interference can be observed in each spatial mode of the signal beam due to induced coherence, as long as the corresponding mode in the idler beam is not obstructed between the crystals. Therefore, information about the transmission at each point on the object is obtained in the interference visibility on the camera. It is possible to recover an image of the object without detecting photons scattered by it. Moreover, the scheme allows to detect light with a different wavelength than that illuminating the object. In the experiment [16], the wavelengths of signal and idler photons differed almost by a factor of 2. The signal beam is at 810 nm, a wavelength at which an EMCCD camera is very sensitive, while the object is probed at a wavelength of 1550 nm, where direct single photon detection is challenging with current technologies. Picture taken from [16].

## 2.5 Quantum Imaging with Undetected Photons

Despite the initial demonstration of induced coherence without induced emission (Sec. 2.4.2) was performed more than 25 years ago, only recently several applications of this effect have been identified (e.g. [16, 89–96]). A particularly fruitful idea was to use the effect for imaging with undetected photons [16]. This scheme allows to obtain images of an object without detecting light that interacted with it. As such, the object can be probed at a different wavelength than the detected light. Exploiting correlations between signal and idler photons in a multimode scenario, this experiment has been the starting point for my research activities presented in this thesis and it has also inspired several experiments in other research groups. Due to its relevance particularly for the experiments presented in Chapter 3, the main points of quantum imaging with undetected photons experiment are explained in some detail below. This section also serves to introduce the notation used in the later chapters.

### 2.5.1 Principle

The idea is based on the experiment by ZWM [13] (Sec. 2.4.2) in a spatially multimode scenario. The experimental setup is depicted in Fig. 2.11 [16]. Two SPDC photon pair sources (2 mm

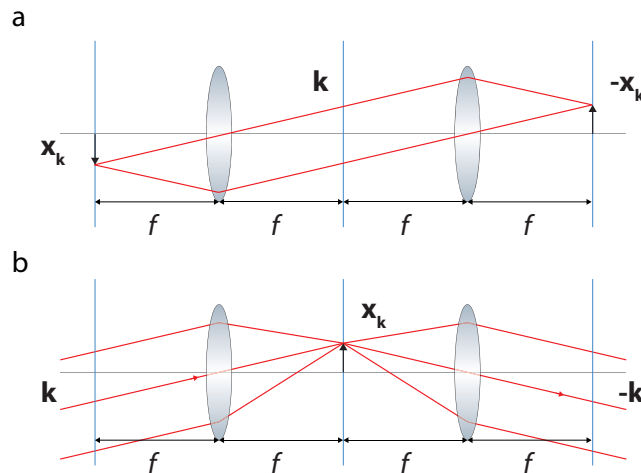


**Figure 2.12:**  $4f$  lens system. An idealized positive lens maps a plane wave to a point at focal distance. A combination of two lenses can, therefore, be used to map a point to a plane wave and back to a point, i.e. for point-to-point imaging (a). The same lens system maps a plane wave to another plane wave (b).

long ppKTP crystals NL1 and NL2) are illuminated by coherent laser beams. The two signal beams (yellow in Fig. 2.11) are superposed on a beam splitter and subsequently detected on a camera. The idler beam from the first source is aligned to be indistinguishable from the idler beam emerging from the second source (red in figure). Upon overlapping two idler beams from different sources, interference between the two signal beams is observed. An object  $O$  to be imaged is placed in the idler beam between the two nonlinear crystals. Each point on the object affects transmission and phase shift of a distinct spatial mode of the idler beam between the crystals. This affects visibility and fringe-shift of the observed interference at the corresponding mode of the signal beam. Therefore, an image can be recovered in the interference pattern on the camera (EMCCD). The idler beam that interacts with the object does not need to be detected. The scheme enables imaging of the transmission as well as the phase shift of an object, while the wavelength of the detected photons can differ from the wavelength of the photons impinging on the object.

From a fundamental perspective, the physical interpretation of this experiment is fascinating. Instead of detecting light scattered from the object, the information about the object can be retrieved because the object selectively introduces the possibility to obtain path information about the signal photons. At spatial modes that pass through a transparent point on the object, the source of a photon pair is indistinguishable and interference in the corresponding mode of the superposed signal beam is observed. At points where the object obstructs idler photons, the corresponding spatial modes of the signal beams cannot interfere, as it is in principle possible to acquire path information by a hypothetical measurement on the idler photon.

## 2.5.2 Lens Systems and Spatial Modes

The mapping between points on the camera to points on the object is performed using a number of  $4f$ -lens systems [58] (Figs. 2.11 and 2.12).

A  $4f$  imaging system consisting of  $L2$  and  $L2'$  in the pump beam ensures that the pump beam is focused equally into the two nonlinear crystals (by  $L1$ ). In this way, photon pairs are emitted by both sources with identical momentum correlation (cf. Sec. 2.3.1).

The idler beam is imaged between NL1 and NL2 with the help of a second  $4f$  system ( $L3$  and  $L3'$ ). This ensures indistinguishable idler beams from the two sources. The object is placed at focal distance between the two lenses. Thus, a plane wave component of the idler beam emerging

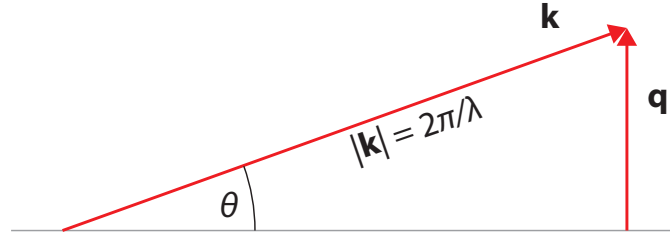


**Figure 2.13:** Illustration of the transverse component  $\mathbf{q}$  of a plane wave mode with wave vector  $\mathbf{k}$ . Under the condition of narrow frequency filtering, a one-to-one correspondence between the  $\mathbf{k}$ -vectors and their transverse components can be assumed in the experiment.

from NL1 is mapped to a point on the object and thus experiences an attenuation as well as a phase shift that corresponds to the optical properties at a particular point on the object.

The two signal beams are detected after a beam splitter BS and a lens L5, which maps one plane wave component from either of the two signal beams to a distinct point on the camera. Therefore, the detection probability at a particular point on the camera depends on the ability of the signal beams to interfere at this point, i.e. in the corresponding plane wave mode.

Under the assumption of perfect momentum correlation between signal and idler photons<sup>18</sup>, a signal photon detected in a selected plane wave mode (i.e. on a selected point on the camera) is accompanied by an idler photon in a plane wave mode of the idler beam that can be inferred with certainty. This plane wave mode is mapped to a point on the object. Therefore, a point to point correlation exists between the transmission of the object and the interference visibility on the camera.

The transmission of the object is therefore retrieved by a measurement of the signal photon visibility at each point on the camera. The idler beam does not need to be detected. This is an advantage over other quantum imaging schemes (e.g. ghost imaging), because it is possible to perform this method even if no suitable detector for the wavelength of the idler photons is available. A phase shift acquired by the idler beam upon its passage through the object manifests itself in a phase shift of the recorded interference fringe on the camera. A measurement of the relative phase shifts of the interference recorded at different points on the camera allows to reconstruct point by point the phase shift imposed by the object. This fact is interesting in itself as the same object would produce different phase shifts if placed in the signal or the idler beams due to their wavelength difference.

### 2.5.3 Quantitative Description

In the following, a brief quantitative description of the phenomenon is presented, which is based on the treatment in [16, 97].

Each of the two individual photon pair sources produce photons in the state

$$|\psi_{NL_j}\rangle = \int d\mathbf{q}_S d\mathbf{q}_I C(\mathbf{q}_S, \mathbf{q}_I) |\mathbf{q}_S\rangle_{S_j} \otimes |\mathbf{q}_I\rangle_{I_j}, \quad (2.34)$$

where  $\mathbf{q}_S$  and  $\mathbf{q}_I$  stand for the transverse components of a wave vector (spatial mode) in the signal and idler beams (Fig. 2.13). The signal and idler beams of the  $j$ th crystal are labeled  $S_j$  and  $I_j$ , respectively. The correlation between signal and idler photons is encoded in the coefficients  $C(\mathbf{q}_S, \mathbf{q}_I)$ .

As an individual photon pair is produced in a superposition of the two sources, its quantum state can be written as

$$|\Psi\rangle = |\psi_{NL_1}\rangle + e^{i\varphi_0} |\psi_{NL_2}\rangle, \quad (2.35)$$

<sup>18</sup>The momentum correlation is maximized in the experiment by employing a large ( $w_P \approx 300 \mu\text{m}$ ) pump spot at the crystals.

with a phase factor  $\varphi_0$  between the two emissions. When an object of transmission  $T$  is located between the two sources, the alignment of the two idler beams results in

$$|\Psi\rangle = \int d\mathbf{q}_S d\mathbf{q}_I \left[ C(\mathbf{q}_S, \mathbf{q}_I) \left( T(\mathbf{q}_I) e^{i\varphi_I(\mathbf{q}_I)} |\mathbf{q}_S\rangle_{S1} + e^{i\varphi_0} |\mathbf{q}_S\rangle_{S2} \right) |\mathbf{q}_I\rangle_I + \sqrt{1 - T(\mathbf{q}_I)^2} |\mathbf{q}_S\rangle_{S1} |\mathbf{q}_I\rangle_w \right], \quad (2.36)$$

where  $|\mathbf{q}_I\rangle_w$  represents the state of an idler photon that is either absorbed or reflected by the object and the common idler beam is denoted by  $I$ . Equation 2.36 is obtained by applying the approach of Sec. 2.4.2 [13, 14] on each spatial mode.

We can simplify Eq. 2.36, by assuming perfect momentum correlation and zero transverse momentum of the pump wave vector,  $\mathbf{q}_P = 0$ , that is  $C(\mathbf{q}_S, \mathbf{q}_I) \propto \delta(\mathbf{q}_S + \mathbf{q}_I)$ . In this case,

$$|\Psi\rangle = \int d\mathbf{q}_S C(\mathbf{q}_S, -\mathbf{q}_S) \left( T(-\mathbf{q}_S) e^{i\varphi_I(-\mathbf{q}_S)} |\mathbf{q}_S\rangle_{S1} + e^{i\varphi_0} |\mathbf{q}_S\rangle_{S2} \right) |\mathbf{q}_I\rangle_I + \sqrt{1 - T(-\mathbf{q}_S)^2} |\mathbf{q}_S\rangle_{S1} |\mathbf{q}_I\rangle_w. \quad (2.37)$$

The signal beams are superposed on a beam splitter in a way that a transverse wave vector of the first signal beam interferes with the same transverse wave vector of the second signal beam (we project onto  $\frac{1}{\sqrt{2}}(|\mathbf{q}_S\rangle_{S1} + i|\mathbf{q}_S\rangle_{S2})$ ). The photon detection rate at one point on the camera is proportional to the average photon number in one mode  $\mathbf{q}_S$  after the beam splitter<sup>19</sup>,

$$R(\mathbf{q}_S) \propto 1 + T(-\mathbf{q}_S) \cos(\varphi_I(-\mathbf{q}_S) - \varphi_0). \quad (2.38)$$

Equation 2.38 describes an interference fringe with visibility  $T(-\mathbf{q}_S)$  and phase  $\varphi_I(-\mathbf{q}_S) - \varphi_0$ . Thus, the spatially dependent transmission of an object  $T(\mathbf{x}_O)$  is recovered in the visibility, whereas a phase shift introduced by the object manifests itself in position dependent phase shifts in the camera image. This can be made explicit by considering the mapping between spatial modes and points on the object and camera planes.

The quantum state of a photon pair is decomposed into plane wave components at the plane of the crystal (cf. Eq. 2.34). The lens systems in the signal beam<sup>20</sup> map one  $\mathbf{q}_S$  to the point  $\mathbf{x}_C$  on the camera (Fig. 2.14),

$$\mathbf{x}_C = \frac{f_C \lambda_S}{2\pi} \mathbf{q}_S. \quad (2.39)$$

Conversely, in the idler beam, one spatial mode  $\mathbf{q}_I$  is mapped to the point

$$\mathbf{x}_O = \frac{f_I \lambda_I}{2\pi} \mathbf{q}_I \quad (2.40)$$

on the object (Fig. 2.15). These relations are consequences of the geometrical configuration of the lenses.

The momentum correlation of the photon pairs implies that for an individual photon pair,

$$\mathbf{q}_S + \mathbf{q}_I \approx 0. \quad (2.41)$$

This allows to write Eq. 2.38 in terms of transverse position on the camera  $\mathbf{x}_C$  and on the object  $\mathbf{x}_O$ ,

$$R(\mathbf{x}_C) \propto 1 + T(\mathbf{x}_O) \cos(\varphi_I(\mathbf{x}_O) - \varphi_0). \quad (2.42)$$

It follows from Eqs. 2.40 and 2.39 that the magnification depends on both wavelengths and is given by (cf. [16, 97]),

$$M = \frac{f_C \lambda_S}{f_I \lambda_I}. \quad (2.43)$$

<sup>19</sup>Eq. 2.38 can be obtained in an analogous way as Eq. 2.22 or using the interaction picture [97].

<sup>20</sup>In Fig. 2.11, the signal beam from NL1 passes the lenses L4, L4', and L5/L6, whereas the signal beam from NL2 passes only through L5/L6 between crystal and camera.

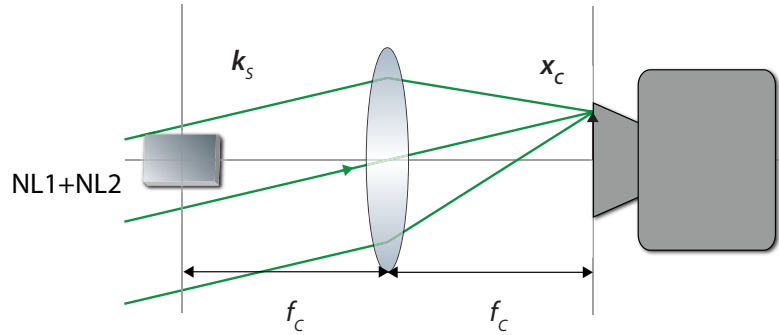


**Figure 2.14:** Mapping of a plane wave of the signal beam onto a point on the camera as used in quantum imaging with undetected photons. The lens after the beam splitter (Fig. 2.11) ensures that one  $\mathbf{k}$ -vector from either of the two crystals is mapped to one point on the camera. In the paraxial limit, the  $\mathbf{k}$ -vector  $\mathbf{k}_S$  arrives at the point on the camera  $\mathbf{x}_C/f_C = \mathbf{q}_S/|\mathbf{k}_S|$ . Therefore,  $\mathbf{x}_C = \mathbf{q}_S(f_C\lambda_S)/(2\pi)$ . The detection allows to infer a signal photon's momentum, however it does not allow to infer, which crystal it was emitted from.

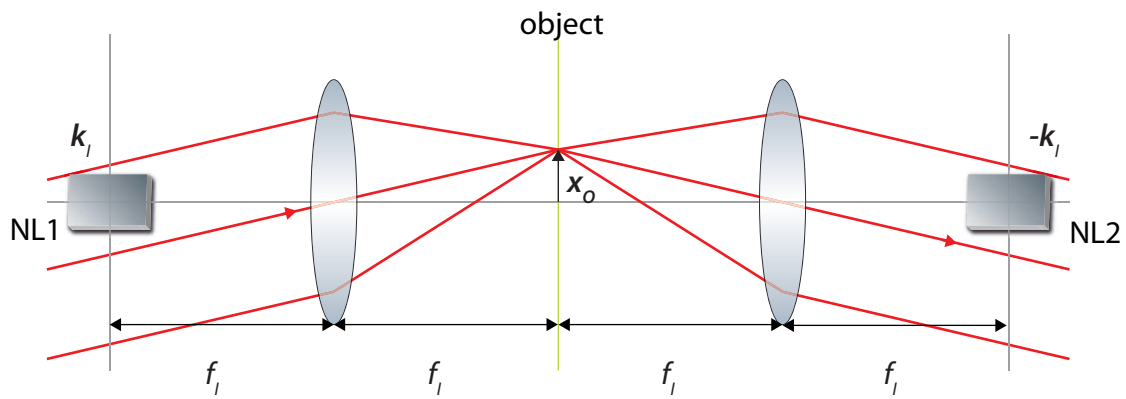


**Figure 2.15:** Mapping of a plane wave component of the idler beam onto a point on the object in quantum imaging with undetected photons. In the idler beam, the object is placed in the center of the  $4f$  system in a way that one  $\mathbf{k}$ -vector from NL1 is mapped to one point on the object and subsequently to a  $\mathbf{k}$ -vector at NL2. In conjunction with perfect correlation between the signal and idler  $\mathbf{k}$ -vectors, this system creates a correspondence between points on the object with points on the camera.

## 2.6 Other Applications of Induced Coherence

Interference effects due to the alignment of photon paths have been investigated for some time in connection with frequency correlations of down-converted photons [98–101]). These efforts led to the demonstration of infrared spectroscopy by detecting visible light in 2016 [89]. This experiment used a scheme similar to the one described in Sec. 2.4.3, in which both signal and idler beams were aligned. The idler photon carried a wavelength in the mid infrared (IR), whereas the signal photon was in the visible range. An object (in this case CO<sub>2</sub> gas) between the two SPDC processes absorbs idler photons at characteristic frequencies in the IR range, which results in a changed visibility of the corresponding spectral components of the detected signal photons. The same scheme has been used to determine the refractive indices of materials at different wavelengths than the detected photons by analyzing the corresponding phase shift. [93]. Furthermore, it has been shown that it is possible to determine polarization rotations of undetected photons in a birefringent sample [94].

Other applications worth mentioning are the exploitation of the coherence length requirements by performing a quantum version of optical coherence tomography [95, 96]. Using multiple possibilities for the idler photon to be reflected between the two possible SPDC processes, it is possible to associate an idler path length with a given depth of the object, at which the reflection happened. By scanning the optical path length of the signal photons, different “depth sections” on the object can be probed.

It has been shown that the alignment of paths from different sources can be used as a tool to generate a large class of high-dimensionally entangled states [102]. It is possible to make the idler beams indistinguishable by overlapping them not in space but in time [103], or in frequency [104]. Further applications can be found in a recent review [90].

## 2.7 The Role of Stimulated Emission

### 2.7.1 Stimulated Emission as an Interference Effect

In probabilistic photon emission processes such as spontaneous parametric down-conversion, photon pairs are emitted with a certain probability into modes that are initially in the vacuum state. It can be shown that if initially,  $n$  photons are already present in one of the modes into which down-converted photons are emitted, the probability of photon pair emission is enhanced.

Mathematically, this follows from the identity

$$\hat{a}^\dagger|0\rangle = |1\rangle, \hat{a}^\dagger|n\rangle = \sqrt{n+1}|n+1\rangle. \quad (2.44)$$

Consequently, the probability of creating a photon in a mode that is already occupied by  $n$  photons is enhanced by a factor of  $n+1$ , compared to the vacuum case. That is, the emission of photons is stimulated by the presence of indistinguishable photons in the same mode. This effect can be interpreted as a result of the coherent addition of probability amplitudes for indistinguishable events. The  $n+1$  photons in the mode can be arranged in different indistinguishable ways with the corresponding probability amplitudes interfering constructively [3].

The condition for stimulated emission to occur in parametric down-conversion is that the stimulating photon(s)<sup>21</sup> are indistinguishable in principle from the down-converted photons. Remarkably, this condition is very similar to the condition to observe interference in the ZWM experiment (see Sec 2.4.4).

<sup>21</sup>The  $n$  photons already present in the mode before the emission.

### 2.7.2 Significance in Laser Pumped Induced Coherence

The question arises, whether stimulated emission occurs in experiments in which coherence is induced by aligning photon paths. In particular, whether the idler beam from the first source in the ZWM-experiment (Sec. 2.4.2) is stimulating the emission of photon pairs at the second crystal. It has been shown that stimulated photons are coherent to the stimulating light [105,106]. Therefore, the occurrence of stimulated emission could in principle explain (at least partially) the observed interference between the two signal beams.

Although the above description is quantum mechanical, the phenomenon of stimulated emission can alternatively be explained in the framework of classical nonlinear optics [50]. This fact led to a long-standing discussion [107–110] about whether or not quantum mechanics is needed to describe experiments on induced coherence.

Stimulated emission can only occur in situations in which at least two photon pairs are present in the setup at the same time (cf. Eq. 2.44). This requires at least two pump photons to “be present” in the setup at the same time. In the original experiment [13,14], the pump was a weak laser beam that can be modeled as a coherent state

$$|\alpha\rangle \propto \sum_{n=0}^{\infty} \frac{\alpha^n}{\sqrt{n!}} |n\rangle, \quad (2.45)$$

with the mean photon number per mode  $|\alpha|^2$ . As long as the mean photon number is much smaller than 1, the one-photon term ( $n=1$ ) term dominates over terms involving larger photon numbers. Consequently, the probability of simultaneous photon pair creation in the two crystals is negligibly small.

The ZWM experiment was performed in this regime, which inspired the name “induced coherence *without induced emission*” [14]. However, the effect of stimulated emission is present, due to the non-zero probability of emitting two or more photons in the same mode. This applies to all performed experiments on induced coherence to date for which laser pumps were used. Although generally negligible, it would be interesting to perform an experiment with induced coherence in which the possibility of stimulated emission is definitely ruled out. We analyzed this scenario in a recent paper [111].

In the case of induced coherence *without* induced emission (i.e. only one photon pair is present in the setup at a time), the interferometric visibility is linearly proportional to the transmission of the idler beam between the two crystals (cf. Eq. 2.22). Physically, this accounts for the rate of photon pairs emitted by NL2 being constant and independent of the transmission  $T$ .

On the other hand, in the regime of stimulated emission (many photon pairs present in the setup at any given time), the transmission of the idler beam affects the number of idler photons already present in the mode into which NL2 emits. Thus, the rate of stimulated photon pairs is dependent on  $T$ . As a result, the visibility as a function of the transmission deviates from the linear dependence of  $V = T$  (cf. Eq. 2.22), but is instead given by  $V = T\sqrt{(1+n)/(1+T^2n)}$  [108], where  $n$  denotes the mean photon number and equal pump power and gain in the two crystals have been assumed. This fact in principle leads to the possibility to determine whether spontaneous or stimulated emission dominates in a particular experiment by measuring  $V(T)$  [107,108] (Fig. 2.16).

The linear dependence of the visibility on the amplitude transmission of the idler beam (already reported in [13]) can be regarded as “signature of quantumness” in the sense that a semi-classical description (in which stimulated emission is a non-negligible effect leading to coherence between the signal beams) predicts a different dependence.

Soon after the demonstration of frustrated two-photon creation via interference [15], a classical explanation for this effect was proposed [112]. However, it was later pointed out that this model cannot reproduce the visibility ( $> 50\%$ ) that was observed by Herzog et al., but would lead to a visibility of only 3% for the experimental parameters used in the original experiment [113,114].

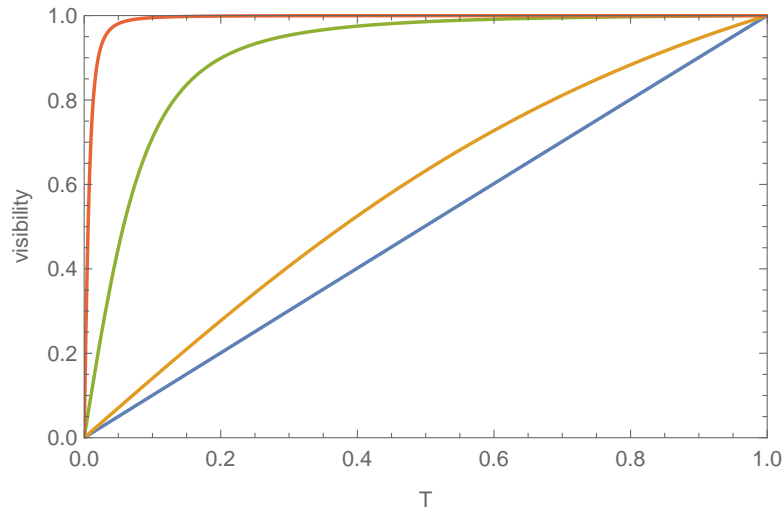


**Figure 2.16:** Dependence of the visibility on the amplitude transmission of the idler beam between the two crystals in a ZWM experiment. The colors represent mean photon numbers per spatio-temporal mode, 10000 (red), 100 (green), 1 (yellow), 0.01 (blue). The higher the mean photon number, the higher the probability of stimulated emission and the greater the deviation of  $V(T)$  from the linear dependence. The linear dependence only occurs in the “quantum” regime in which stimulated emission is negligible. This plot was generated using the results of [108], under the assumption that both NL1 and NL2 emit at equal rates.

It should be noted that ZWM interference in the “classical” regime, in which stimulated emission is the dominant effect, is useful for several applications. The possibility for imaging with stimulated emission was demonstrated experimentally [110]. Moreover, it was shown that a better signal-to-noise ratio for imaging could be achieved in the high-gain regime [109], in particular, if the gain balance of the two sources is optimized [115, 116].

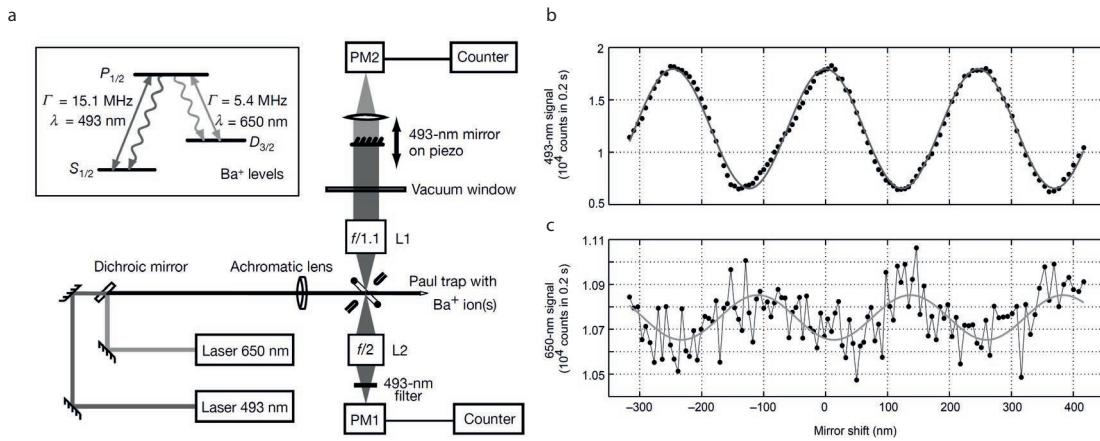


**Figure 2.17:** Eschner's experiment. In the setup (a), an ion in a trap emits spontaneously in all directions at 493 nm. The emitted light is reflected back through the ion by a piezo controlled mirror. The intensity of the light detected at the opposite side shows a sinusoidal modulation as the position of the mirror is varied (b). At the same time, the population of the excited state is probed using a separate laser, which shows an anticorrelated modulation (c). This experiment shows that not only the amount of emitted light is modulated by the mirror position but also the lifetime of the excited state. As the ion is involved in the interference process, the phenomenon is more than merely destructive interference between the reflected and the directly emitted light. Pictures taken from [127].

## 2.8 Atoms and Mirrors

### 2.8.1 Spontaneous Emission in the Vicinity of Mirrors

The experimental scheme to observe frustrated down-conversion [15], Sec. 2.4.3, is related to a phenomenon in cavity quantum electrodynamics: if an excited atom is located in the vicinity of a reflecting surface, its rate of spontaneous emission is modified depending on the exact distance between atom and mirror.

The phenomenon was first noted for radio waves by Purcell as early as 1946 [117]. In the 1970s, experimental demonstrations were performed with molecules on a dielectric substrate (e.g. [118]). Since then, the effect has been shown in a variety of different systems, such as atoms in cavities [119–123], solid-state materials [124, 125] and in superconducting qubits [126].

As an example of how this effect is observed, we consider a particularly interesting experiment [127, 128] that was performed in 2001 (Fig. 2.17). An ion located in a trap was excited with a laser beam. A mirror was placed in the vicinity of the ion and the rate of spontaneous emission into the opposite direction of the mirror was observed. The results showed a modulation of the detection rate, depending on the distance between ion and mirror. At the same time, the excitation of the ion was probed, showing a modulation with the opposite phase. That is, during suppressed emission, the ion is more likely to remain in the excited state than during enhanced emission, and vice-versa. This shows that the phenomenon cannot be viewed as interference of the emitted light alone, but the entire process of emission and de-excitation of the ion takes part in the interference.

### 2.8.2 Discussion about Physical Origin and Time-Dependence

Following its discovery, the effect sparked a discussion about its physical origin [129–131]. If the emission probability of an atom is reduced by not being in vacuum, how does the atom “know” about the presence of the mirror in the first place? In particular, the question was raised, whether the atom’s “own source field” changes the emission probability after being reflected back to the

atom, or whether the rate is changed due to a modified vacuum mode structure imposed by the mirror [129]. This led to the related question about how the atom behaves in an environment that changes in time [132], i.e. when the mirror is inserted or removed.

Several theoretical studies suggested that an atom adapts to the boundary conditions after some delay time corresponding to the distance to the mirror(s) [133–135]. Nevertheless, in a situation in which the mirror is positioned such that spontaneous emission is suppressed, a sudden replacement of the mirror by a detector is predicted to lead to the immediate detection of photons [134, 136]. This causes problems with the assertion that the atom remains in its excited state during suppressed emission, as the energy of the immediately detected photon corresponds to a decay of the atom, which at first sight is at odds with causality.

In [136, 137], the following interpretation was given as an attempt to resolve this problem: the atom starts radiating towards the mirror as if it were in vacuum until the time a photon would take to travel towards the mirror and back to the atom. After this time delay, the probability of the atom being in the excited state remains constant. It is, however, smaller than unity. Formally, the eigenstates of the atom in vacuum are not equal to the eigenstates of an atom-mirror coupled system. If placed close to a mirror, the atom is not in the same excited state as it was in vacuum. Instead, the atom-mirror system is in an “excited” state, which corresponds to a distribution of the energy in the atom and the space between atom and mirror.

The physical intuition about why spontaneous emission rates are modified by mirrors is not completely clear up to this date. This is indicated by the wide range of interpretations present in the literature, a few of which are stated below. One viewpoint is that the modulated emission rate is an interference fringe resulting from the coherent addition of the probability amplitudes for the different emission directions. As the mirror reflects light emitted into one direction, it becomes indistinguishable from the direct emission in the opposite direction. The situation can be described in analogy to a single photon interference experiment (e.g. [138]).

Another possible interpretation can be given as the presence of mirrors alters the density of vacuum modes available for emission [119, 122, 126, 127] and as a result, the transition rate given by Fermi’s golden rule is modified.

### 2.8.3 Can an Optical Experiment Clarify the Interpretation?

Spontaneous emission by an excited atom is a probabilistic process as is spontaneous parametric down-conversion. The suppression or enhancement of SPDC in the experiment on frustrated down-conversion [15] exhibits striking analogies to the suppression or enhancement of spontaneous emission of an atom in front of a mirror. In both cases, a mirror is placed in the vicinity of the emitter, which reflects the emitted light back towards its origin. The spontaneous emission rate towards the opposite direction is modulated by the exact positioning of the mirror(s) (Fig. 2.18).

Nevertheless, several limits to this analogy need to be noted. In contrast to a nonlinear crystal, the spatial extent of an atom is much smaller than the wavelength of the emitted light. Therefore, the atom can be “placed” in a node or in an anti-node of a standing wave pattern. A nonlinear crystal, however, extends over a much larger distance than the wavelength, even larger than the coherence length of the emitted light. Another important difference between the two scenarios is given by the coherence length requirements for the distances between emitter and mirror. Suppressed spontaneous emission from an atom can only be observed if the atom is located at a distance to the mirror that lies within the coherence length. On the other hand, down-conversion from nonlinear crystals can be observed for a much larger distance between crystal and mirrors that can even exceed the pump coherence length [15, 87]. The coherence requirements in the optical experiment are more complex and involve the coherence lengths of the pump laser as well as that of the SPDC photons (see Sec. 2.4.4).

In light of the analogy between the two phenomena, a modification to the optical experiment

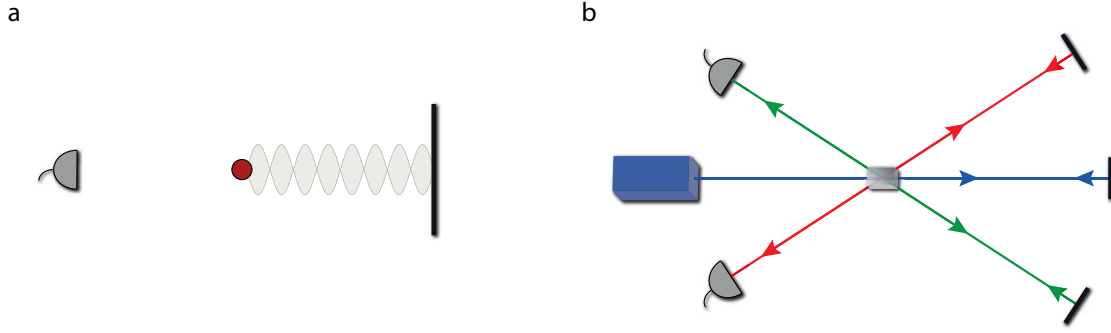


**Figure 2.18:** Analogies and differences between inhibited spontaneous emission by an excited atom (a) and frustrated down-conversion (b). The schemes of the two experiments are similar, as well as the corresponding observations. In both cases, varying the mirror position alters the emission rate in the opposite direction, which can be observed using intensity measurements. In the spontaneous emission case (a), the effect can be observed only if the distance between atom and mirror is smaller than the coherence length of the emitted light. In contrast, the coherence length requirements in the optical experiment are more complex (see Sec. 2.4.4) and allow the distance between crystal and mirror to be larger than the coherence length. The difference can be understood considering the analogy between the excitation of the atom and the occupation of the traveling pump mode, which is further discussed in Chapter 5.

to observe frustrated down-conversion was proposed [114, 139], with the aim of clarifying the interpretation of its physical origin. A better understanding of the optical experiment could lead to insights about the atomic case as well and therefore contribute to the resolution of this long-standing discussion.

In the experimental scheme of frustrated two-photon emission by interference [15], the following situation was analyzed. In the case of complete suppression of down-conversion by the presence of mirrors, what would happen if one of the mirrors was suddenly replaced by a detector? In the proposed experiment, one measures the arrival times of photons at this detector. After changing the experimental arrangement (i.e. inserting the detector), it takes a finite amount of time until the changed environment can affect the crystal. Under the assumption that the crystal itself entirely stops to emit photons during the suppression of down-conversion, photon pairs would only be emitted at a time  $\tau_s = l/c$  after the detector was inserted, where  $l$  stands for the distance between crystal and mirror and  $c$  represents the speed of light. Consequently, a total delay of  $\tau = 2l/c$  is expected for the then emitted photons to arrive at the inserted detector [136, 139]. If instead, the detector registers photons immediately, it would rule out explanations of this phenomenon according to which the nonlinear crystal does not emit photons at all during the suppression of down-conversion. Despite the issue has been addressed experimentally before [140], the question of whether or not such a delay exists has not been conclusively answered to this date.

A related phenomenon was addressed in an optical experiment, showing that the rate of second-harmonic generation can be modified similarly in the presence of mirrors [141]. It was later demonstrated that during the suppression of second-harmonic generation in the opposite direction of the mirror, photons can be detected in the reflection from a semi-transparent glass slide placed between mirror and non-linear material [142].

In Chapter 5, an experiment is presented that realizes the above proposal and establishes an upper bound for a hypothetical delay in a frustrated down-conversion experiment.



# 3

## Interference Fringes in Induced Coherence Without Induced Emission

The content of this chapter is based on the publications “Interference fringes controlled by noninterfering photons” [143] and “Quantifying the momentum correlation between two light beams by detecting one” [91].

### 3.1 Motivation

In the experimental demonstration of induced coherence without induced emission, the alignment of the idler beams causes the two signal beams to be mutually coherent (Fig. 3.1a). Ideally, the resulting interference can attain 100% visibility [14]. On the other hand, no interference is observed if the two idler beams are completely misaligned. In this case, full path information about the signal photons can in principle be obtained by measurements on idler photons (Fig. 3.1b).

Naturally, the question arises, how the system behaves in the intermediate case of slightly misaligned idler beams. In this case, a partial reduction of visibility has been predicted and qualitatively observed [80]. However, the misalignment of the idler beam can be implemented by displacing a lens, which ultimately functions by introducing a spatially dependent phase and thus can be viewed as a phase object. It has been shown that in a spatially multimode scenario, imaging with undetected photons is possible for phase objects without a significant reduction of visibility [16] (Sec. 2.5). This shows that the distinction between introducing path information and introducing a phase object is not entirely clear.

In this chapter, we explore the above mentioned intermediate situation with the aim of gaining a deeper understanding of the phenomenon of induced coherence without induced emission. As shown below, this allows us to experimentally address questions about the role of different wavelengths and of the momentum correlation between signal and idler photons.

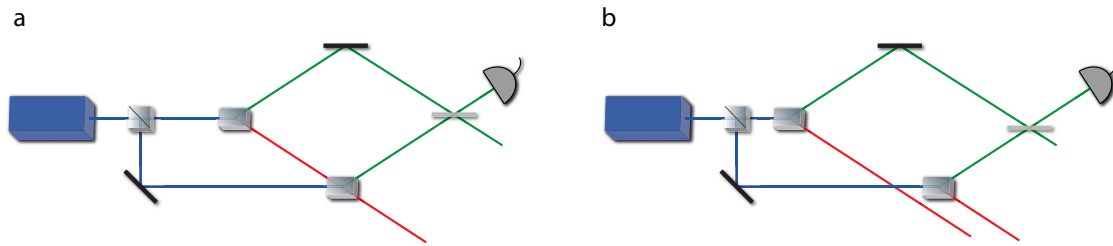


**Figure 3.1:** The effect of path alignment in coherent photon pair emission from either of two sources. The two signal beams interfere with ideally 100% visibility if the two idler beams are aligned to be indistinguishable (a). If the idler beams are misaligned, such that the origin of a particular photon can be identified, no interference is observed (b). In this chapter, we investigate the intermediate case of a slight misalignment between the two idler beams.

We demonstrate that in a spatially multimode Zou, Wang, Mandel (ZWM) interferometer (Secs. 2.4.2 and 2.5), it is possible to observe spatial interference fringes, if the idler beam between the two crystals is slightly misaligned. This interference pattern exhibits similarities to the spatial fringes observed in traditional interferometers when the interfering beams are slightly misaligned with respect to each other. However, in contrast to traditional interferometry, the phase shift leading to the interference pattern is not introduced in any of the interfering beams, but in the undetected idler beam. Thus, the fringes are created without interacting with the interfering photons. Moreover, the idler photons in our experiment are of a different wavelength than the interfering light.

### 3.1.1 Specific Questions and Experiments

In a first experiment, we study the formation and the properties of spatial interference fringes in a multimode ZWM interferometer. We compare them to analogous fringes in classical interferometry and find that the interference fringes created via induced coherence are in many aspects similar to their classical counterparts. However, we also note important differences between the two cases that arise from the fact that phase shifts are controlled in a beam that is not itself interfering.

In general, the formation of interference fringes depends on the wavelength of the interfering light. The idler photons in our experiment are of a different wavelength than the interfering signal photons. This leads to the question, which wavelength determines the interference pattern in our system. We investigate this question by producing and studying a circular interference pattern that occurs in the signal beam, if an appropriate phase shift is introduced in the idler beam.

In a second experiment, we analyze how the fringe pattern is affected by a changed momentum correlation between signal and idler photons. To this end, we implement a system to tune the momentum correlation between signal and idler photons and experimentally demonstrate how the pattern is affected by changing the correlation strength. We show that it is possible to quantify the correlation between signal and idler photons by analyzing the obtained interference fringes. This is remarkable, as the observation of the pattern relies on the detection of signal photons only.

The correlation between two photons is a property that neither of the individual photons carry themselves, but a property that is “encoded” in the photon pair as a whole. The possibility to access it by first order intensity measurements on one of photons raises fundamental questions about how information is stored in quantum systems. In our experiment, we access information about the correlation by using two sources and only one detector, instead of the traditional approach using one source and two detectors in coincidence.

The results are also relevant for applications as quantum imaging with undetected photons, as spatial correlations between signal and idler beams are a necessary condition to access spatial information about the idler beam in the signal beam. These correlations form the basis for applications of ZWM interference for imaging.

## 3.2 Experimental Setup

The experimental setup is depicted in Figs. 3.2 and 3.3. It is based on the implementation of quantum imaging with undetected photons [16].

A laser beam (Coherent Sapphire SF, 532 nm CW, pump power 150 mW) is split on a beam splitter<sup>22</sup> and illuminates two identical 2 mm long non-linear crystals NL1 and NL2. Photon pairs are emitted collinearly by the crystals at 810 nm (signal) and 1550 nm (idler) wavelength through the process of type-0 SPDC. The pair production rate is small enough to render the probability of simultaneous emission of multiple pairs negligible and essentially only one photon pair is present in the setup at a time. Thus, stimulated emission plays no practical role in our experiment (cf. Sec. 2.7). Signal and idler beams are separated from each other using dichroic mirrors (DM1 and DM2). The idler beam emerging from NL1 is directed through NL2 and aligned to be indistinguishable from the idler beam generated at NL2. After emerging from NL2, the common idler beam is discarded (via DM3) and remains undetected. Both signal beams are superposed on a beam splitter (BS) and subsequently detected by an EMCCD camera (Andor Luca R).

A number of lens systems are present in the setup. These constitute three separate  $4f$  imaging systems for the pump, signal and idler beams, respectively, as described in Sec. 2.5. The combination of  $L_{P1}$  and  $L_{P2}$  ensures equal pump spots at the two crystals by imaging the plane CPp onto NL2.  $L_{I1}$  and  $L_{I2}$  image the idler beam from the center plane of NL1 onto the center plane of NL2. A third imaging system, consisting of  $L_{S1}$  and  $L_{S2}$  images the signal beam from NL1 to the plane CPs, which is at the same distance from BS as NL2. This ensures that after the combined beam passes the final lens  $L_C$ , one point on the camera corresponds to one transverse wave vector of the signal beam at either of the two crystals. Loosely speaking, the camera sees the Fourier transform of the superposed signal beam.

The lens systems effectively cancel the spatially dependent phase shift arising from the free-space propagation of the idler beam between NL1 and NL2. The same holds for the signal beam, where the phase shifts due to unequal propagation distances to the camera from  $S1$  and from  $S2$  are compensated by the lens system in the signal beam.

If the two idler beams are overlapped and the coherence length requirements (see Sec. 2.4.4) are met, no measurement can be performed on an idler photon leaving the setup that would reveal the origin of its corresponding signal photon. As a result, interference is observed on the camera.

<sup>22</sup>The beam splitter is experimentally implemented by a combination of a polarizing beam splitter (PBS) and a half-wave plate (HWP) oriented at  $45^\circ$  in the reflected path. In this way, both outgoing beams are horizontally polarized. Their relative intensity and phase can be tuned by controlling the initial polarization of the pump laser.

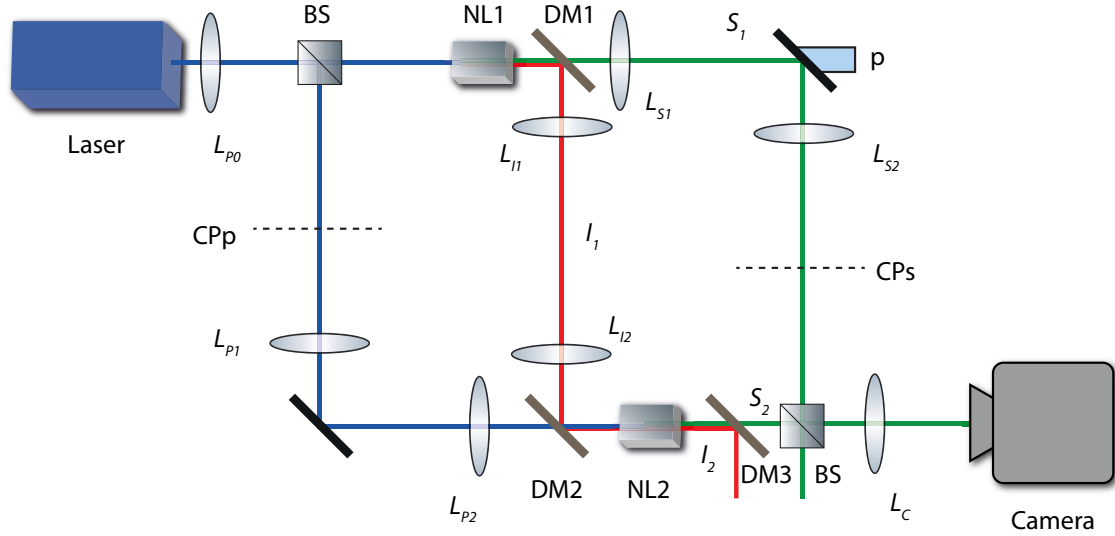


**Figure 3.2:** Experimental setup for the observation of interference fringes controlled with undetected photons. Two nonlinear crystals, NL1 and NL2 are pumped coherently in a way that one pair of photons is emitted at a time by non-degenerate collinear SPDC. The signal beams  $S_1$  and  $S_2$  (green) are superposed at a beam splitter (BS) and subsequently detected. The idler beams  $I_1$  and  $I_2$  (red) are aligned to be indistinguishable using two dichroic mirrors (DM1 and DM2). If no information about the origin of a photon pair can be obtained, even in principle, interference between the two possible paths of the signal photon is observed.

The pump beam is focused by  $L_{P0}$  into NL1. The lenses  $L_{P1}$  and  $L_{P2}$  are positioned in a  $4f$  configuration in order to image the plane CPp onto NL2. As CPp is at the same distance from BS as NL1, equal pump spots are produced in both crystals. Another  $4f$  system in the idler beam ( $L_{I1}$  and  $L_{I2}$ ) forms an image of the idler beam from NL1 at NL2 in a way that the two idler beams are indistinguishable in each spatial mode. The signal beam emerging from NL1 is imaged using lenses  $L_{S1}$  and  $L_{S2}$  onto the plane CPs, which is at the same distance from the final BS as NL2. In this way, spatially dependent phase-shifts due to the additional propagation of signal photons from NL1 compared to NL2 are effectively canceled. A final lens  $L_C$  is located at focal distance in front of the camera mapping one transverse k-vector at CPs or at NL2 to one point on the camera. A piezoelectric crystal (p) is attached to a mirror in the signal beam, which allows to scan the interferometric phase by fine-tuning the path length.

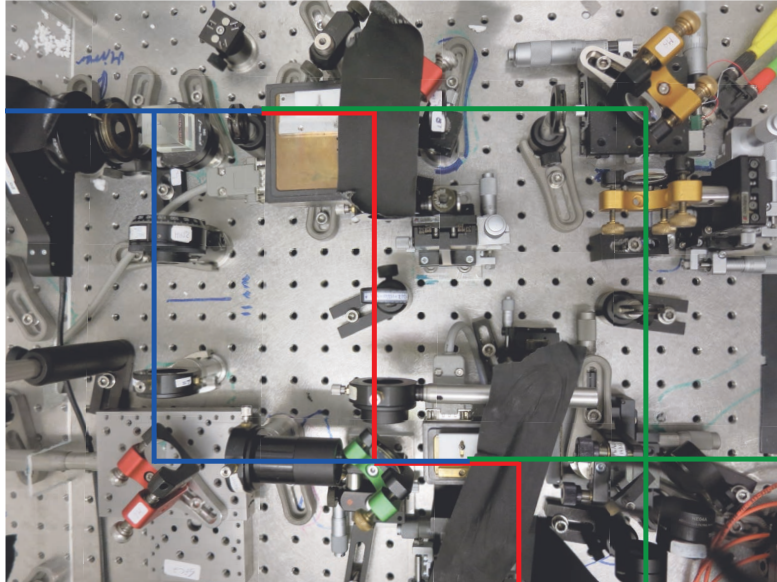


**Figure 3.3:** Photograph of the setup. The blue line traces the path of the pump beam, the red (green) lines signify the idler (signal) beams. See description in Fig. 3.2.

### 3.3 Observation of Spatial Interference Fringes

If the setup is well aligned and the two idler beams are overlapped to be indistinguishable, the signal beam observed on the camera exhibits a uniform intensity modulation upon varying a spatially independent interferometric phase. That is, all points on the camera undergo the same transition from minimum to maximum intensity, as illustrated in Fig. 3.4a. The variation of this phase is implemented by translating the mirror in the signal path by a small distance using a piezoelectric crystal (p in Fig. 3.2). The resulting variation of the path length of  $S_1$  relative to  $S_2$  introduces a phase shift in the  $S_1$  beam, which is independent of the spatial mode.

The situation changes, if we depart from perfect alignment. If a lens in the idler beam ( $L_{I1}$ ) is displaced, spatially varying interference fringes are observed. The shape of these fringes depends on how the lens is moved. A translation of the lens in transverse direction leads to a striped pattern, whereas a translation along the beam propagation axis results in a circular pattern (see Fig. 3.4b and 3.4c).

The behavior is familiar from conventional interferometers, if the misalignment would be performed in one of the two interfering beams. A tilt of one of the beams results in a linear phase shift (constant phase gradient) causing straight fringes to be observed. Circular fringes occur upon defocusing one of the beams with respect to the other or by introducing an additional propagation distance. These fringes in a classical scenario are sometimes referred to as “Haidinger fringes” (e.g. [144, Sec. 9.4.]).

Note that if the observed pattern would be detected with a single detector that integrates the intensity across the beam, the recorded signal would correspond to an interference fringe with reduced visibility. A stronger misalignment causes more fringes to be averaged over, corresponding to a lower visibility. This observation can explain the reduced visibility reported in [80].

In the following, we investigate the formation and the properties of circular fringes, which occur if a lens in the idler beam is translated along the beam propagation axis. In the experiment, signal photons carry almost twice the energy of idler photons. This fact allows to study the role of the different wavelengths in the formation of the fringes, which is done in the following section. We further find that the pattern is strongly connected to the momentum correlation between signal and idler photons, which is analyzed in Sec. 3.5. This leads to the possibility of quantifying their transverse momentum correlation without the need for detecting the idler beam.

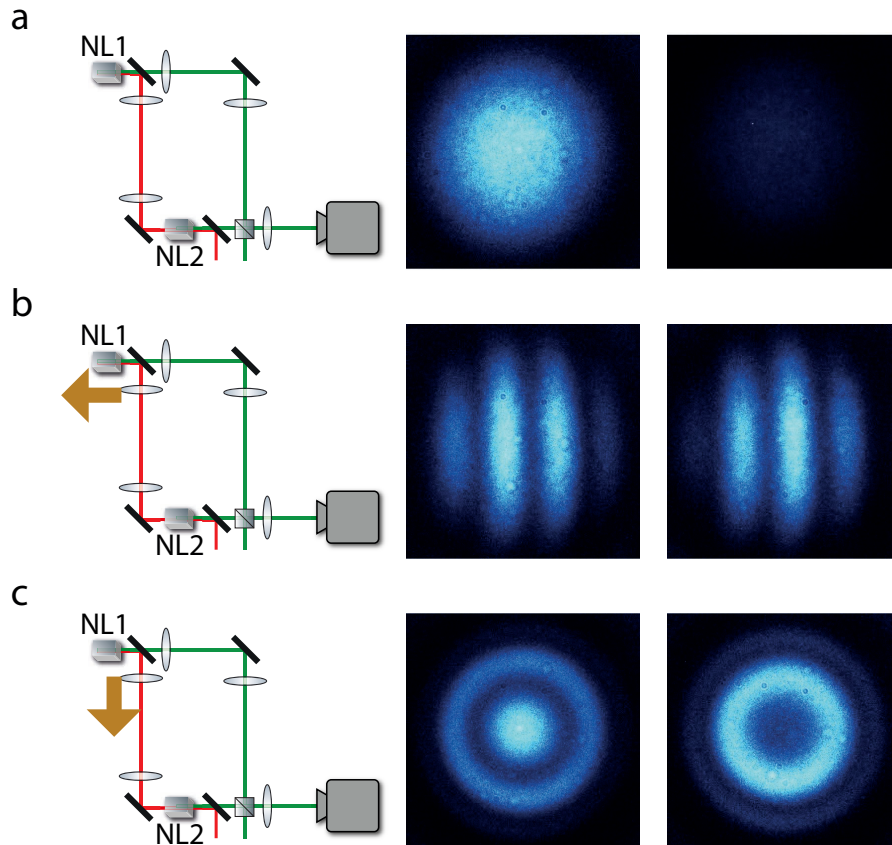


**Figure 3.4:** Effect of a lens shift in the idler beam on the interference pattern observed in the superposed signal beam. In the initial alignment (a), the beam spot on the camera varies uniformly if the interferometric phase is scanned. The images on the right side have been taken at two settings of the interferometric phase that differ by a  $\pi$  phase shift. If a lens is translated transversely to the beam axis (b), a striped fringe pattern appears, analogous to a relative tilt of two interfering beams in a traditional interferometer. If the lens is instead translated along the beam axis (c), a circular pattern is observed. This pattern corresponds to a relative propagation between two interfering beams in traditional interferometry.

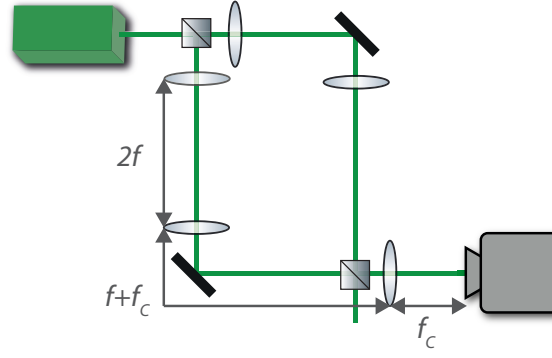


**Figure 3.5:** Analogous classical Mach-Zehnder interferometer with initially identical imaging systems in both paths. The imaging systems consist of two lenses with focal length  $f$ , initially arranged in a  $4f$  configuration. The superposed beam is detected after another lens at its focal distance  $f_c$  in front of the camera. An interference pattern forms if the imaging system in one of the paths is misaligned with respect to that in the other path. A misalignment in transverse direction with respect to the optical axis results in a striped interference pattern. On the other hand, if one of the lens systems is defocused with respect to the other, circular fringes occur. For a fixed distance of the corresponding lens shift, the spacing of the fringes depends on the wavelength of the interfering light.

## 3.4 Wavelength Dependence

### 3.4.1 Goal of the Experiment

In our experiment (Fig. 3.2), the wavelength of idler photons is different from the wavelength of signal photons. The question arises, which wavelength is responsible for the appearance of the fringe pattern that is observed in the signal beam by translating a lens in the undetected idler beam.

We focus on the circular fringes that arise if the lens is translated along the beam propagation axis. The goal of the experiment is to determine, which wavelength characterizes the appearance of the fringes. To this end, we measure the radii of minima and maxima of the pattern as we vary the location of the lens  $L_{I1}$  in Fig. 3.2. We analyze the results by comparing the spacing of the fringes to the spacing of analogous fringes in a classical interferometer and determine the corresponding wavelength.

### 3.4.2 Analogy to Classical Interferometry

In order to understand the role of the different wavelengths of signal and idler photons in the formation of fringes in multimode ZWM interference, we first analyze the wavelength dependence of analogous fringes in a classical scenario.

Consider a conventional two path interferometer, in which two beams are derived by splitting a single beam on a semi-reflecting surface (the method of “division-of-amplitude” [145, Sec. 7.5.]). The beam is recombined at a second beam splitter and subsequently detected on a camera. In each path, analogous lens systems as in our experiment are present (Fig. 3.5). The camera is located at focal distance from the final lens, such that distinct transverse plane wave modes are detected at distinct points on the camera. In the initial alignment, a spatially uniform interference pattern is observed, i.e. the entire beam interferes either constructively or destructively.

Translating a lens in one of the two beams along the propagation direction leads to a spatially dependent phase shift. This phase shift can be approximately described by the phase shift arising from an additional free space propagation about a distance  $d$  of one beam with respect to the

other (see Appendix A.1.2),

$$\varphi(\mathbf{q}) = \frac{d|\mathbf{q}|^2\lambda}{4\pi}. \quad (3.1)$$

Here,  $\lambda$  stands for the wavelength of the interfering light and  $\mathbf{q}$  represents the transverse component of a wave vector (Fig. 2.13). The parameter  $d$  is defined as  $d = (f^2 l)/(f^2 + l^2)$ , where  $l$  is the distance the lens is translated and  $f$  is the focal length of the lens. Physically, it represents the distance, which the image plane moves due to the lens shift. In the regime of our experiment, it is approximately equal to the lens shift distance  $l$ . See Appendix A.1.2. We used a small angle approximation, i.e. we assumed  $|\mathbf{q}| \ll |\mathbf{k}|$ .

After combining the two beams and detecting the superposed beam at the focal plane of a lens (focal length  $f_C$ ), each point  $\mathbf{x}_C$  on the camera detects light in the mode  $\mathbf{q} = \mathbf{x}_C \frac{2\pi}{f_C \lambda}$  (cf. Eq. 2.39). In each spatial mode, interference between the two possible paths is observed, leading to a detected intensity on the camera  $R \propto 1 + \cos(\varphi)$ , with  $\varphi$  denoting the relative phase between the two paths. Considering all spatial modes corresponding to different points on the camera, the following pattern is observed (using Eq. 3.1),

$$R(\mathbf{x}_C) \propto 1 + \cos\left(\frac{d\pi}{\lambda f_C^2} |\mathbf{x}_C|^2 + \varphi_0\right), \quad (3.2)$$

where the phase term  $\varphi_0$  incorporates all phase shifts that do not depend on the transverse coordinate  $\mathbf{x}_C$ .

Equation 3.2 describes circular fringes, which are subject to the following condition for minima and maxima (cf. [145, 146]),

$$\frac{d}{2f_C^2} |\mathbf{x}_C|_n^2 + \varphi_0' = n\lambda, \quad (3.3)$$

where integer  $n = 1, 2, 3, \dots$  correspond to maxima and half integer  $n = \frac{1}{2}, \frac{3}{2}, \frac{5}{2}, \dots$  correspond to minima. Here,  $|\mathbf{x}_C|_n$  is the transverse distance from the optical axis (beam center) to the minimum (maximum) labeled by  $n$ , i.e. the radius of the corresponding dark (bright) fringe.

It follows that the spacing of minima and maxima in the circular fringe pattern can be used to determine the wavelength  $\lambda$  of the interfering light, given the other parameters are known (in particular  $d$ ). We use the condition Eq. 3.3 to determine the wavelength governing the fringes in our experiment.

### 3.4.3 Performed Measurements

In our experiment (Fig. 3.6), the setup is first aligned to the “zero” position, in which a uniform interference pattern is observed on the camera<sup>23</sup>. From this position, the lens  $L_{II}$  is displaced about different distances and the resulting interference patterns are recorded. Examples of the resulting images are displayed in Fig. 3.6. Note that no coincidence or heralded detection was employed for these observations. The fringes become more closely spaced, as the lens is translated further from the initial position. The spacing of the resulting fringe pattern is analyzed in order to find the wavelength that characterizes the pattern.

### 3.4.4 Results

The images of circular interference patterns resulting from the above procedure are analyzed as follows. A computer algorithm is used to evaluate the radial positions of minima and maxima for each lens shift (Fig. 3.7). These radii were found to be proportional to the square root of their order ( $|\mathbf{x}_C|_n \propto \sqrt{n}$ ), which is familiar from the fringes in a traditional interferometer.

<sup>23</sup>The procedure to find this position is explained in Appendix A.1.1.

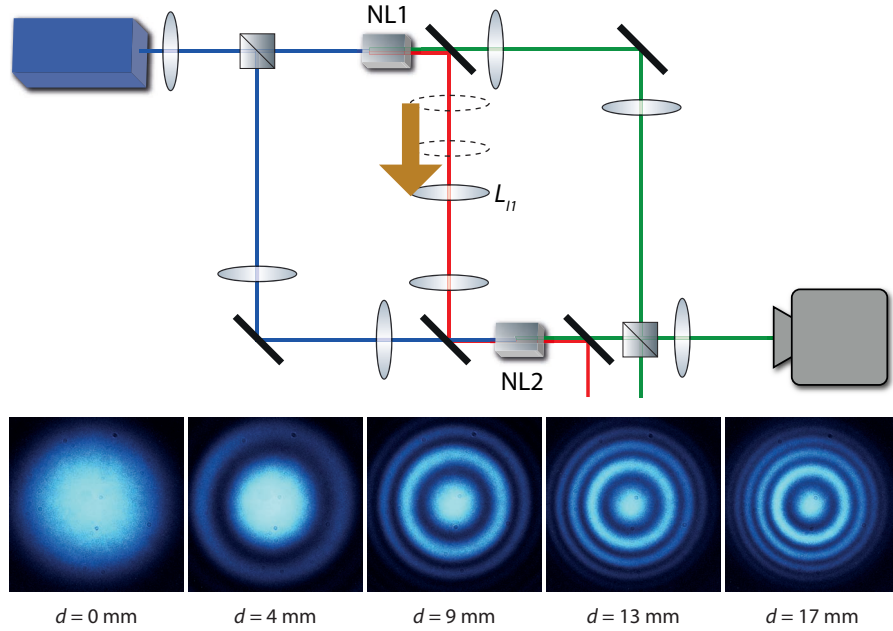


**Figure 3.6:** Circular fringes in the signal beam due to a lens shift in the idler beam. Interference fringes are observed on the camera if a lens in the idler beam ( $\lambda_I = 1550$  nm) is translated along the direction of beam propagation. The lens shift results in a spatially dependent phase shift in the idler beam corresponding to an additional propagation distance of  $d$ . The resulting pattern is observed in the signal beam ( $\lambda_S = 810$  nm). In analogy to traditional interferometry, a large lens translation distance corresponds to a narrow spacing of the fringes.

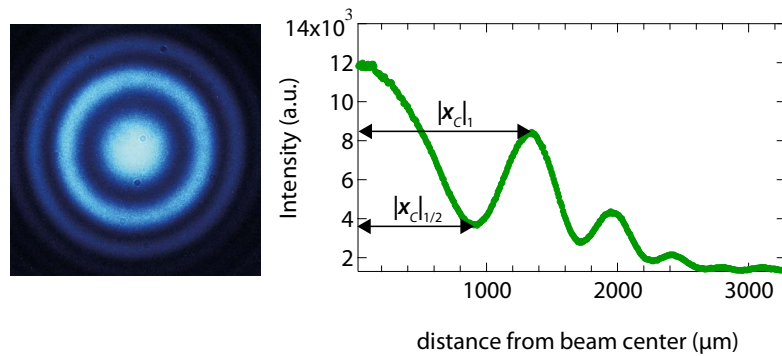


**Figure 3.7:** Evaluation of the radial intensity distribution of our circular fringes for the example of  $d = 9$  mm. The radial positions of minima and maxima are determined using a computer algorithm. These positions are subsequently used to evaluate the wavelength characterizing the pattern.

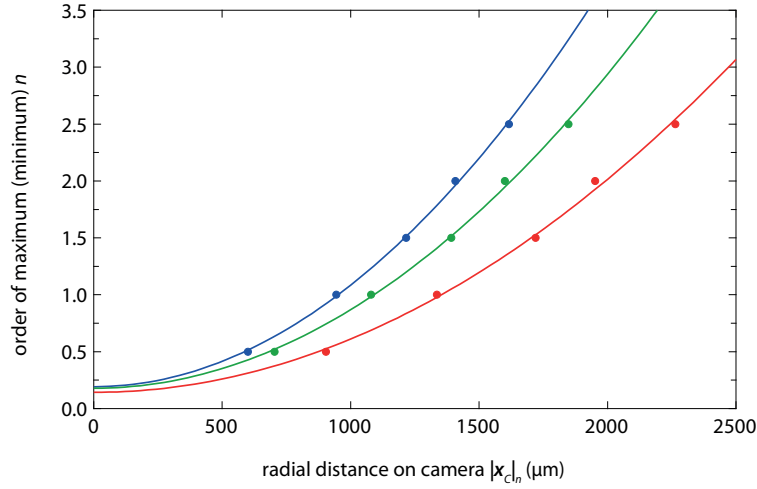


**Figure 3.8:** Fringe spacing for different lens shifts. Each curve corresponds to a single fringe pattern, obtained with a fixed value of  $d$ . The order of each minimum/maximum (see Eq. 3.3) is plotted against its radial position on the beam cross section. The points represent the radii of the first two minima and the first three maxima after the central maximum of the pattern. The presented data are obtained through lens shifts with  $d = 9$  mm (red),  $d = 13$  mm (green),  $d = 17$  mm (blue). An  $n \propto |x_C|_n^2$  dependence familiar from traditional interferometry is observed. The quadratic coefficients obtained by parabolic fits to the data (Eq. 3.5) are used to evaluate the wavelength dependence. Error bars representing the position uncertainties due to statistical fluctuations are smaller than the dots.

In order to determine the wavelength corresponding to the pattern, the minimum/maximum condition Eq. 3.3 is employed,

$$\frac{d}{2f_C^2} |x_C|_n^2 + \varphi'_0 = n\lambda_{eq}. \quad (3.4)$$

Again,  $d$  stands for the equivalent propagation distance<sup>24</sup>. The wavelength  $\lambda_{eq}$  governing the pattern is determined as follows.

Equation 3.4 can be rewritten as

$$n = a|x_C|_n^2 + b, \quad (3.5)$$

where

$$a = \frac{d}{2f_C^2 \lambda_{eq}}, \quad (3.6)$$

and  $b$  subsumes phase terms that are independent of the transverse position on the camera.

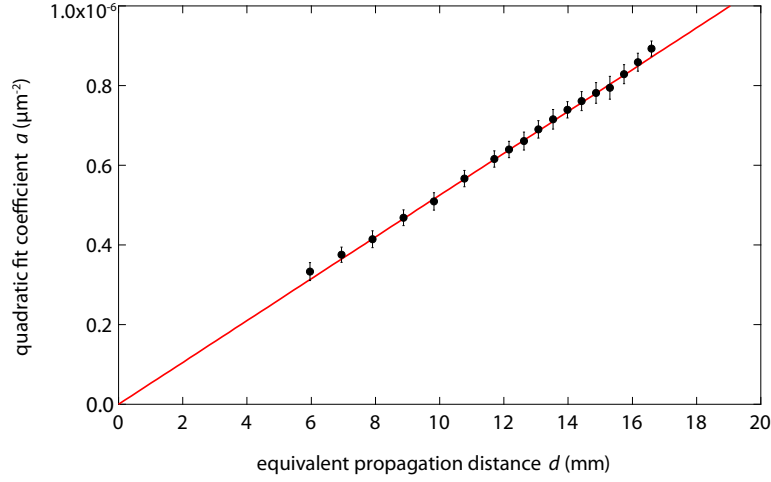
For each picture corresponding to a specific equivalent propagation distance  $d$ , the  $n$  are plotted as a function of  $|x_C|_n$  and equation 3.5 is fitted to the data (see Fig. 3.8). In this way, for each value of  $d$ , the quadratic fit coefficient  $a$  is obtained as a measure for how closely the fringes are spaced. If the two interfering beams are pictured as classical coherent light,  $a$  corresponds to the curvature of the phase-front of one of the beams with respect to the other.

Figure 3.9 shows the dependence of  $a$  on the equivalent propagation distance  $d$ . These values are used to determine the wavelength via Eq. 3.6. As a result, the wavelength governing the fringes was determined to

$$\lambda_{eq} = 420 \pm 7 \text{ nm}. \quad (3.7)$$

Note that this wavelength is smaller than any of the involved physical wavelengths of pump (532 nm), signal (810 nm) and idler (1550 nm) photons (Fig. 3.10). Instead, the result agrees

<sup>24</sup>Defined as  $d = (f_I^2 l) / (f_I^2 + l^2)$ , where  $l$  is the distance the lens is translated with respect to its initial position and  $f_I$  is the focal length of the lens in the idler beam.



**Figure 3.9:** Dependence of the “wavefront curvature” on the lens shift. The values of the quadratic coefficients (black dots) obtained from fits to the data of Fig. 3.8 are plotted as a function of the equivalent propagation distance. The observed linear dependence agrees well with the theoretical prediction (red line).

with the theoretical prediction of an equivalent wavelength, which is given by a combination of signal and idler wavelengths,

$$\lambda_{eq} = \frac{\lambda_S^2}{\lambda_I} \quad (3.8)$$

This result is explained theoretically in Sec. 3.4.5. The physical origin of this phenomenon is discussed in Sec. 3.4.6.

### 3.4.5 Quantum State in the Experiment

The appearance of the equivalent wavelength can be understood considering the quantum state of light in our experiment. Each of the two nonlinear crystals emits photon pairs in correlated pairs of spatial modes labeled by transverse wave vectors  $\mathbf{q}_S$  and  $\mathbf{q}_I$  in the respective beam (Fig. 3.12). This results in the quantum state of the emitted light from one crystal,

$$|\psi_{NLj}\rangle = \int d\mathbf{q}_S d\mathbf{q}_I C(\mathbf{q}_S, \mathbf{q}_I) |\mathbf{q}_S\rangle_{Sj} |\mathbf{q}_I\rangle_I, \quad (3.9)$$

where  $C(\mathbf{q}_S, \mathbf{q}_I)$  is the probability amplitude of source  $j$  emitting a photon pair into the two spatial modes  $\mathbf{q}_S$  and  $\mathbf{q}_I$  of the signal beam from the  $j$ th source  $S_j$  and the common idler beam  $I$ , respectively.

In the following, we assume perfect transverse momentum correlation between signal and idler photons, which is represented by  $C(\mathbf{q}_S, \mathbf{q}_I) = C(\mathbf{q}_S)\delta(\mathbf{q}_S + \mathbf{q}_I)$ , with  $C(\mathbf{q}_S)$  denoting the probability amplitude of detecting a signal photon with transverse k-vector  $\mathbf{q}_S$ . The quantum state of light emitted by an individual source can be simplified (using  $\mathbf{q}_I \rightarrow -\mathbf{q}_S$ )

$$|\psi_{NLj}\rangle = \int d\mathbf{q}_S C(\mathbf{q}_S) |\mathbf{q}_S\rangle_{Sj} |-\mathbf{q}_S\rangle_I. \quad (3.10)$$

We consider the case of perfect overlap and transmission of the idler beams ( $T=1$ ). A photon

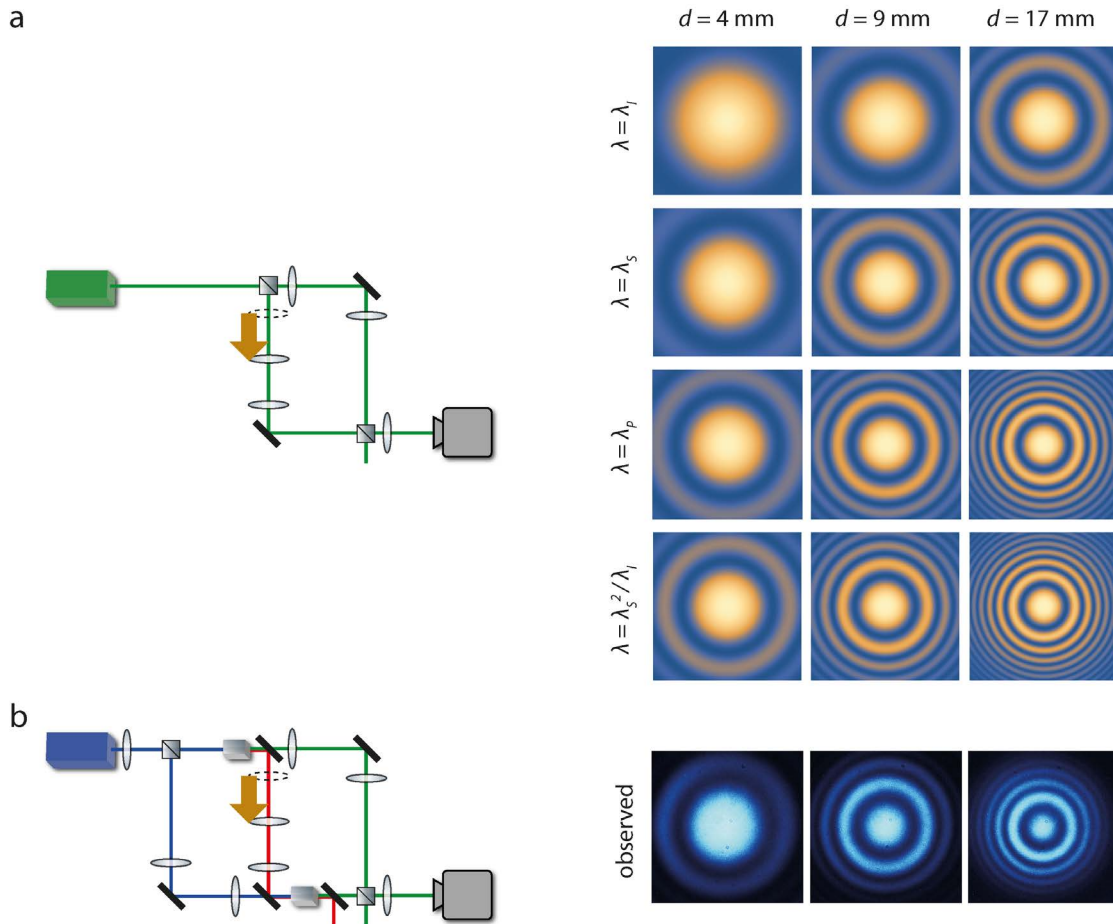


**Figure 3.10:** Wavelength comparison of circular fringes in traditional interferometry and circular fringes produced by induced coherence without induced emission. In a classical interferometer (a), the translation of one of the lenses along the beam propagation axis results in circular fringes. The spacing of these fringes for a is determined by the wavelength of the interfering light. This situation is illustrated for a Mach-Zehnder interferometer with classical light of idler ( $\lambda_I$ ), signal ( $\lambda_S$ ), and pump ( $\lambda_P$ ) wavelengths. The spacing of the observed fringes produced in induced coherence without induced emission (b) corresponds to the combination of the involved wavelengths  $\lambda_S^2 / \lambda_I$ , which corresponds to a closer fringe spacing than a classical interferometer with any of the actual physical wavelengths, even the pump.

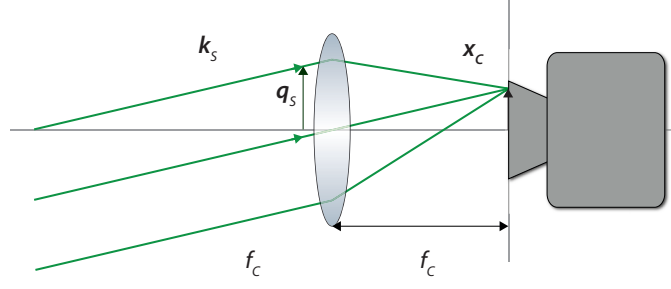


**Figure 3.11:** Geometrical scheme of the detection system. A lens placed at focal distance ( $f_C$ ) in front of the camera maps one transverse component  $\mathbf{q}_S$  of a  $\mathbf{k}_S$  of the signal beam from either of the two crystals to one point  $\mathbf{x}_C$  on the camera. Thus, upon detecting a photon on the camera, its transverse momentum is known, however there is no way to determine, whether the photon originated from NL1 or from NL2.

pair emitted in a superposition of NL1 and NL2 can be described by the state

$$|\Psi\rangle = \int d\mathbf{q}_S C(\mathbf{q}_S) |\mathbf{q}_S\rangle_{S1} |-\mathbf{q}_S\rangle_I + \int d\mathbf{q}_S e^{i(\varphi_I(-\mathbf{q}_S) - \varphi_0)} C(\mathbf{q}_S) |\mathbf{q}_S\rangle_{S2} |-\mathbf{q}_S\rangle_I, \quad (3.11)$$

which can be simplified to

$$|\Psi\rangle = \int d\mathbf{q}_S C(\mathbf{q}_S) \left( |\mathbf{q}_S\rangle_{S1} + e^{i(\varphi_I(-\mathbf{q}_S) - \varphi_0)} |\mathbf{q}_S\rangle_{S2} \right) |-\mathbf{q}_S\rangle_I. \quad (3.12)$$

A spatially dependent phase shift introduced in the idler beam between the crystals is denoted by  $\varphi_I(\mathbf{q}_I)$ . All other spatially independent phase terms are subsumed in  $\varphi_0$ .

As indicated in Fig. 3.11, the camera is located at the back focal plane of a lens that maps each  $\mathbf{q}_S$  of the superposed signal beam to a point on the camera  $\mathbf{x}_C$ ,

$$\mathbf{x}_C = \frac{f_C \lambda_S}{2\pi} \mathbf{q}_S. \quad (3.13)$$

The detection rate at a particular point on the camera is computed using the state of the corresponding spatial mode of the signal beam,

$$|\Psi_{\mathbf{x}_C}\rangle = C(\mathbf{q}_S) \left( |\mathbf{q}_S\rangle_{S1} + e^{i(\varphi_I(-\mathbf{q}_S) - \varphi_0)} |\mathbf{q}_S\rangle_{S2} \right) |-\mathbf{q}_S\rangle_I. \quad (3.14)$$

and is given by

$$R(\mathbf{x}_C) \propto 1 + \cos(\varphi_I[-\mathbf{q}_S(\mathbf{x}_C)] - \varphi_0). \quad (3.15)$$

The intensity at the point  $\mathbf{x}_C$  is therefore determined by the phase  $\varphi_I[-\mathbf{q}_S(\mathbf{x}_C)]$ , which can be explicitly written using Eqs. 3.1 and 3.13,

$$\varphi_I[-\mathbf{q}_S(\mathbf{x}_C)] = \frac{d|-\mathbf{q}_S(\mathbf{x}_C)|^2 \lambda_I}{4\pi} = \frac{d\lambda_I}{4\pi} \frac{4\pi^2}{\lambda_S^2 f_C^2} |\mathbf{x}_C|^2 = |\mathbf{x}_C|^2 \frac{d\pi}{\lambda_{eq} f_C^2}. \quad (3.16)$$

Note the dependence on the “wavelength”  $\lambda_{eq} = \lambda_S^2/\lambda_I$  in contrast to the classical case Eq. 3.2.

### 3.4.6 Discussion

#### 3.4.6.1 Intuitive Understanding of the Equivalent Wavelength

Under the assumption of perfect momentum correlation between signal and idler photons, the joint momentum distribution of the photon pairs is proportional to a Dirac delta function,

$$P(\mathbf{q}_S, \mathbf{q}_I) \propto \delta(\mathbf{q}_S + \mathbf{q}_I). \quad (3.17)$$

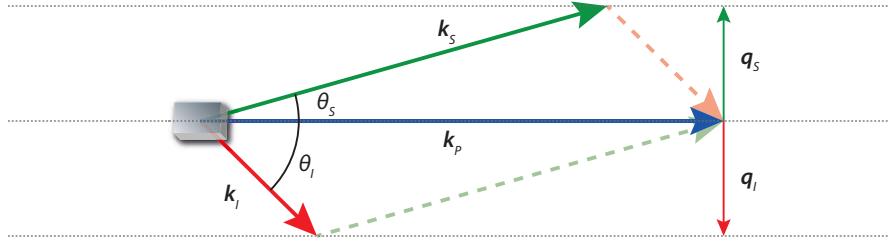


**Figure 3.12:** Correlated emission angles in non-degenerate SPDC. Momentum conservation in the SPDC process leads to the condition  $\mathbf{k}_P = \mathbf{k}_S + \mathbf{k}_I$ , which, given the pump beam propagates along the optical axis, implies  $\mathbf{q}_S + \mathbf{q}_I = 0$ . Due to the difference in wavelengths, the same magnitude of transverse wave vectors ( $\mathbf{q}_S = -\mathbf{q}_I$ ) corresponds to different angles of the respective  $\mathbf{k}$ -vectors. Geometrically,  $|\mathbf{q}_{S/I}|/|\mathbf{k}_{S/I}| = \sin(\theta_{S/I}) \approx \theta_{S/I}$ . Therefore,  $\theta_S/\theta_I = \lambda_S/\lambda_I$ . The phase shift and transmission introduced at a spatial mode corresponding to  $\theta_I$  in the idler beam thus affects the interference observed at  $\theta_S = \theta_I \lambda_S/\lambda_I$ . This results in a wavelength dependent image magnification as well as in a dependence of our interference fringes on a combination of the two wavelengths.

Due to momentum conservation in the SPDC process, the  $\mathbf{k}$ -vectors of signal and idler sum vectorially to the  $\mathbf{k}$ -vector the pump field (see Fig. 3.12). In the case of non-degenerate photon pairs, this corresponds to a different emission angle for a signal photon and its partner idler photon,

It follows from geometrical arguments and from  $|\mathbf{k}| = 2\pi/\lambda$  (Fig. 3.12) that the angles are related by

$$\frac{\theta_S}{\theta_I} \approx \frac{\lambda_S}{\lambda_I}. \quad (3.18)$$

The corresponding joint probability distribution of the two emission angles is

$$P(\theta_S, \theta_I) = \delta(\theta_S - \frac{\lambda_S}{\lambda_I} \theta_I). \quad (3.19)$$

The phase shift introduced at a particular wave vector of the idler beam affects the interferometric phase in the detection of its partner signal photon. As a result of Eq. 3.19, this photon will be detected at an angle different from the angle at which the phase shift was introduced by a factor  $\frac{\lambda_I}{\lambda_S}$ .

A similar wavelength dependent scaling between signal and idler photon gives rise to the magnification in quantum imaging with undetected photons (see Sec. 2.5).

### 3.4.6.2 Application: Wavelength Measurement of Undetected Photons

The interference pattern as it appears on the camera depends on the distance of the lens shift as well as on the “equivalent wavelength”  $\lambda_{eq} = \frac{\lambda_S^2}{\lambda_I}$ . By detecting only signal photons, the fringe pattern, as well as  $\lambda_S$  can be determined. This is sufficient to determine the wavelengths of idler photons even if the pump wavelength is not known. This fact might be useful in the characterization of photon pair sources.

### 3.4.6.3 Fringes and Stimulated Emission

The appearance of the equivalent wavelength is not limited to the quantum phenomenon of induced coherence without induced emission. The same observation (Although with reduced visibility [107–110]) should be possible in a setup which uses stimulated emission of photons in order to induce coherence (see Sec. 2.7).

#### 3.4.6.4 Analogy and Differences to Classical Interference

An interesting feature of the spatial interference fringes produced in our experiment is the qualitative similarity to classical interferometry. The same manipulation on one of the two interfering beams in a classical interferometer (tilt, defocusing) leads to interference fringes that are similar in their appearance. For example tilting one path with respect to the other produces straight fringes whereas defocusing one beam with respect to the other results in circular fringes.

In a classical interferometer, the formation of these patterns is often pictured as a relative tilt or focus of two wavefronts of the superposed beams. In our case, the attribution of a wavefront is impossible as one cannot assign a well defined phase-front to one photon of a photon pair (not even as a random variable). Instead the photon pair as a whole is represented by a product state and thus is multiplied by a single phase factor.

## 3.5 Quantifying the Momentum Correlation Between Two Photons by Detecting One

### 3.5.1 Goal of the Experiment

We showed in the previous section that the mapping of the phase shift acquired at a particular idler momentum to a particular point on the camera is based on the momentum correlation between signal and idler photons. In the following, we drop the assumption of perfect correlation and turn to the case of imperfect momentum correlation. We analyze, how the strength of the correlation between signal and idler photons affects the observed interference pattern. In the experiment described in this section, we aim to demonstrate that it is possible to quantify the momentum correlation between signal and idler photons by first order measurements of signal photons only, i.e. without detecting idler photons.

In more precise terms, the correlation is encoded in the conditional variance of the transverse momentum distribution of signal and idler photons,  $\sigma^2(\mathbf{q}_I|\mathbf{q}_S)$  (see Sec. 2.3.1). We aim to experimentally determine this quantity by analyzing the fringe pattern produced in the signal beam using induced coherence without induced emission.

### 3.5.2 Momentum Correlation in Laser Pumped SPDC

In photon pair sources based on SPDC in bulk nonlinear crystals, the momentum correlation of the emitted photons depends on the properties of the pump laser beam [55].

Loosely speaking, the angular spectrum of the pump beam<sup>25</sup> manifests itself in the angular spectrum of the coincident photons [55, 57] (see Sec. 2.3.1). More precisely, the probability distribution governing the transverse momenta of signal and idler photons is given by

$$P(\mathbf{q}_S, \mathbf{q}_I) \propto |A(\mathbf{q}_P)|^2 = |A(\mathbf{q}_S + \mathbf{q}_I)|^2, \quad (3.20)$$

where  $A(\mathbf{q}_P)$  denotes the angular spectrum of the pump beam. Momentum conservation in the SPDC process leads to the fact that the pump wave vector is equal to the sum of signal and idler wave vectors. In terms of their transverse components,  $\mathbf{q}_S + \mathbf{q}_I = \mathbf{q}_P$ .

A Gaussian laser beam can be written in the angular spectrum representation as (e.g. [147])

$$A(\mathbf{q}_P) \propto \exp(-|\mathbf{q}_P|^2 w_P^2 / 4), \quad (3.21)$$

where  $w_P$  is the Gaussian beam waist. It follows that a narrow focus (small  $w_P$ ) corresponds to a broad range of transverse momenta of the pump photons, whereas a large focus spot (large  $w_P$ ) approaches the ideal case of a plane wave pump, which can be described with a single transverse momentum.

Substituting Eq. 3.21 into Eq. 3.20 leads to a “joint angular spectrum” of the photon pairs given by

$$P(\mathbf{q}_S, \mathbf{q}_I) \propto \exp(-|\mathbf{q}_S + \mathbf{q}_I|^2 w_P^2 / 2). \quad (3.22)$$

Intuitively, the phase matching condition holds for every k-vector of the pump beam, resulting in a sharp correlation between the down-converted photons produced using a plane wave pump and a weak correlation in the case of a narrow pump focus.

### 3.5.3 Fringe Visibility with Tuned Momentum Correlation

The effect of a changed momentum correlation on the circular fringes in induced coherence without induced emission is tested as follows. First, a circular fringe pattern is produced by

<sup>25</sup>The angular spectrum of a light beam is basically the set of complex amplitudes corresponding to each transverse k-vector [58]

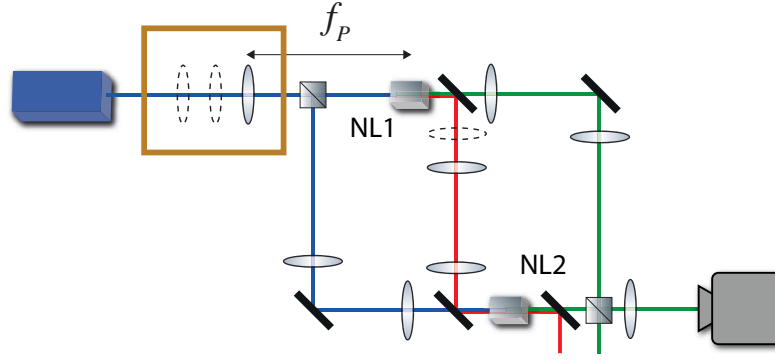


**Figure 3.13:** Setup to observe spatial fringes by induced coherence without induced emission while tuning the momentum correlation between signal and idler photons. The pump laser is focused equally into the crystals NL1 and NL2 using the imaging system in the pump beam (see Fig. 3.2). The pump focus spot size is tuned by choosing different focal lengths and distances for the lens to focus the pump beam (inside yellow box). Circular fringes are produced as in the previous section by displacing a lens in the idler beam.

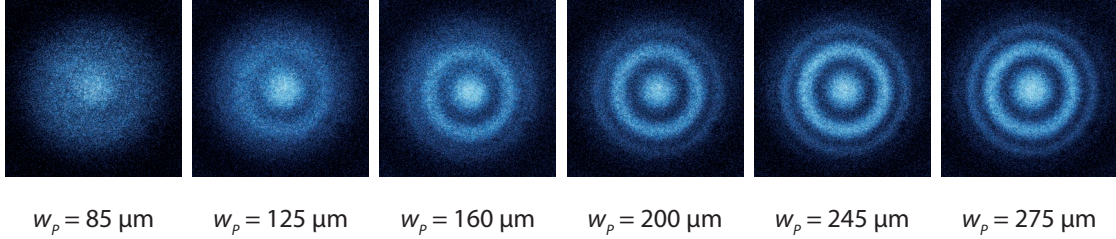


**Figure 3.14:** Observation of interference fringes with varying pump focus. A narrow pump waist (strong focus) at the two crystals results in an interference pattern with lower visibility than in the case of loosely focused pump beams. The Gaussian beam waist of the pump beam at both crystals ( $w_p$ ) is indicated. This effect can be attributed to the varied momentum correlation between signal and idler photons.

translating a lens in the idler beam. Subsequently, the momentum correlation is tuned by varying the focus spot size of the pump beam at both crystals simultaneously while keeping the position of the lenses in signal and idler beams constant (Fig. 3.13). The appearance of the resulting interference patterns changes as depicted in Fig. 3.14. It can be seen that the fringe contrast is reduced for a narrower focus, i.e. if the employed photon pairs are less strongly correlated.

### 3.5.4 Quantitative Description

#### 3.5.4.1 Quantum State in the Experiment

Analogously to Sec. 3.4.5, Eq. 3.9, we write the quantum state of a photon pair produced by one of the two sources with a common idler beam  $I$  as

$$|\psi_{NLj}\rangle = \int d\mathbf{q}_S d\mathbf{q}_I C(\mathbf{q}_S, \mathbf{q}_I) |\mathbf{q}_S\rangle_{Sj} |\mathbf{q}_I\rangle_I, \quad (3.23)$$

where  $Sj$  denotes the  $j$ th signal beam. In contrast to the treatment in Sec. 3.4.5, here we do not make a priori assumptions on  $C(\mathbf{q}_S, \mathbf{q}_I)$ .

The quantum state of the system is again given by a superposition of a photon pair originating at either of the two crystals,

$$|\Psi\rangle = \int d\mathbf{q}_S d\mathbf{q}_I C(\mathbf{q}_S, \mathbf{q}_I) |\mathbf{q}_S\rangle_{S1} |\mathbf{q}_I\rangle_I + \int d\mathbf{q}'_S d\mathbf{q}'_I e^{i(\varphi_I(\mathbf{q}_I) - \varphi_0)} C(\mathbf{q}'_S, \mathbf{q}'_I) |\mathbf{q}'_S\rangle_{S2} |\mathbf{q}'_I\rangle_I, \quad (3.24)$$

which can be simplified to

$$|\Psi\rangle = \int d\mathbf{q}_S d\mathbf{q}_I C(\mathbf{q}_S, \mathbf{q}_I) \left( |\mathbf{q}_S\rangle_{S1} + e^{i(\varphi_I(\mathbf{q}_I) - \varphi_0)} |\mathbf{q}_S\rangle_{S2} \right) |\mathbf{q}_I\rangle_I. \quad (3.25)$$

In contrast to Eq. 3.12, here it is not possible to directly carry out the integration over  $\mathbf{q}_I$  as we dropped the assumption of perfect momentum correlation and  $C(\mathbf{q}_S, \mathbf{q}_I)$  is essentially arbitrary.

We are interested in the photon detection probability at one point on the camera. Under the assumption of ideal lens systems, selecting one point  $\mathbf{x}_C$  on the camera corresponds to selecting a fixed transverse momentum  $\mathbf{q}_S = 2\pi/(f_C \lambda_S) \mathbf{x}_C$  of the signal photon (cf. Eq. 3.13). The detection probability at that point is calculated using the state describing light in the mode  $\mathbf{q}_S$  of the signal beam. This state reads

$$|\Psi_{\mathbf{q}_S}\rangle = \int d\mathbf{q}_I C(\mathbf{q}_S, \mathbf{q}_I) \left( |\mathbf{q}_S\rangle_{S1} + e^{i(\varphi_I(\mathbf{q}_I) - \varphi_0)} |\mathbf{q}_S\rangle_{S2} \right) |\mathbf{q}_I\rangle_I. \quad (3.26)$$

It follows that the detection rate on the camera is given by

$$R(\mathbf{x}_C) \propto \int d\mathbf{q}_I |C(\mathbf{q}_S(\mathbf{x}_C), \mathbf{q}_I)|^2 (1 + \cos[\varphi_I(\mathbf{q}_I) + \varphi_0]) d\mathbf{q}_I. \quad (3.27)$$

Using the fact that  $|C(\mathbf{q}_S(\mathbf{x}_C), \mathbf{q}_I)|^2 = P(\mathbf{q}_S(\mathbf{x}_C), \mathbf{q}_I)$  represents the joint probability distribution of signal and idler momenta, which can be expressed as  $P(\mathbf{q}_S(\mathbf{x}_C), \mathbf{q}_I) = P(\mathbf{q}_I|\mathbf{q}_S(\mathbf{x}_C))P_S(\mathbf{q}_S(\mathbf{x}_C))$ , Eq. 3.27 can be written in terms of the conditional probability distribution of an idler momentum given a certain momentum of the signal photon,

$$R(\mathbf{x}_C) \propto P_S(\mathbf{q}_S(\mathbf{x}_C)) \int P(\mathbf{q}_I|\mathbf{q}_S(\mathbf{x}_C)) (1 + \cos[\varphi_I(\mathbf{q}_I) + \varphi_0]) d\mathbf{q}_I, \quad (3.28)$$

where (cf. Eq. 3.22)

$$P(\mathbf{q}_I|\mathbf{q}_S) \propto \exp(-|\mathbf{q}_S + \mathbf{q}_I|^2 w_p^2/2). \quad (3.29)$$

The interferometric visibility<sup>26</sup> at one point  $\mathbf{x}_C$  on the camera is independent of the multiplicative factor  $P_S(\mathbf{q}_S)$ .

Instead, the visibility depends solely on the conditional probability distribution  $P(\mathbf{q}_I|\mathbf{q}_S)$ , and on the phase shifts  $\varphi_I(\mathbf{q}_I)$ . In the following, we investigate, how the momentum correlation strength can affect the obtained visibility.

### 3.5.4.2 Effect of Correlation Strength

An interpretation of Eq. 3.28 allows to obtain some intuition about the role of the momentum correlation in the formation of an interference pattern in our experiment.

Consider first the hypothetical case of perfectly anticorrelated momenta between signal and idler photons. In this case,  $P(\mathbf{q}_I|\mathbf{q}_S) \propto \delta(\mathbf{q}_I + \mathbf{q}_S)$ . Equation 3.28 reduces to

$$R(\mathbf{x}_C) \propto P_S(\mathbf{q}_S) (1 + \cos[\varphi_I(-\mathbf{q}_S) + \varphi_0]), \quad (3.30)$$

which represents an interference pattern with visibility one. The reason is that one point on the camera is only affected by the phase shift of exactly one spatial mode of the idler beam. This situation is illustrated in Fig. 3.15. It corresponds to the approximation made in Secs. 2.5 and 3.5.

In the other extreme case of completely uncorrelated signal and idler photons, the probability distribution for idler photons with momentum  $\mathbf{q}_I$  is independent of the signal photon's momentum. We can write  $P(\mathbf{q}_I|\mathbf{q}_S) = P_I(\mathbf{q}_I)$ . In this case,

$$R(\mathbf{x}_C) \propto P_S(\mathbf{q}_S) \int P_I(\mathbf{q}_I) (1 + \cos[\varphi_I(\mathbf{q}_I) + \varphi_0]) d\mathbf{q}_I = P_S(\mathbf{q}_S) f(\varphi_0), \quad (3.31)$$

---

<sup>26</sup>Defined as  $V := \frac{R_{max} - R_{min}}{R_{max} + R_{min}}$ , where the minimum and maximum refers to a variation of  $\varphi_0$

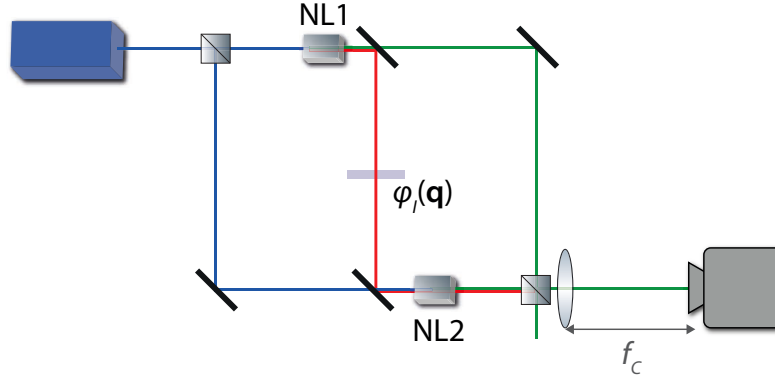


**Figure 3.15:** Schematic representation of a scenario with perfect momentum correlation. A signal photon is detected at a particular point on the camera, corresponding to a particular transverse momentum. As the photons are perfectly correlated, the momentum of the partner idler photon can be inferred precisely. In the experiment, a momentum-dependent phase shift is introduced in the idler beam. Due to the perfect correlation, an exact value of phase shift is acquired by the idler photon and observed as phase shift in the signal beam interference at this point. Each point on the camera corresponds to a different transverse momentum of the signal photons and thus to different phase shifts. This results in a transverse position dependent interference pattern. See Eq. 3.30.

where the factor  $f$  is the same for every point on the camera  $\mathbf{x}_C$ . It is impossible to see a spatially varying interference pattern, as the phase shifts imparted on all  $\mathbf{q}_I$  are contributing equally to the intensity at any point on the camera.

In general, photon pairs exhibit a momentum correlation that corresponds to neither of the above extreme cases. Instead, the correlation is imperfect, i.e.  $P(\mathbf{q}_I|\mathbf{q}_S)$  has a finite width. In this case, the phase shifts introduced on a range of  $\mathbf{q}_I$ s contribute to the intensity in a single spatial mode of the signal beam, i.e. on a single point on the camera. The weaker the correlation and the faster the phase shift  $\varphi_I(\mathbf{q}_I)$  varies with  $\mathbf{q}_I$ , the lower the interferometric visibility. The situation is illustrated in Fig. 3.16. The intensity at the camera is given by Eq. 3.28

It follows that a suitably varying  $\varphi_I(\mathbf{q}_I)$  is essential in order to use the pattern for determining the strength of the momentum correlation.

### 3.5.5 Performed Measurements

#### 3.5.5.1 Tuning Momentum Correlation Strength by Pump Focusing

In order to allow for tunable momentum correlation between signal and idler photons, a variable focus of the pump laser beam into the two nonlinear crystals is implemented. To this end, lenses of various focal lengths ( $f = \{200, 300, 400, 500, 600, 700\}$  mm) are positioned at the respective focal distances from NL1 on magnetic mounts that allow to remove and reposition the lenses precisely and in a reproducible way. In our setup, this allows the selection of pump focus spots between  $85 \mu\text{m}$  and  $275 \mu\text{m}$  by inserting the corresponding lens (see Fig. 3.14).

Due to the imaging system in the pump beam ( $L_{P1}$  and  $L_{P2}$ ), the same pump spot is produced in both NL1 and NL2. It suffices to change the focus at NL1 to simultaneously change the focus spot at both crystals. For each lens configuration, the Gaussian waist of the pump beam is measured using a standard knife-edge technique.

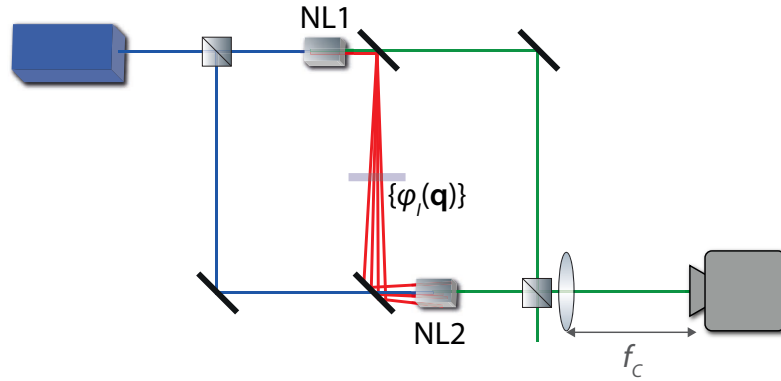


**Figure 3.16:** Formation of an interference pattern with imperfect momentum correlation. Again, a signal photon is detected on the camera with a particular transverse momentum. In the case of imperfect momentum correlation, the momentum of the partner idler photon can be inferred only up to a non-negligible uncertainty. Consequently, the phase shift acquired by the idler photon that corresponds to the detection of a signal photon at a specific point, is to some extent ambiguous. As a result, the interferometric phase observed at the point on the camera is an average over the range of possible phase shifts corresponding to the range of possible momenta of the idler photon. This averaging leads to less pronounced minima and maxima of the pattern, i.e. to a reduced visibility. See Eq. 3.28.

### 3.5.5.2 Introduced Phase Shift and Image Acquisition

The fringes are produced in the same way as in Sec. 3.4.3. A lens in the idler beam is translated along the beam axis, introducing the phase shift

$$\varphi_I(\mathbf{q}_I) = \frac{\lambda_I d}{4\pi} |\mathbf{q}_I|^2. \quad (3.32)$$

For the momentum correlation measurement, we use a fixed lens shift distance, corresponding to  $d = 11.7$  mm.

The pump beam is focused into the crystals, sequentially using lenses of different focal lengths. In each pump configuration, the interferometric phase ( $\varphi_0$ ) is scanned using a piezo attached to a mirror in the signal beam (see Fig. 3.2). Camera images are recorded for 30 different values of interferometric phase.

### 3.5.6 Image Analysis

The obtained images are analyzed as follows (Fig. 3.17). For each point on the camera, intensity values for different interferometric phase shifts  $\varphi_0$  are determined. The resulting interference fringe for each pixel is characterized by evaluating the interferometric visibility. This procedure results in an “image” of the visibility distribution on the beam

Algorithmically, the center of the beam is determined by maximizing the cross-correlation between opposite radial directions.

### 3.5.7 Results

The cross section of each visibility image is evaluated (Fig. 3.18). In general, the visibility is maximum at the center of the beam and drops with the distance from the center.

This behavior can be understood as follows. By detecting a signal photon at a particular point on the camera, its transverse momentum is known. It is possible to infer the transverse momentum of the partner idler photon up to the uncertainty  $\sigma(\mathbf{q}_I|\mathbf{q}_S)$ , i.e. the uncertainty in the correlation.

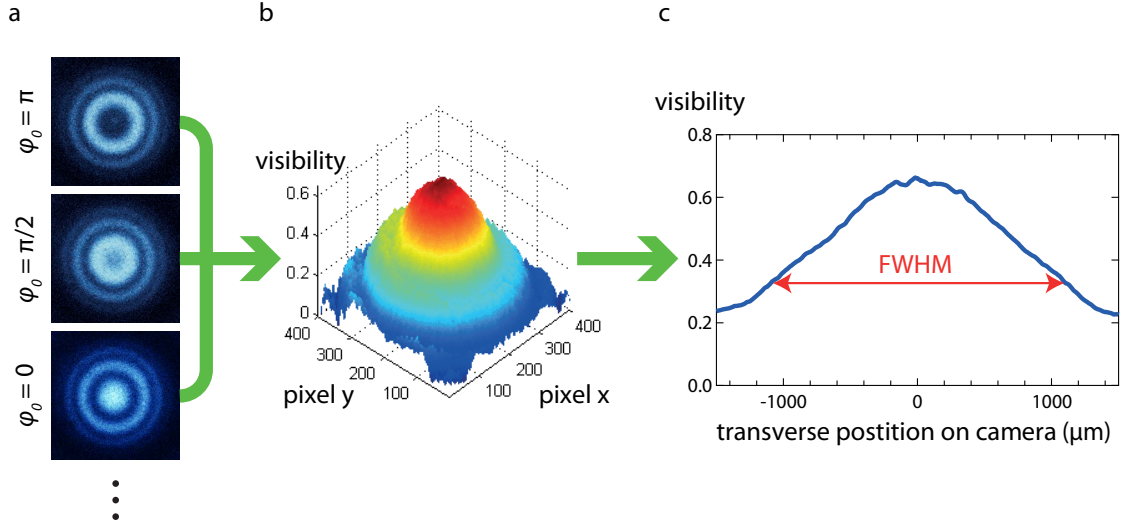


**Figure 3.17:** Quantitative analysis of the interference pattern. For a given lens shift (here  $d = 11.7$  mm) and for each pump focus parameter ( $w_P = 200 \mu\text{m}$  in this image), interference fringes are recorded for 30 different values of the spatially uniform interferometric phase  $\varphi_0$ . This results in phase shifted interference fringes on the camera (a). The corresponding visibilities at each point on the camera are evaluated by fitting a sinusoidal function to the phase-dependent intensity value. This allows to construct an “image” of the visibility (b). The characteristic full width at half maximum (FWHM) of the transverse cross section is evaluated as the transverse profile of this image (c).

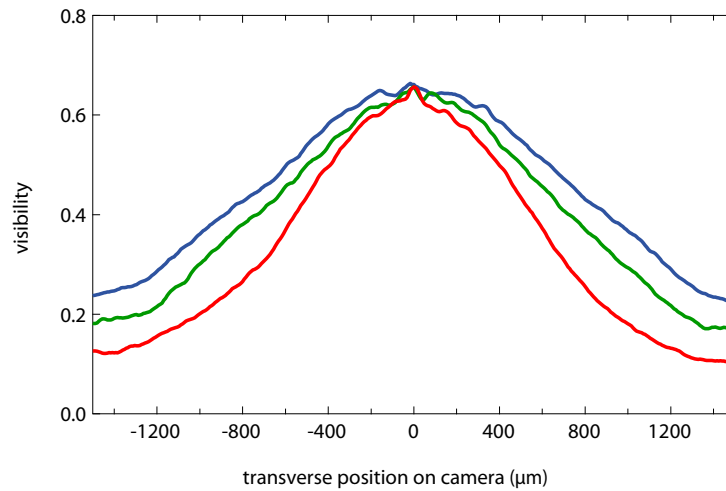


**Figure 3.18:** Transverse visibility profiles. The observed visibility as a function of the transverse position in the camera is plotted for pump waists of  $w_P = 125 \mu\text{m}$  (red),  $w_P = 160 \mu\text{m}$  (green), and  $w_P = 200 \mu\text{m}$  (blue). In all cases, the visibility decreases as the distance from the center increases. A larger pump waist corresponds to a slower decrease.

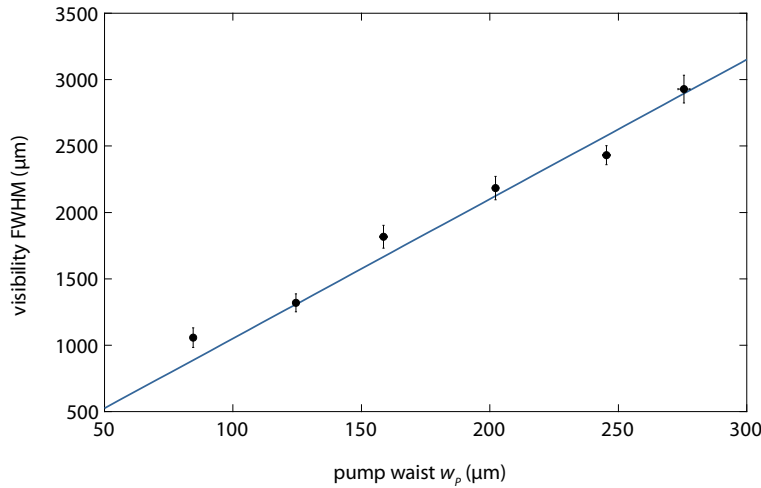


**Figure 3.19:** Dependence of the visibility cross section on the momentum correlation. The FWHM of the visibility profiles (black dots) are plotted against the pump waist. A wider pump waist corresponds to a sharper momentum correlation and to a slower decrease of visibility with the distance from the beam center. This slower decrease is manifested in a larger FWHM of the visibility profile. The observed data agree with the theoretical prediction (blue line), which is obtained by a numerical simulation based on Eq. 3.28 and does not include any free parameters.

The phase-shift of the observed interference at this point is determined by the phase shift imparted on the corresponding idler photon. In the case of a non-zero uncertainty of the idler photon's momentum, this phase shift is not uniquely determined.

The larger this uncertainty, and the faster the phase shift varies (the larger  $d\varphi_I(\mathbf{q}_I)/d\mathbf{q}_I$ ) within that uncertainty, the larger the range of possible phase shifts, which the idler photon can obtain.

As a result, the observed interference pattern is an average over many possible patterns, each corresponding to a particular phase shift acquired by the idler photon. Due to this averaging, the observed fringe appears blurred and the visibility is reduced.

The introduced phase shift is proportional to the square of the transverse momentum of the idler photon,  $\varphi_I \propto \mathbf{q}_I^2$ . Therefore,  $\varphi_I$  varies faster for larger  $\mathbf{q}_I$  than for small ones. The slowest variation is observed in the center of the beam (where  $\mathbf{q}_I$  is close to zero), which therefore constitutes the maximum visibility along the beam cross-section.

### 3.5.7.1 Reconstruction of the Correlation Strength

In order to quantify the strength of the momentum correlation, the full width at half maximum (FWHM) of the visibility cross section turned out to be a practical measure. The obtained FWHM values for the experimentally implemented pump focus spots are shown in Fig. 3.19, in comparison to the theoretical prediction. The dependence appears linear.

In order to relate the visibility FWHM to an actual numerical value corresponding to the strength of the momentum correlation between signal and idler photons, the following parametrization of the conditional probability distribution was used.

$$P(\mathbf{q}_I|\mathbf{q}_S) \propto \exp \left[ -|\mathbf{q}_S + \mathbf{q}_I|^2 / (2\sigma^2) \right], \quad (3.33)$$

Here,  $\sigma^2$  denotes the variance of the distribution, which is a measure for how well the momenta of signal and idler photons are correlated. The parametrization of Eq. 3.33 corresponds to the angular spectrum of a Gaussian pump beam. It can be shown that given the implemented idler

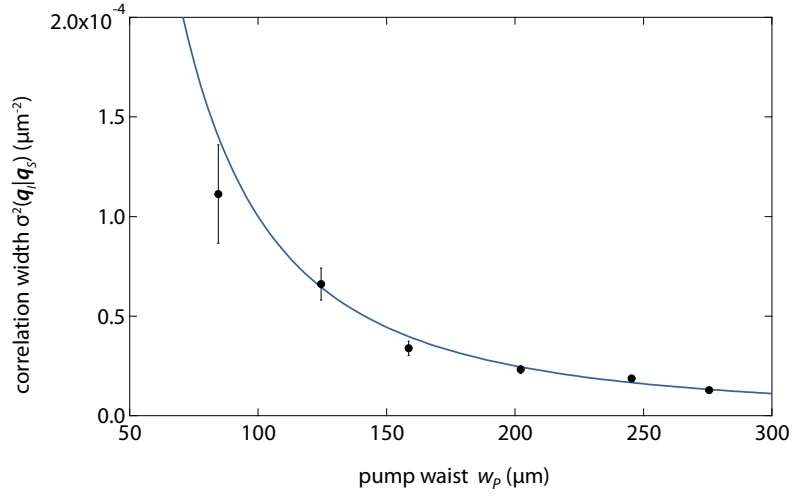


**Figure 3.20:** Reconstructed momentum correlation between signal and idler photons by measurements of signal photons only. The uncertainty of the transverse momentum of an idler photon, given the transverse momentum of its partner signal photon is determined with our method. The results (black points) are plotted against different pump waists. For comparison, the theoretical prediction (with no free parameters) is plotted as blue line.

phase distribution (Eq. 3.1), a one-to-one relation between the correlation strength  $\sigma^2$  and the FWHM of the visibility exists (see [146]). As a result, it is possible to numerically compute  $\sigma^2$  from the measured FWHM values. This was done by using Eqs. 3.33, 3.28 and 3.32 to numerically compute an expected visibility pattern and its FWHM for arbitrary  $\sigma$ . The obtained numerical relation was inverted to determine  $\sigma$  for the measured values of the visibility FWHM.

The results are shown in Fig. 3.20. A comparison of Eq. 3.33 to Eq. 3.22 leads to a theoretical prediction for a variance of  $\sigma_{theo}^2 = 1/w_p^2$ . The corresponding prediction  $\sigma^2(\mathbf{q}_I|\mathbf{q}_S) = 1/w_p^2$  is represented as the blue curve in Fig. 3.20. It can be seen that the prediction matches closely with the measurement results.

### 3.5.8 Summary of the Method

It is possible to understand the method intuitively by considering the steps in the formation of an interference pattern in our setup. The intensity of the detected signal beam at a particular point on the camera is controlled by the phase shift introduced in the corresponding spatial mode of the idler beam. In the case of perfect correlation, this is exactly one plane wave mode of the idler beam (i.e. a particular momentum of an idler photon).

Selecting one point on the camera, the momentum of the signal photon is known. In the case of perfect correlation, the transverse momentum of the partner idler photon can be inferred with certainty. Therefore, the phase shift affecting the point on the camera can be inferred accordingly. If, on the other hand, the photons are less correlated, the detection of a signal photon does not allow to infer the momentum of the partner idler photon with certainty. The introduced phase shift is therefore not uniquely determined and could be different for each detected signal photon. As a result, the detected intensity at one point on the camera is obtained by averaging over a range of possible phase shifts, corresponding to a range of possible idler momenta. The consequent reduction of visibility is quantified in our method.

### 3.5.9 Discussion

#### 3.5.9.1 Comparison to Traditional Methods and Possible Uses of Our Method

Using our method, it is possible to obtain a measure for the strength of the momentum correlation between signal and idler photons from intensity measurements on signal photons only. The method therefore allows to access a property of a higher order correlation (proportional to intensity squared) in lower order (intensity on the camera).

Instead of using one photon pair source and two detectors to determine the momentum correlation, we used one detector and two identical sources, which are arranged such that a photon pair is produced in a superposition of the two sources. Unlike traditional methods based on coincidence detection, our method is based on the effect of induced coherence without induced emission which is observed using only one detector. Due to the fact that the underlying principle is fundamentally different, it is of interest to point out some advantages and disadvantages of our method. A disadvantage is that the measurement is more indirect than measuring the correlation by direct coincident detection of both photons. It therefore involves more assumptions, in particular the use of the parametrization in Eq. 3.33, which assumes a particular form of the conditional probability distribution. It is, however possible to generalize the method to a large class of other distributions [146]. The obvious advantage of our method is that it is unnecessary to detect the second photon. Therefore, it can be applied to characterize sources, in which one of the photons is difficult or impossible to detect, for example, because it is at a wavelength which is technically difficult to access (e.g. far-infrared or terahertz-radiation). It could also find applications in the detection of other particles than photons, for which coincidence detection is challenging (e.g. certain species of atoms). In the future, the method could be extended to measure not only momentum correlation but other correlations as well. For example, the method could be readily used in to determine frequency correlations by detecting only one particle. A particularly interesting avenue of research is to measure the correlations in complementary observables. This would enable an experimental test of entanglement without detecting all involved particles<sup>27</sup>.

The fact that the idler photon remains undetected also allows to perform subsequent measurements on the idler photon, while simultaneously measuring the momentum correlation. Information about both photons is collected by destroying only the signal photon.

#### 3.5.9.2 Relation to Spatial Resolution of Quantum Imaging with Undetected Photons

The results are closely connected to the questions about spatial resolution in the application of quantum imaging with undetected photons. Using the same arguments as in Sec. 3.5.4.1, an imperfect momentum correlation is expected to affect the image resolution. In fact the pictures presented in Fig. 3.14 could be viewed as images of the same phase object which is more blurred with weaker momentum correlation.

<sup>27</sup>Experimental tests of entanglement by measuring only one subsystem have thus far been demonstrated only for globally pure states, see e.g. [148–153].

### 3.6 Conclusions

We have shown that the effect of induced coherence without induced emission in a multimode setting can be used to create spatial interference fringes. These fringes are produced by manipulating neither of the two interfering beams, but by manipulating a third light beam that remains undetected. We demonstrated that the fringes are characterized not by one of the involved wavelengths alone, but by a combination of the wavelength of the beam in which the manipulations are performed and the wavelength of the interfering beams (Eq. 3.8). Furthermore, we have shown that the momentum correlation in the employed photon pairs is tightly connected to the formation of the pattern. We used this connection to determine the correlation strength between signal and idler photons without detecting idler photons.

Both experiments in this chapter allow to access information about the correlation between signal and idler photons. The wavelength dependent scaling responsible for the appearance of an “equivalent wavelength”, allows to access the mean value of  $P(\mathbf{q}_I|\mathbf{q}_S)$ , whereas the “sharpness” of the interference pattern allows to obtain the variance  $\sigma^2(\mathbf{q}_I|\mathbf{q}_S)$ .

From a fundamental physics standpoint, these experiments raise questions about the information content of correlated photonic systems. As the correlation is in general a property of the photon pair as a whole, it is intuitive that both photons need to be detected in order to measure it. One might ask, at what time such a joint measurement actually happens, either when the first or when the second photon is detected, or when the electronic signals of the detectors are compared to each other in a coincidence circuit? The possibility to perform an equivalent measurement without the need for coincidence detection stimulates the investigation of these questions.

# Controlling Partial Polarization by Path Distinguishability

This chapter is based on the publication “Partial Polarization by Quantum Distinguishability” [92].

## 4.1 Motivation and Goal

In experiments to observe the effect of induced coherence without induced emission (see e.g. Secs. 2.4.2, 2.5 and the previous chapter), the alignment of two idler beams ensures that the detection of an idler photon does not reveal information about the origin of a signal photon. However, path information is not only eliminated in the idler beam, but also in the signal beam itself. This is done by detecting signal photons after a beam splitter. The ability of a signal photon to interfere can be controlled by varying the transmission of the idler beam between the two sources [13, 14]. In this way, partial path information is introduced, which deteriorates the observed visibility.

In this chapter, we investigate a different situation, in which path distinguishability is introduced by rotating the polarization of one of the two signal beams. In the extreme case of mutually orthogonal polarizations, a signal photon cannot interfere at the beam splitter, regardless of the transmission in the idler beam. The question arises, how in this case, signal photons are affected by varying the degree of distinguishability of the possible origins of idler photons.

The polarization of light can be described as field correlations (“coherence”) between mutually orthogonal polarization components [145]. It has been shown that the degree of coherence in an optical system is equal to the degree of indistinguishability [46]. Thus, by tuning the amount of distinguishability of two mutually orthogonal polarization components, the degree of polarization of the light beam can be controlled.

The goal of this experiment is to construct such a situation. We show that in our system, the degree of polarization can be tuned by varying merely the path distinguishability available through a different photon. The presented experiment demonstrates that the effect of induced coherence without induced emission can be used to “induce polarization” without induced emission. As

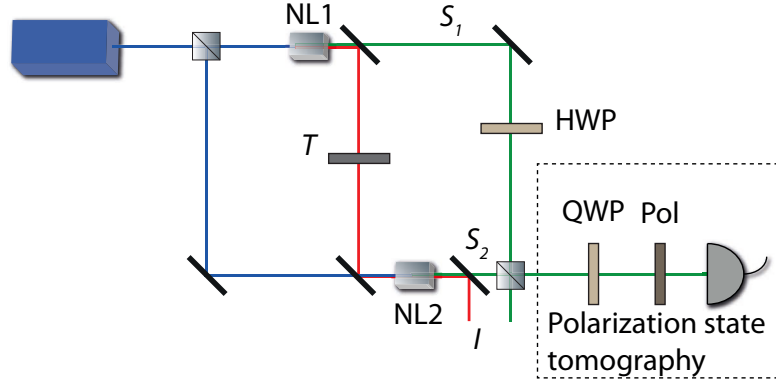


**Figure 4.1:** Setup of the experiment. Similar to the previous experiments, two nonlinear crystals NL1 and NL2 coherently emit photon pairs by type-0 SPDC. The two idler beams are aligned to be indistinguishable and the two signal beams are superposed at a beam splitter. Lens systems (here omitted for clarity) are used to align the beams (see Fig. 3.2). Initially, all photons are horizontally polarized. The polarization of the signal beam emerging from NL1 is rotated by an angle  $\gamma$  using a half wave plate (HWP). Polarization state tomography is performed on the superposed signal beam using a combination of a quarter wave plate (QWP) and a polarizer (Pol). A variable attenuator ( $T$ ) is positioned in the idler beam between the crystals, which is used to control the coherence between the two possible ways of emitting a signal photon. Both HWP and  $T$  are used to introduce distinguishability between the two possible sources, however of two fundamentally different kinds.

such, it is possible to control the degree of polarization of a light beam without interacting with it. Moreover, our experiment demonstrates a situation, in which the origin of partial polarization cannot be explained classically (see [154]).

## 4.2 Degree of Polarization

The degree of polarization ( $DoP$ ) is defined as the ratio between the polarized portion of a light beam and the total beam intensity,  $DoP = I_{pol}/I$  [147]. It can be expressed in terms of Stokes parameters or via the “one-point coherency matrix” [145],

$$J = \begin{bmatrix} \langle E_x^* E_x \rangle & \langle E_x^* E_y \rangle \\ \langle E_y^* E_x \rangle & \langle E_y^* E_y \rangle \end{bmatrix}$$

with the expectation values of electrical fields at mutually orthogonal polarization directions  $x$  and  $y$  at a single point in space. Using this matrix, the degree of polarization can be written as [145, 155]

$$DoP = \sqrt{1 - \frac{4 \det J}{(\text{tr } J)^2}}. \quad (4.1)$$

It is unity for fully polarized light and zero for unpolarized light.

## 4.3 Experimental Setup

In the experiment, we determine how the degree of polarization of the superposed signal beam depends on the two kinds of path information introduced in the signal and the idler beam. To this end, the experimental setup described in the previous chapter was modified in several aspects (see Fig. 4.1).

The two nonlinear crystals NL1 and NL2 are pumped coherently such that either of them can emit photon pairs. The idler beams are overlapped to be indistinguishable and a variable

attenuator of transmission  $T$  placed in the idler beam between the two sources. Both nonlinear crystals initially emit horizontally (H) polarized photons. A half-wave plate (HWP) is placed in the signal beam emerging from NL1, which rotates the linear polarization by an angle  $\gamma$ . That is, the initially horizontally polarized  $S_1$  beam is transformed according to  $|H\rangle_{S1} \rightarrow \cos \gamma |H\rangle_{S1} + \sin \gamma |V\rangle_{S2}$ .

After superposing both signal beams on a non-polarizing beam splitter, the combined beam is detected behind a quarter-wave plate (QWP) and a linear polarizer (Pol). These elements are used to perform polarization state tomography [156] on the signal photons leaving the interferometer.

## 4.4 Performed Measurements

In the experiment, quantum state tomography is performed on the signal beam for different values of  $T$  and different rotations  $\gamma$  of the polarization of the  $S_1$  beam. In each setting of  $\gamma$  and  $T$ , the interferometric phase is set to constructive interference by maximizing the intensity in the horizontal polarization of the outgoing photons (after setting QWP and P to project onto H).

Experimentally, different settings of  $T$  are implemented using a variable neutral density filter (Thorlabs NDC-100S-4M) in the idler beam between the two crystals. For each setting, the transmission is determined using a separate laser and a power meter before and after the filter. The filter has a physical width of approximately 2 mm and thus introduces an additional delay in the optical path of the idler beam. After inserting the filter, the setup needs to be realigned in order to satisfy the coherence length requirements (Sec. 2.4.4). For this reason, the maximal value of  $T$  is implemented with the filter in place at the “full transmission” setting instead of removing it completely.

The polarization state tomography is performed by rotating QWP and Pol successively to project photons onto a set of different basis states<sup>28</sup> and measuring the respective count rates per 15 seconds each. A maximum likelihood estimation is used to “fit” the best matching density matrix to this set of measurements [156].

The coherency matrix  $J$  is computed from each reconstructed density matrix. For each setting of  $T$  and  $\gamma$ , the corresponding degree of polarization [145] is determined using Eq. 4.1 [92].

---

<sup>28</sup>horizontal: H, vertical: V, diagonal: D, anti-diagonal: A, right and left circular: R and L.

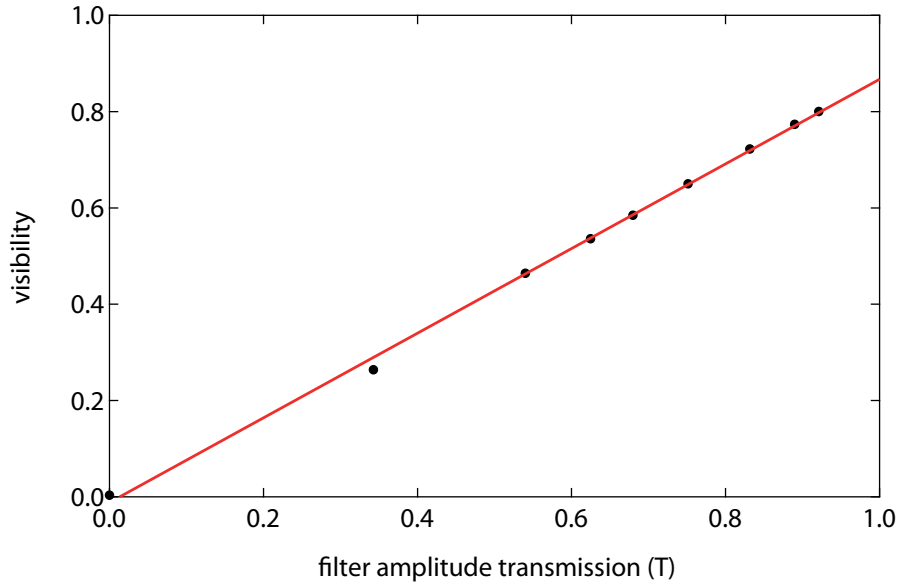


**Figure 4.2:** Visibility observed in the horizontal polarization component as a function of the transmission of the idler beam. The linear dependence on  $T$  for our experiment is a signature of the low gain, “quantum” regime (see Sec. 2.7). This result confirms that our experiment operates in this regime. The linear fit evaluates to  $V = (0.863 \pm 0.006)T$ , indicating a visibility of 86% that can be achieved without any filter.

## 4.5 Results

### 4.5.1 Degree of Polarization and Path Distinguishability

The dependence of the degree of polarization of the signal beam on the transmission in the idler beam is shown in Fig. 4.3.

In the case of no polarization rotation, both signal beams are horizontally polarized. Consequently, the  $DoP$  of the superposed beam is maximum for all values of idler transmission (blue curve in Fig. 4.3). The signal beams interfere with a visibility proportional to  $T$  (Fig. 4.2). The linear dependence confirms that stimulated emission can be neglected and our experiment operates in the “quantum regime” (see Sec. 2.7).

In the case of orthogonal polarizations of the signal photons from the two sources, the interferometric visibility is zero. However, in this case, the  $DoP$  can be controlled by tuning the transmission of the idler beam between the crystals (green curve in Fig. 4.3). It theoretically varies linearly between zero and one without being accompanied by a change in intensity. In the experiment, the  $DoP$  could be adjusted between  $0.081 \pm 0.003$  and  $0.92 \pm 0.01$ . We attribute the deviation from the ideal case  $0 \leq DoP \leq 1$  to the fact that our non-polarizing beam splitter was in fact slightly polarizing and the intensities of the two sources were not perfectly balanced. Moreover, due to imperfect alignment of the idler beams and residual reflections, the maximum observed visibility did not exceed 86%. These imperfections were taken into account in the theoretical simulations of our measurement results in Fig. 4.3.

In the intermediate case of non-orthogonal polarizations of the two signal beams, partial interferometric visibility is observed together with partial polarization. As can be seen from Fig. 4.3, the results agree well with the theoretical predictions (see Sec. 4.6).

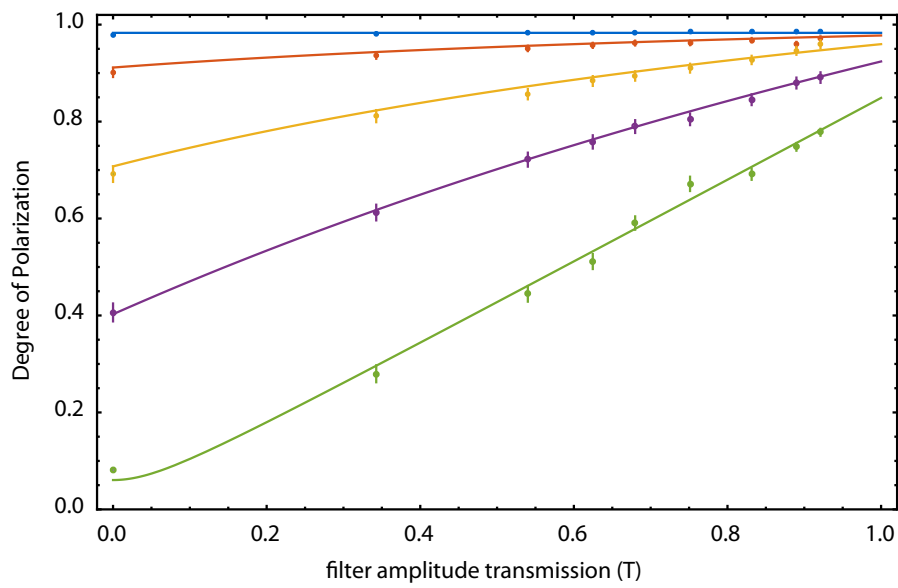


**Figure 4.3:** Degree of Polarization (*DoP*) of the superposed signal beam as a function of the transmission in the idler beam between the two crystals. The data points are obtained by evaluating the DoP from the reconstructed density matrices. The results are compared to the theoretical predictions (solid lines) taking into account experimental imperfections (see text). Different colors signify different polarization rotations of the  $S_2$  beam with respect to the horizontally polarized  $S_1$  beam:  $\gamma = 0^\circ$  (same polarization, blue),  $\gamma = 22^\circ$  (red),  $\gamma = 44^\circ$  (yellow),  $\gamma = 66^\circ$  (purple),  $\gamma = 90^\circ$  (orthogonal polarization, green).

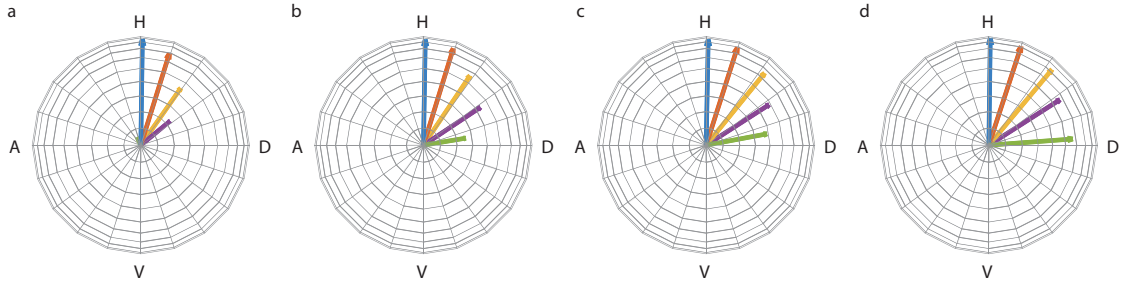


**Figure 4.4:** Bloch/Poincaré sphere representation of the reconstructed polarization states of the signal photons. The arrow colors represent the polarization rotation of the HWP ( $\gamma = 0^\circ$  (blue),  $\gamma = 22^\circ$  (red),  $\gamma = 44^\circ$  (yellow),  $\gamma = 66^\circ$  (purple),  $\gamma = 90^\circ$  (green)). The different plots correspond to different transmission values of the attenuator in the idler beam ( $T = 0$  (a),  $T = 0.54$  (b),  $T = 0.68$  (c),  $T = 0.92$  (d)). In the case of zero transmission, the polarization goes from completely polarized to completely unpolarized. In the case of maximum transmission (92%), the degree of polarization is almost unchanged by varying  $\gamma$ . However the polarization state varies between D and H.

#### 4.5.2 Reconstructed Quantum States

It is interesting to analyze how the polarization state changes as the distinguishability is varied during this experiment. In Fig. 4.4, the polarization of the outgoing signal beam is represented on Bloch/Poincaré spheres for different settings of  $\gamma$  and  $T$ .

In the case of zero transmission  $T = 0$  (Fig. 4.4a), the signal beams from the two individual sources are mutually incoherent and no interference can be observed. By increasing  $\gamma$ , the polarization of the  $S_1$  beam is rotated from H to V, while the  $S_2$  beam remains horizontally polarized. Thus the relative intensity between (mutually incoherent) horizontal and vertical components is modified from initially zero vertical polarization to 50% with  $\gamma = 90^\circ$ . The beam therefore undergoes a transition from fully polarized to unpolarized upon rotating  $S_1$  from H to V.

In the ideal case of perfectly indistinguishable idler beams ( $T = 1$ ), the rotation of the first signal beam's polarization does not change the degree of polarization of the superposed beam. The reason for this is that the two beams are fully coherent. This coherence manifests itself as interference in the case of equally polarized signal beams. On the other hand, the coherent superposition of two orthogonal polarizations results in a fully polarized state that is a superposition of two orthogonal directions. Varying the interferometric phase rotates the resulting state on the Bloch sphere. Depending on the relative polarization direction between the two signal beams, intermediate states are possible. Experimentally, the case  $T = 1$  cannot be realized perfectly due to imperfect alignment of the two idler beams and residual losses on the propagation between the two crystals. Nevertheless, a weaker dependence of the DoP on  $\gamma$  is observed for increased transmission  $T$  (see Figs. 4.3 and 4.4).

Interestingly, if  $T$  and  $\gamma$  are both in the intermediate range, the degree of polarization depends on the relative phase of the interferometer. This can be confirmed by the general expression of the DoP (Eq. 4.6). Intuitively, the horizontal polarization components partially interfere, while any vertical polarization component can only come from NL1 and its intensity is thus phase-independent. This results in a phase dependent intensity balance of the horizontal and vertical polarization components.

This fact raises interesting questions about how to relate the degree of polarization to path information that is in general phase-independent. An experiment addressing the issue of phase-dependent path information in a different context is presented in Chapter 6.

## 4.6 Theoretical Quantum States in the Experiment

The results can be understood considering the quantum state of light in our system. The HWP in the  $S_1$  signal beam is represented by the transformation

$$|H\rangle_{S_1} \rightarrow \cos \gamma |H\rangle_{S_1} + \sin \gamma |V\rangle_{S_1}, \quad (4.2)$$

where  $\gamma$  varies between  $0^\circ$  (no rotation) and  $90^\circ$  ( $H \rightarrow V$ ).

The quantum state in this system before the HWP can be described analogously to Eq. 2.21 in a notation that includes the polarization degree of freedom,

$$|\psi\rangle = (T|H\rangle_{S_1} + e^{i\varphi}|H\rangle_{S_2}) |H\rangle_I + \sqrt{1 - T^2} |H\rangle_{S_1} |H\rangle_{I_l}. \quad (4.3)$$

The mode  $I_l$  represents the portion of the idler beam lost due to absorption or imperfect alignment between the two crystals. Using Eq. 4.2, we obtain

$$|\psi\rangle = (T \cos \gamma |H\rangle_{S_1} + T \sin \gamma |V\rangle_{S_1} + e^{i\varphi} |H\rangle_{S_2}) |H\rangle_I + \sqrt{1 - T^2} |H\rangle_{S_1} |H\rangle_{I_l}. \quad (4.4)$$

The photon detection rate without polarizer in front of the detector is given by

$$R \propto 1 + T \cos \gamma \cos \varphi, \quad (4.5)$$

which exhibits interference with visibility  $V = T \cos \gamma$ .

The degree of polarization of the beam emerging from the final beam splitter is [92]

$$DoP = \frac{\sqrt{\cos^2 \gamma + T^2(\sin^2 \gamma + \cos^2 \gamma \cos^2 \varphi) + 2T \cos \gamma \cos \varphi}}{1 + T \cos \gamma \cos \varphi} \quad (4.6)$$

For the phase setting  $\varphi = 0$  (constructive interference in H), it reduces to

$$DoP = \frac{T + \cos \gamma}{1 + T \cos \gamma}. \quad (4.7)$$

The theoretical curves shown in Fig. 4.3 are computed based on this formula with experimental conditions taken into account.

## 4.7 Discussion

By examining Eq. 4.7, it is clear that the degree of polarization depends on two different kinds of introduced path information. The “degree of indistinguishability” of the idler beams is represented by  $T$ , whereas  $\cos \gamma$  can be regarded as a measure of the indistinguishability of the two signal beams. From this point of view, the degree of polarization depends on the two kinds of path information in a symmetric way. These two kinds of path information are of fundamentally different nature. Whereas the information present in the signal beam’s polarization can in principle be “quantum erased”, by detecting it behind a polarizer, the distinguishability introduced by the idler photons cannot be erased (as long as no coincidence detection is used, see Sec. 2.4.1 and 2.4.2.)

Partial polarization can be obtained only if path information is introduced in both ways, i.e.  $T < 1$  and at the same time  $\cos \gamma < 1$ . On the other hand, if either  $T = 1$ , or  $\cos \gamma = 1$  (i.e. path information is introduced at most in one of the two ways), the beam is fully polarized with  $DoP = 1$ . A fully unpolarized beam can theoretically be obtained by setting both  $T = 0$  and  $\cos \gamma = 0$ .

It is interesting to ask the general question of whether partial polarization is a result of detecting a statistical mixture of completely polarized photons, or whether every individual photon

is partially polarized. As the quantum states in our experiment are reconstructed from a large number of photon detections, the results themselves do not conclusively favour one interpretation over the other. However, our experiment allows to translate the above question to the question of whether partial source-information exists for every single photon in a ZWM interferometer, or whether a definite fraction of photons are fully distinguishable and the remaining photons completely indistinguishable. A discussion of the analogous question in the spectral domain is addressed in [98].

## 4.8 Conclusion

We have shown that the degree of polarization of photons can be controlled without interacting with the photons directly. This was done by superposing two beams with different polarization on a beam splitter and varying their mutual coherence in a third beam. The amount of distinguishability of the two idlers results in an arbitrary degree of polarization of the signal photons.

Our experiment thus demonstrates a situation, in which partial polarization results from distinguishability between mutually orthogonal polarization components. As the underlying effect of induced coherence without induced emission cannot be quantitatively described by classical theory (see Sec. 2.7), quantum mechanics is needed to explain the physical origin of (partial) polarization in our experiment.

# Delayed-Choice Frustration of Down-Conversion

## 5.1 Motivation and Goal

It has been shown that the spontaneous emission rate of an atom is modified compared to its free-space value, if the atom is placed in the vicinity of a reflecting mirror (e.g. [118, 125]). The physical interpretation of this effect is subject of discussion (see Sec. 2.8), particularly in the case of completely suppressed emission in the direction opposite of the mirror. Specifically, the question was raised, whether the atom entirely stops to emit (even towards the mirror), or whether the rate of detected photons is suppressed by destructive interference [136].

The optical effect of suppressed or enhanced down-conversion in the vicinity of mirrors (Sec. 2.4.3) bears strong analogies to this problem, as discussed in Sec. 2.8.3. The analogy is particularly intuitive considering the original experimental implementation of “frustrated two-photon creation via interference” [15] (Fig. 5.1). In the case of suppressed emission of SPDC towards the detectors, the following question may be asked: does the crystal emit photon pairs towards the mirrors, or does no down-conversion take place at all [114, 139]?

The experiment described in this chapter aims to investigate this question. We effectively realize a situation in which one of the mirrors in Fig. 5.1 is suddenly replaced by a detector, as proposed in [114, 139]. If, during suppressed emission, no photons are emitted at all by the crystal, it would take the light travel time between mirror and crystal for the changed environment to affect the emission properties at the crystal. Only then, photon pairs would be emitted. This would result in a measurable delay of photon detections at the inserted detector. We experimentally determine, whether such a delay exists.

Our experiment can be regarded as an instance of a delayed-choice experiment, which investigates quantum complementarity in an unusual situation. As discussed in Sec. 5.7, it can be interpreted as a test, whether a photon pair “decides” a priori (before the time it could be emitted by the first SPDC process), if it interferes or if it originates from a definite one of the SPDC processes. In that sense, we investigate, whether the mere existence of a photon pair can be

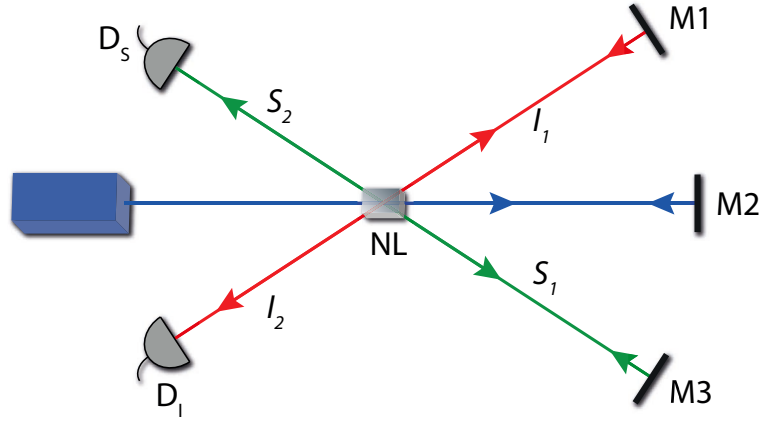


**Figure 5.1:** Experimental setup for the observation of frustrated down-conversion as implemented in [15]. A pump laser passes through a nonlinear crystal in two directions, allowing for photon pair generation either in the modes  $S_1$  and  $I_1$ , or in the modes  $S_2$  and  $I_2$ . These two alternatives are aligned to be indistinguishable by reflecting the photon beams back through the crystals. A photon arriving at the detector does not carry any information by which of the two alternatives it had initially been emitted. The rate of detected photon pairs can be suppressed or enhanced depending on the precise distances between the mirrors and the crystal.

regarded as a real property independent of measurement, or rather a quantum property of the electromagnetic field mode, which can be in a superposition state.

## 5.2 Outline of the Experiment

The goal of this experiment is to test whether a suddenly inserted detector during suppressed emission would register photons immediately or after a time delay. To this end, we implement a fast switch, which directs the photon beam towards a detector instead of the mirror (Fig. 5.2). This switch is realized using an electro-optical modulator (EOM) in conjunction with a polarizing beam-splitter (PBS), as proposed in [114, 139]. The EOM (see Appendix A.2.3) can rotate a photon’s polarization, which causes it to travel via one or via the other output beam of the PBS, either towards the mirror or towards the detector.

The experiment is performed as follows. The setup is adjusted to observe the suppression of SPDC, such that ideally no photons are emitted by the system of two indistinguishable SPDC processes. In this configuration, we switch from mirror to detector. As this new situation corresponds to a measurement of which of the two processes a photon pair originated from, no interference is observed and photons are detected. The time to switch from mirror to detector is faster than the light travel time between nonlinear crystal and EOM. Thus, given it is constrained by the speed of light, the information that a detector had been inserted cannot affect the crystal immediately after the switching.

The arrival times of photons at the “inserted” detector on a short time-scale after the switching are analyzed. From the observed data, we aim to determine, whether the photons had already been emitted by the time the switching was performed, or whether they were emitted from the crystal only after the mirror was switched off.

This goal imposes several interdependent requirements on our experimental apparatus. First, the timing resolution needs to be short enough to distinguish whether the rise in count rate occurs immediately or a few nanoseconds later, i.e. after a light signal from the switch could in principle have triggered an emission at the crystal. This is accounted for by choosing the distance



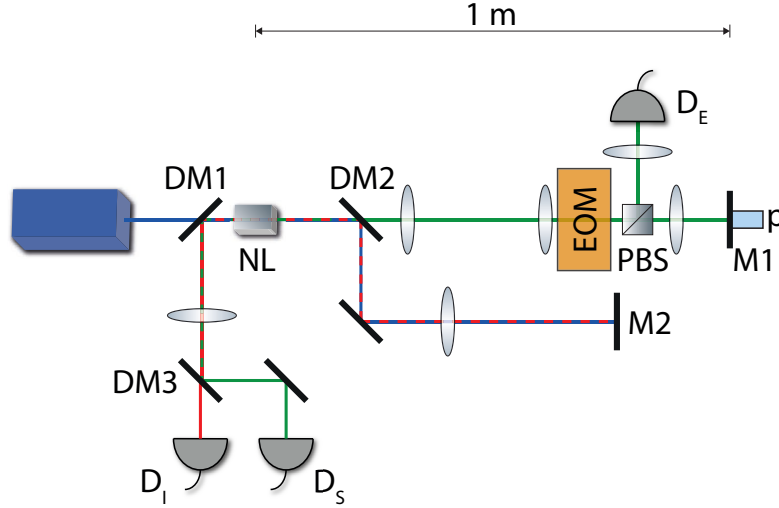


**Figure 5.3:** Implementation of the experimental setup. A laser beam illuminates a nonlinear crystal (NL) which emits collinear photon pairs with non-degenerate wavelengths (signal: 841 nm, idler 782 nm). The pump laser and idler beams are reflected back through the crystal via DM2 and M2. The signal beam passes an electro-optical modulator (EOM) and is either reflected back through the crystal via M1 if the EOM is off or detected at  $D_E$  with the EOM switched on. With the EOM off, signal and idler photons are detected by two detectors  $D_S$  and  $D_I$ . A photon pair can arrive at the detectors in two indistinguishable ways, giving rise to an interfering rate of photon detections. The distance between NL and the mirrors M1 and M2 is 1 m. The EOM is located 77 cm behind NL.

## 5.3 Implementation

### 5.3.1 Experimental Setup

The setup is depicted in Fig. 5.3. A pump laser (Toptica DL 100, 405 nm, CW) illuminates a non-linear crystal (20 mm ppKTP), which emits horizontally polarized photon pairs at 782 nm (idler) and 841 nm (signal) wavelength by collinear type-0 SPDC. Subsequently, the laser is back-reflected using dichroic mirror DM2 and mirror M2 to pass through the crystal a second time. In this way, down-converted photon pairs can be emitted in either of two opposite directions.

The signal and idler beams generated during the first pass of the pump beam are reflected back through the crystal as well. The idler beam follows the same path as the pump beam and is reflected by DM2 and M2, whereas the signal beam is transmitted by DM2 and reflected by M1. The reflected photon beams are aligned to be indistinguishable from the down-converted beams created in the second pass of the pump beam and subsequently detected behind (5 nm bandwidth) bandpass filters, using single-mode fiber coupled avalanche photo-diodes  $D_S$  (signal) and  $D_I$  (idler). Photons arrive at the detectors in the same pair of spatio-temporal modes, irrespective of whether they were initially emitted from the crystal in forward or in backward direction. The indistinguishability between the two alternatives of creating a photon pair leads to interference, which results in a phase dependence of the rate of emitted photon pairs.

Using an electro-optical modulator (EOM) followed by a polarizing beam splitter (PBS) in the signal beam, we implement a switch that is capable of effectively inserting a detector ( $D_E$ ) in place of mirror M1. For details about the operation and the alignment of the EOM, see Appendix A.2.3. The detector  $D_E$  detects only signal photons generated in the first (forward) SPDC process.

As long as the EOM is switched off, it does not alter the photon's polarization. The signal photons remain horizontally polarized and traverse the PBS. If the EOM is switched on, however,

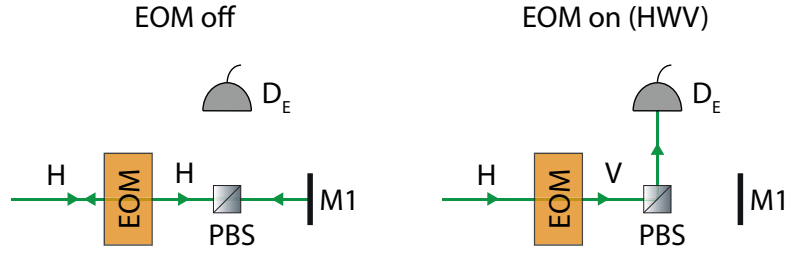


**Figure 5.4:** Principle of using the EOM in combination with a PBS for switching the photon path. As long as no voltage is applied, horizontally polarized photons pass through the EOM and are reflected back via mirror M1. A voltage is applied, which results in a delay of the diagonal polarization component by half the wavelength with respect to the antidiagonal component (half-wave-voltage, HWV). As a result, the polarization of photons passing through the cell is rotated from initially horizontal to vertical. Vertically polarized photons are reflected by the PBS towards the detector  $D_E$  instead of being reflected.

the polarization of signal photons generated in the first SPDC process is rotated from horizontal to vertical. Consequently, signal photons are reflected by the PBS towards  $D_E$  (Fig. 5.4). In this case, the setup corresponds to a measurement of the origin of each photon pair. Pairs created by the first pass of the pump beam through the crystal are registered at  $D_E$  and  $D_I$ , whereas photon pairs created in the second pass of the pump beam through the crystal arrive at detectors  $D_S$  and  $D_I$ .

### 5.3.2 Distances and Switching Times

The distance between NL and the mirrors M1 and M2 is 1 m, corresponding to a light travel time of  $\approx 6.7$  ns both ways. The path length differences are fine-adjusted to meet the coherence requirements for observing interference (Sec. 2.4.4). The EOM is situated at 77 cm after NL, such that photons take at least a time of 2.5 ns to travel to the EOM, after they have been emitted from the crystal. The EOM is switched by applying a voltage, which is performed in less than 2 ns (see Appendix A.2.3 for details on the measurement of the switching time). It is thus possible to change the configuration between the measurement of a photon's origin and the observation of interference on a time-scale faster than the “flight-time” of photons between crystal and mirror.

### 5.3.3 Lens Systems

A number of lenses are installed in the setup, which are used to ensure indistinguishability of the photon pairs. Idler and pump beams are imaged from the crystal back onto the crystal during their passage through the half-cavity between NL and M2. This is done using an achromatic lens, which is traversed twice between the two crystal passes in a way that it forms a  $4f$  imaging system. The signal beam is also imaged between the two crystal passes. However, as it passes through the small aperture of the EOM (4 mm diameter), this is done using three lenses, each of which is passed twice. In this configuration,  $4f$ -imaging is performed between the crystal and the EOM (ensuring a small beam inside the EOM) as well as on the path between EOM and M1 which is passed twice (see Fig. 5.3). All detectors are situated in the Fourier plane of the crystals. The imaging systems ensure that a plane wave of either signal or idler beam as decomposed at the crystal corresponds to a plane wave after being reflected back onto the crystal. This “mode-matching” is essential for maximizing the interferometric visibility.

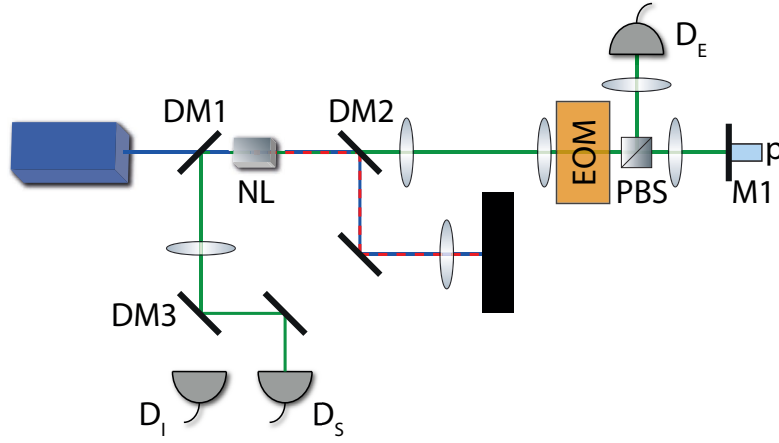


**Figure 5.5:** Experimental setup for the reference measurement. Switching and detection times are calibrated by blocking both idler and pump beams after they exit the nonlinear crystal. In this configuration, the pump beam passes the crystal only in a single direction. Photon pairs can only be generated during this pass of the pump beam through the crystal and are emitted towards the right. Signal photons can be either detected at  $D_E$ , if the EOM is switched on, or reflected back via M1-DM1-DM3 and be detected by  $D_S$  (with the EOM switched off). No interference occurs in this configuration.

## 5.4 Characterization and Calibration

### 5.4.1 Reference Measurement

The time-dependence of the EOM's switching profile is characterized as follows. Both pump and idler beams are blocked after the first pass of the pump beam through the crystal (Fig. 5.5). In this configuration, the setup is simply a photon pair source consisting of a nonlinear crystal pumped by a laser beam. Consequently, no interference can occur as there is only one possible way for photon pairs to be emitted. The EOM is switched periodically with a repetition rate of 100 kHz and an on-time of 50 ns.

Photon detections at all three detectors ( $D_S$ ,  $D_I$ , and  $D_E$ ) as well as the electronic trigger signal used for switching the EOM are recorded using a time-tagging-module (TTM). The photon arrival times are assigned to 660 ps long time-bins. The time differences between an EOM trigger signal (see Appendix A.2.2) and successive photon detections are evaluated. This produces a histogram of photon detections at a given time after the previous switching signal (in a similar way as a triggered oscilloscope). The results of the calibration measurement are presented in Fig. 5.6.

The arrival time data exhibits periods in which the EOM is switched off (gray background) and a period (about 47 - 98 ns after the trigger signal) in which the EOM is switched on (white). During the EOM off-time, signal photons are detected at  $D_S$ , whereas when the EOM is switched on, they are detected at  $D_E$ . At any time, only background noise is detected at  $D_I$ , which is expected as the idler beam is blocked. Note that the count rates are normalized and the time origins of the traces of  $D_S$  and  $D_I$  have been shifted in order to allow for direct comparison (compensating for unequal response times of the detectors). The shifts are determined by analyzing coincident detections between all detector combinations (see Appendix A.2.4.2).

From the data, several parameters are extracted that are used for later analysis. The time between the count rate of  $D_E$  rising from 10% to 90% is evaluated to  $1.9 \pm 0.1$  ns (see Appendix A.2.3). The time difference between the recording of the EOM trigger signal and the registration of photons at  $D_E$  is roughly 47 ns. This number includes electronic delays in the EOM driver, cables, as well as the response times of the detectors. The measured switching profile is used

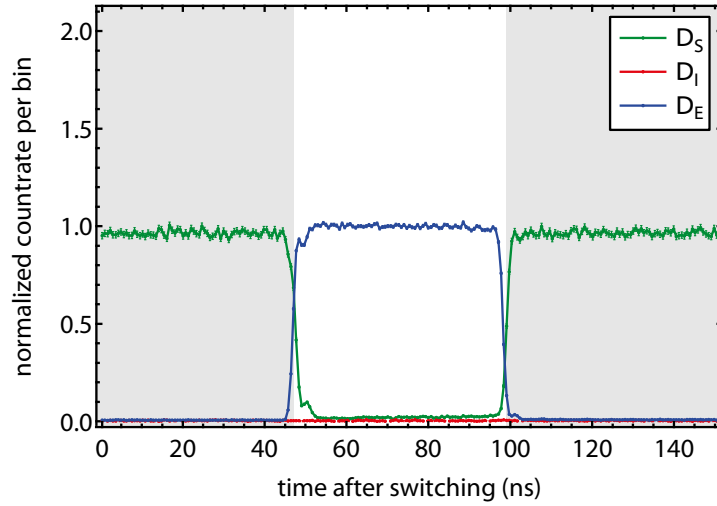


**Figure 5.6:** Result of the reference measurement with blocked idler and pump beams. The curves show the accumulated counts per (660 ps wide) time bin in the respective detector. The time scale represents the time between an electronic signal triggering the EOM and the arrival of photons at the detectors. The origins have been shifted for  $D_S$  and  $D_I$  such that the arrivals of two photons belonging to the same pair appear in the same time bin. Note that this does not affect the trace of  $D_E$ , which is used for further evaluation. During this measurement, pump and idler beams were blocked after the crystal (see Fig. 5.5) and  $D_I$  only detects residual background. While the EOM is switched off (gray background), signal photons produced in the crystal are reflected by M1 and subsequently detected at  $D_S$ . Consequently, during this time, no photons arrive at  $D_E$ . From  $t \approx 47$  ns to  $t \approx 98$  ns, the EOM is switched on (white background). During this time, signal photons arrive at  $D_E$ . The count rates are normalized with a value of 1 corresponding to the detection rate from one SPDC process.

to compute the predictions for both delayed and immediate scenarios (Sec. 5.6.2) in the case of suppressed down-conversion.

## 5.5 Measurement During Destructive Interference

After the calibration, all blocks are removed and an interfering photon pair emission rate was observed. The interferometric phase is set to destructive interference using the piezo attached to mirror M1 (Fig. 5.3). The EOM is switched periodically (repetition rate 100 kHz, 50 ns on-time) and time-tags of photon detections at all detectors are recorded.

### 5.5.1 Visibility and Stability

During the measurement, the visibility is monitored by performing a phase scan every 60 seconds. This is done using a piezoelectric crystal attached to mirror M1. After each visibility measurement, the interferometric phase is reset to observe a minimum in the count rate at the detectors  $D_S$  and  $D_I$ . The start and end times of these visibility measurements are recorded using the TTM and the corresponding time periods are excluded from later evaluation<sup>29</sup>. As an illustration of this procedure, Fig. 5.7 shows a segment of the raw count rate of  $D_S$  during the experimental run. The count rates slightly fluctuate around the minimum until every minute, the phase is scanned to observe the maximum count rate and subsequently reset to the minimum. The results of the visibility measurements during the entire experiment are presented in Fig. 5.8. The measured values are  $78 \pm 2\%$  at  $D_S$  and  $76 \pm 2\%$  at  $D_I$ .

Note that throughout this chapter, the term “visibility” is used to quantify how close the experiment comes to the theoretically perfect suppression and enhancement of photon pair emission. In analogy to its use in traditional interferometry, the visibility is defined as  $V = (I_{max} - I_{min}) / (I_{max} + I_{min})$ , where  $I_{max(min)}$  denotes the maximum (minimum) photo counting rate at the respective detector as the interferometric phase is varied. It is possible to interpret  $V$  as fraction of photons that perfectly interfere, whereas the fraction  $1 - V$  is unaffected by a change of phase.

In a standard interferometer, the probabilities for a fraction  $V$  of the photons leaving the beam-splitter on one or the other output path is modified by changing the relative path lengths in the interferometer. The total number of detected photons in both outputs remains constant, which can be checked by summing the number of detection events in the two output paths (proportional to  $\sin(\phi/2)^2$  and  $\cos(\phi/2)^2$ ).

The physical interpretation of visibility in the interference phenomenon considered here is different. In contrast to a traditional interferometer, the interference phenomenon does not alter the the probabilities of a photon leaving a beam splitter in one or the other path, but the absolute number of down-converted photons emitted by the system. If photon emission is completely suppressed, this probability is zero; there is no other bright output port, in which the “missing” down converted photons could be detected. Instead, at least theoretically, the second output of this interferometer corresponds to the occupation of the respective pump mode.

<sup>29</sup>As during the visibility measurements, the phase setting deviates from destructive interference.

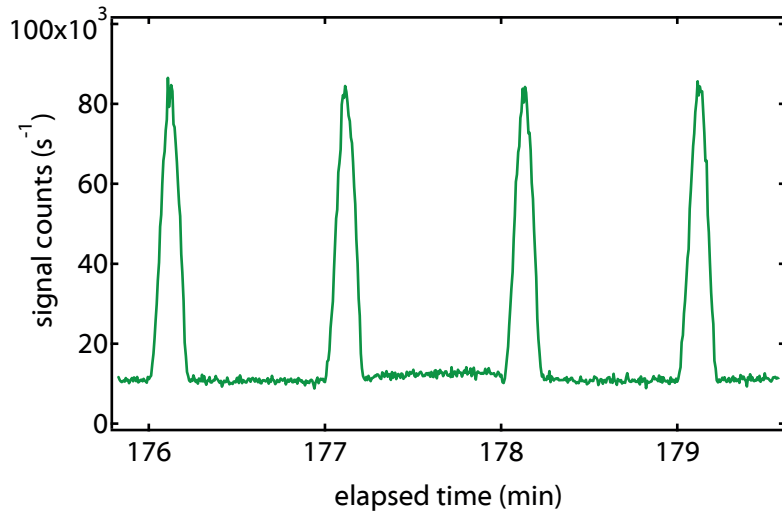


**Figure 5.7:** Excerpt of the single detection rate in the signal beam measured at  $D_S$ . Every 60 seconds, a phase scan is performed and the visibility is evaluated. Subsequently, the phase is adjusted back to the minimum value. Small phase fluctuations during the time of destructive interference between two consecutive scans are considered in the data analysis.

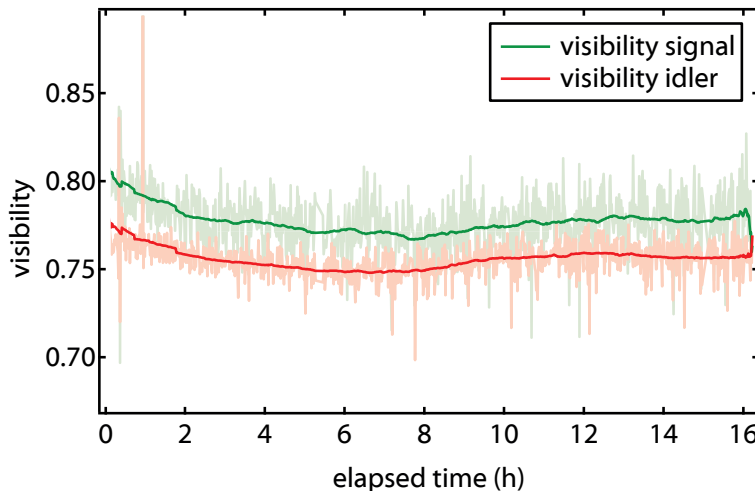


**Figure 5.8:** Measured visibility of signal (green) and idler (red) during the experimental run. The light colored curves show the results of each individual visibility measurement during the experimental run, whereas the dark colored lines are moving averages. Over the entire experimental run, the mean visibilities were determined to  $78 \pm 2\%$  in the signal and  $76 \pm 2\%$  in the idler beams.

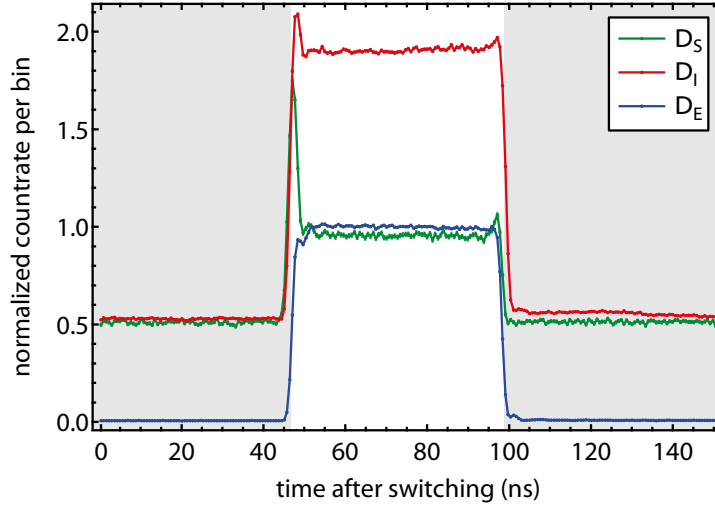


**Figure 5.9:** Time resolved detection events during suppressed emission. While the EOM is switched off (gray background),  $D_E$  detects only noise photons. The count rates at  $D_S$  and  $D_I$  are reduced due to destructive interference. From  $t \approx 47$  ns to  $t \approx 98$  ns, the EOM is switched on (white background) and the system is no longer interfering. In this case, signal photons emitted from the crystal into one direction arrive at  $D_E$  and signal photons emitted in the opposite direction arrive at  $D_S$ . All idler photons are registered at  $D_I$ . The “spikes” observed at  $D_S$  and  $D_I$  during the transient time between the on and off states are attributed to a phase shift introduced by the EOM during the switching. The same delay-corrections and normalization are used as in Fig. 5.6.

## 5.6 Results

### 5.6.1 Time Dependent Frustrated Down-Conversion

The resulting histograms of photon arrival times at all three detectors are presented in Fig. 5.9. During the EOM off-time (shaded area), the system shows destructive interference and a minimum in the count rate of  $D_S$  and  $D_I$  is observed. Practically no photons are recorded at  $D_E$  during this time ( $6.1 \pm 0.6 \times 10^{-3}$  times the rate of a single SPDC process), as the detector is “switched out”. Electronic delays at  $D_S$  and  $D_I$  are compensated for in the same way as in the reference measurement (see Appendix A.2.2).

At the time interval during which the EOM is switched on (white background in figure),  $D_E$  detects signal photons produced in the first (forward) SPDC process. Consequently, interference is lost and the detection rates at  $D_S$  and  $D_I$  increase. Compared to the reference measurement,  $D_I$  records twice as many idler photons during the on-time. This is expected as now two (non-interfering) SPDC processes contribute to this count rate, compared to only one in the calibration measurement. The detected signal photons are roughly equally distributed between  $D_S$  and  $D_E$ . This is expected as the two detectors correspond to photon pairs produced in the two possible SPDC processes. Each of the two detectors receive about the same amount of photons as  $D_E$  detected in the calibration measurement, where only a single SPDC process was pumped.

An interesting feature in Fig. 5.9 is a temporary increase in photon detections at  $D_S$  and  $D_I$  lasting about 2-3 ns during the transient time between on- and off states of the EOM. This increase was not observed in the calibration measurement (compare Fig. 5.6). We attribute it to a phase shift that is accumulated by signal photons traveling through the EOM, while it is switching, before the polarization is completely rotated from horizontal to vertical and which is connected to the piezoelectric ringing of the device. A separate measurement revealed that a similar feature can be observed, when the EOM is rotated in a way that it does not alter the horizontal polarization of photons passing through it, but switches at the same rate, which

results in periodic phase-shifts.

### 5.6.2 Quantitative Predictions for Photon Arrival Times at the Inserted Detector

In order to determine, whether the photons recorded at  $D_E$  are delayed or not, we compare the measured photon arrival times to the arrival times obtained in the calibration measurement. In the absence of a delay, photons could be detected immediately after the insertion of the detector [136, 139]. The photon detection times are expected to exhibit the same time-dependence as in the case of no interference. This can be stated quantitatively as

$$P_{im}(t) = P_r(t), \quad (5.1)$$

where  $P_{im}(t)$  represents the detection probability at the inserted detector  $D_E$  at a given time after the EOM switching signal during suppressed emission in the case of no delay (immediate detection).  $P_r(t)$  is the detection probability given by the technical properties of our EOM and detectors, as it has been determined in the reference measurement (Sec. 5.4).

In contrast, a model according to which no emission happens at the crystal during destructive interference would manifest itself in a shift of the arrival times of interfering photons by the delay time  $\tau$ .

As the experiment does not exhibit perfect visibility ( $V < 1$ ), the emission is not completely suppressed. It is possible to interpret this observation as a fraction  $V$  of photon pairs interfere and a fraction  $1 - V$  of non-interfering photons being constantly present as background. These non-interfering photons could in principle be detected at all times and are thus expected to follow the same time dependence as in the reference measurement,  $P_r(t)$ . If the imperfect visibility is accounted for in the delayed scenario, it leads to the following quantitative prediction,

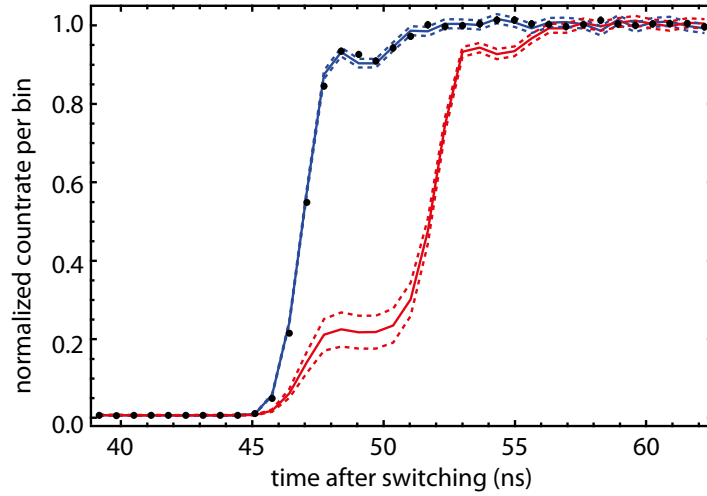
$$P_{delay}(t) = VP_r(t - \tau) + (1 - V)P_r(t). \quad (5.2)$$

A model, according to which the nonlinear crystal needs to be affected by the switching, predicts a delay of the travel time of light between the mirror and the crystal until photons are emitted. After an additional delay of the light travel time between crystal and detector  $D_E$ , photons would be detected. In our setup, this amounts to a total delay of  $\tau = 6.7$  ns.

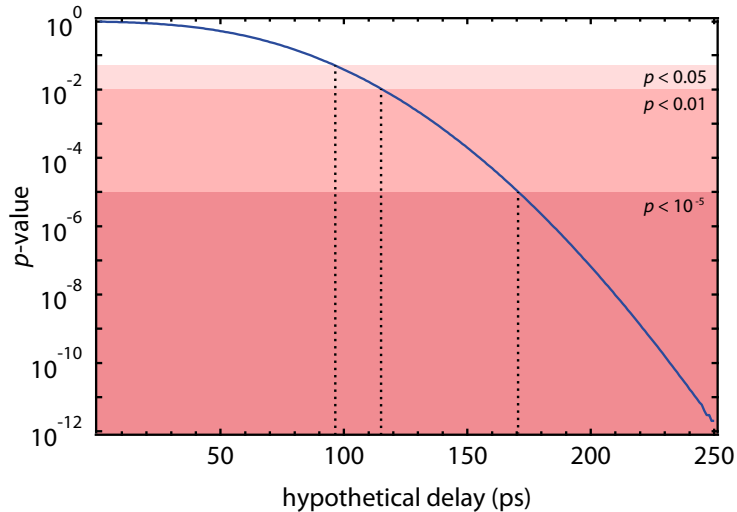
### 5.6.3 Experimental Constraints on Hypothetical Delay

Figure 5.10 depicts the resulting predictions for zero delay ( $P_{im}(t)$ , blue curve, from calibration measurement) and for a delay of 6.7 ns ( $P_{delay}(t)$ , red curve). Both curves were computed numerically using the results of the reference measurement  $P_r(t)$  and the measured average visibility values  $V$ . The data observed during destructive interference are shown as black dots and agree well with the calibration measurement. The results are thus consistent with the absence of a delay.

In order to quantify the compatibility of our data with a model that predicts an arbitrary delay, we compute a  $p$ -value according to a simple test statistic given by the accumulated photon counts at  $D_E$  in the time interval of 46 to 56 ns after the switching. This is used to compare the predictions (Eq. 5.2) of models with different values of delay to our data. The results are depicted in Fig. 5.11. A model that predicts a delay of more than 170 ps is almost impossible to be consistent with the measured data ( $p < 10^{-5}$ ). This delay corresponds to a distance of less than about 5 cm between the first detected photons and the EOM at the time the switching took place. As a result, the first detected photons must have been emitted by the crystal already 2.5 ns *before* the switching took place. The results are consistent with the prediction, according to which an inserted detector can immediately register photons.



**Figure 5.10:** Delay histogram of the data recorded at  $D_E$  (black points) compared to two different predictions. The blue curve represents the histogram corresponding to a prediction of zero delay, which is identical to the histogram obtained in the reference measurement. The red curve is calculated under the assumption that interfering photons are delayed by twice the light traveling time between NL and EOM (6.7 ns). The shoulder at about 0.2 intensity is a result of the imperfect visibility in the experiment. As the photon emission is not completely suppressed during destructive interference, a fraction of the photons can in any case be detected without delay. Both curves exhibit a small oscillation before the maximum intensity is reached (at around 0.9 intensity), which is attributed to piezoelectric oscillations of the Pockels cell. The dashed lines represent 68% confidence bounds of the predicted count rates. The uncertainty is computed taking into account the error in the visibility measurement, counting statistics, detector jitter and the effect of phase drifts during the measurement. The data matches closely with the predictions of a no-delay-scenario.



**Figure 5.11:** Incompatibility of delayed photon hypotheses with the observed data. The red shaded areas signify  $p$ -values below the commonly used thresholds of  $p = 0.05, 0.01$ , and  $10^{-5}$ . The results show to what significance (under our test statistic) the observed data is statistically incompatible with the predictions of a model in which photons are registered at  $D_E$  only after the respective time delay.

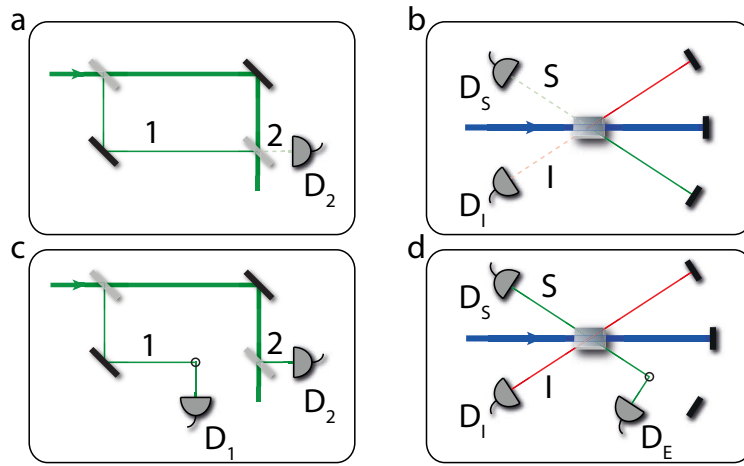


**Figure 5.12:** Analogy of our experiment to a delayed-choice interferometer. Figures a and c on the left-hand side depict a Mach-Zehnder interferometer with beam splitters of low reflectivity. It is possible to observe interference with high visibility at detector  $D_2$ , but low visibility in the other output of the interferometer (a). In analogy (a reflection at one of the beam splitters corresponds to down-conversion in one of the SPDC processes), high visibility can be observed in the suppression and enhancement of the down-converted beams in our setup (b). If a detector  $D_1$  is suddenly inserted into one of the paths of the interferometer (c), it could immediately detect photons. Detection in this experimental configuration corresponds to a measurement of which path was taken by the photon. In (c), a detection at  $D_1$  indicates that the photon was reflected at the first beam splitter, whereas a detection at  $D_2$  corresponds to the second beam splitter. The analogy to our experiment is indicated in (d). There, a detection at  $D_E$  indicates that the photon was down-converted in the first SPDC process, whereas a detection at  $D_S$  corresponds to the second SPDC process. The switching can be performed before or after the photon entered the interferometer without changing the results.

## 5.7 Interpretation and Discussion

The data show that a substantial delay between the insertion of a detector and the emission of photons at the crystal is incompatible with the observations. Our interpretation of this phenomenon is based on the analysis of delayed-choice experiments, as discussed below.

### 5.7.1 Complementarity in Frustrated Down-Conversion

#### 5.7.1.1 Analogy to Mach-Zehnder Interferometer

In the following, we analyze our experiment from the viewpoint of complementarity. This is done by comparing it to a situation in which complementarity has been discussed extensively. The interfering photon pair emission rate in frustrated down-conversion can be interpreted in analogy to the interference in an unbalanced Mach-Zehnder interferometer (MZI) [139] (Fig. 5.12). In this picture, the two possible SPDC processes correspond to two beam splitters with low reflectivity. The low reflectivity stands for the low probability of down-conversion in each individual SPDC process. The reflection from a beam splitter corresponds to the down-conversion of a photon pair, while the transmission through a beam splitter is analogous to a pump-photon passing through a crystal without down-converting.

Using this analogy, most features of the phenomenon of frustrated down-conversion can be recovered. In particular, interference with ideally perfect visibility can be observed in the reflected output of the second beam splitter (path 2 in Fig. 5.12a), which corresponds to the ideally perfect visibility in the rate of emitted photon pairs (paths S and I in Fig. 5.12b). The total suppression of photon pair emission in frustrated down-conversion (no detection events in  $D_S$  or  $D_I$  in

Fig. 5.12b) corresponds to completely destructive interference observed at  $D_2$  in Fig. 5.12a. Low visibility in the other, undetected, output path of the MZI corresponds to the practically unaffected intensity of pump photons exiting our setup.

The complementarity of a single photon in an interferometer is often expressed as complementarity between wave (the observation of interference) and particle behavior (obtaining which-path knowledge) of the photon [30]. Which-path knowledge in the interferometer means knowledge about whether an incoming photon is transmitted or reflected by the first beam splitter. In our experiment, this piece of information corresponds to knowledge about whether or not a pump photon is down-converted during its first pass through the crystal (compare Fig. 5.12c,d). The complementary property of interference can be interpreted as definiteness whether or not a photon leaves the interferometer in one or the other output port of the second beam splitter. In the extreme case of complete destructive interference in one output beam of the MZI, every photon would definitely exit the interferometer in the other. In our experiment, this property corresponds to definiteness whether or not down converted photons can be observed after *both* passes through the crystal.

As the two properties are complementary to each other, the exact knowledge of one precludes any knowledge about the other (see Sec. 2.2).

### 5.7.1.2 Are Photons Emitted During Frustrated Down-Conversion?

It is elusive to analyze the initial question “Does the crystal emit photons towards the mirrors (Fig. 5.12b) when down-conversion is completely frustrated at the detectors?” in light of this analogy. The corresponding question in the Mach-Zehnder setting (Fig. 5.12a) reads “Are photons reflected by the first beam splitter (into beam 1), when destructive interference is observed in the reflected path after the second beam splitter (beam 2)?”.

In quantum mechanics, this question is ill-defined. If it would have a definite answer, it would imply that we have obtained path information while at the same time observing interference. If a photon is definitely reflected by the first beam splitter, it would definitely arrive at the second beam splitter via path 1. This knowledge precludes the observation of interference and thus the second part of the question. In analogy, while observing frustrated down-conversion, it is impossible to give a definite answer to the question whether or not down-conversion occurred in the first pass of the pump beam through the crystal. This answer can only be obtained when a which-path measurement is actually performed, in which case it would be impossible to observe interference. The replacement of the mirror with a detector creates a new experimental situation, in which a different aspect of the quantum system is observed [8, 9].

The above analogy is consistent with the theoretical quantum state of two modes into which a photon pair can be emitted by the first SPDC process (see e.g. [14, 15])

$$|\psi\rangle \approx |0, 0\rangle + g|1, 1\rangle. \quad (5.3)$$

Here, the kets represent the photon occupations of signal and idler modes. The down-conversion efficiency is represented by the constant  $g \ll 1$ , which is generally very small (higher orders of  $g$  have been neglected). The above quantum state represents a superposition of electromagnetic field modes being populated with a photon pair or not. It implies that before the measurement is performed, it is impossible in principle to determine with certainty whether or not an individual photon pair had or had not been emitted in the first SPDC process. The question “Does the crystal emit photons or not”, does only have a definite answer after the photon pair or its absence has been detected (with EOM on). However, this measurement precludes the observation of frustrated down-conversion. Thus, care has to be taken not to make an implicit assumption that the existence of a photon pair would be a real property before it is actually observed.

In the MZI, the quantum state after the first beam splitter is represented by a superposition of the photon being in either of the two paths. If the path of an individual photon is measured

by inserting an additional detector (Fig. 5.12c), one of these possibilities is realized and the photon *can* be detected without delay. Using the same arguments, no delay is expected for the analogous situation in our experiment (Fig. 5.12d), which is consistent with our result.

### 5.7.1.3 Delayed-Choice Frustration of Down-Conversion

In a Mach-Zehnder interferometer, the decision whether to measure path information before the beam splitter or whether to observe interference (obtaining path information after the beam splitter) can be made by inserting or removing the final beam splitter before detecting the photon. It has been shown (e.g. [157, 158]) that even if this choice is made at a time after the photon must have already passed the first beam-splitter, a result is obtained that is consistent with this choice. Interference can be observed, even if the beam-splitter was not yet present in the setup at the time the photon entered the interferometer.

Delayed-choice experiments with interferometers established that a quantum particle does not “decide”, whether it behaves like a wave or like a particle by the time it enters the interferometer. Other delayed-choice experiments demonstrated other aspects of complementarity (see Sec. 2.2.1). For example in delayed-choice entanglement swapping [42], it has been shown that a photon pair is neither definitely entangled nor definitely separable before all involved particles have been detected.

In the case of frustrated down-conversion, we are confronted with a different aspect of complementarity. In analogy to Wheeler’s scheme of a delayed-choice experiment [30], the switching of the EOM can be seen as analogous to switching the second beam splitter in Fig. 5.12a,c on or off. The two complementary observations correspond to the measurement of an interfering (suppressed or enhanced) pair emission rate and to the measurement of whether or not a photon pair was emitted by the first down-conversion process (see also [83]). By realizing a delayed-choice experiment involving these two properties, we demonstrate that whether or not a photon pair is emitted during the first of two alternative SPDC processes is not determined by the time it would be emitted.

When the EOM is switched on, before the measurement is performed, it is possible to make the statistical statement that photon pairs will be detected at  $D_E$  and  $D_I$  with a finite probability ( $\propto g^2$ ). On the other hand, when the EOM is switched off and destructive interference is observed, in principle the statement “the probability of detecting photon pairs at  $D_S$  and  $D_I$  is zero” is possible. This means that no *individual* photon pair can be detected in this experimental configuration. If one interprets a detection probability of zero as “non-existence” of the photon pair, then the possibility of the photon to exist depends on the setting of the EOM. The setting choice, however, can be made at a time *after* the photon would have been emitted in the first SPDC process. In this way, it is possible to choose, whether a photon can exist, after it would have been emitted.

## 5.7.2 Alternative Explanations of Our Results

### 5.7.2.1 Phase-Dependent Up-Conversion in the Second SPDC Process

In principle, the absence of a delay could alternatively be explained by a hidden variable model, according to which photon pairs are (definitely) produced at a constant rate during the first SPDC process and subsequently up-converted during the second passage through the crystal. Such a model would explain the immediate detection of photons from the first SPDC process at  $D_E$ , whenever the EOM is switched on, as well as the absence of detections at  $D_S$  and  $D_I$  when the EOM is switched off. Thus, our results do not directly contradict it.

However, the interpretation of our experiment according to this model would require to accept several counterintuitive ramifications.

An important issue is the consistent explanation of both constructive and destructive interference, i.e. both suppression and enhancement of the rate of detected photon pairs when the EOM is switched off. The observed visibility of  $> 75\%$  (Fig. 5.7) implies that during the observation of frustrated down-conversion (destructive interference), the model needs to account for the up-conversion of more than 50% of the photon pairs emitted in the first SPDC process. At the same time, no down-conversion can occur in the second SPDC process. During constructive interference, the observed photon pair emission rate is  $> 3.5$  times the pair emission rate of a single SPDC process (see Fig. 5.7). If photons are definitely emitted by the first SPDC process at a constant rate, this observation can only be explained if the second SPDC process emits more photon pairs than the first by a factor of at least 2.5.

Depending on the phase setting (relative path lengths), the system needs to switch between these two cases of super-efficient up-conversion and super-efficient down-conversion.

For the up-conversion of *single* photons (with the second photon from a laser beam), up-conversion efficiencies of 90% have been reported, see e.g. [159, 160], however, in contrast to our experiment, strong lasers and cavities have been used. In the low gain regime, up-conversion of down-converted photon *pairs* has been observed [161, 162] with orders of magnitude lower efficiencies. For instance, in [162], a rate of 2200 up-converted photons per second was reported for a flux of incoming photon pairs of about  $10^{12}$  per second, corresponding to an up-conversion efficiency of  $\approx 10^{-9}$ . This is far from the 50% that would be required in order to explain our results by this model.

In our case, the pump beam is present at the second SPDC crystal and thus could increase the effective conversion efficiency. We detected about  $10^5$  down-converted photon pairs per second within our filter bandwidth from a single SPDC process at  $\approx 10$  mW of pump power at  $\lambda = 405$  nm. This corresponds to a down-conversion efficiency of roughly  $10^{-12}$ . Within our theoretical understanding of SPDC processes (e.g. [147, 163]), the same efficiency is expected for up-conversion in the presence of the pump beam. Thus, while the above model is not directly ruled out, its application to our experiment would require to modify the established theory of SPDC.

In Chapter 6, we show for the case of three interfering SPDC processes that already the assumption of each photon pair originating from a definite one of them is inconsistent.

### 5.7.2.2 Interfering Classical Waves

In an attempt to describe the phenomenon of suppressed down-conversion within classical non-linear optics, a similar idea was put forward [112]. In essence, the first of the two SPDC processes was described as a constant source of classical waves, which are modulated during the second passage through the non-linear medium. This model has been refuted as it predicts a lower than observed visibility [113, 114, 139]. Moreover, it predicts a dependence of the visibility on the pump power [113, 114], which also was not observed in our experiment.

In a different approach, *both* SPDC processes were treated as nonlinear interaction of classical fields [84]. In this case, in principle 100% visibility can be achieved, but only in either the signal or the idler beams separately and not simultaneously for both of them. Thus, while classical models were able to recover parts of the observed results, they failed to consistently describe all aspects of this experiment.

## 5.8 Conclusion and Outlook

We have established an upper bound of a few hundreds of picoseconds for a possible delay of observing photons at a suddenly inserted detector during suppressed SPDC. This result is consistent with the quantum mechanical predictions of no delay [136, 139]. An interpretation of

our experiment in analogy to a delayed-choice experiment was presented. We have discussed to what extent alternative models can be ruled out or constrained by our results.

The initial question “does the crystal emit photon pairs towards the mirror in the case of suppressed emission” needs to be addressed from the viewpoint of quantum complementarity, in analogy to the question “through which path does a single photon travel in an interferometer in the case of destructive interference”. The two complementary properties cannot be determined at the same time as this would require two mutually exclusive measurements. A change of the measurement apparatus by switching the EOM on or off introduces different “interactions” that in principle cannot be controlled. Thus the two observations of destructive interference and photons emitted by a definite one of the SPDC processes cannot be comprehended within a single picture, but must be regarded as complementary (see also [9]).

The established experimental restrictions on a delay of photon arrival times at the inserted detector could be made stronger in the future for instance by performing randomized setting choices that are space-like separated from the photon emission events.



# 6

## Complementarity with Three Indistinguishable Sources

### 6.1 Motivation

In the experiment of frustrated down-conversion (see Sec. 2.4.3), a photon pair can be created in two indistinguishable ways, causing interference in the pair emission rate of the system. The idea can be generalized in a straightforward manner to situations with more than two indistinguishable alternatives of photon pair emission. In this case, interference between multiple alternative ways of emitting a photon pair can be observed.

The phenomenon of induced coherence in the case of three sources has been studied previously in situations in which one of the down converted beams from each crystal is aligned to be indistinguishable [164–167], as well as the application of multiple coherent SPDC processes and path alignment for the generation of high-dimensionally entangled states [102].

In this chapter, we investigate the phenomenon of frustrated and enhanced photon pair emission in the case of three sources. We analyze this situation in terms of the complementarity between path information and interferometric visibility.

The duality relations discussed in Sec. 2.2.2 (in particular Eq. 2.8) quantify the tradeoff between interferometric visibility and path distinguishability in two path interference experiments. In the case of fully coherent beams, path distinguishability results in an unbalance of the probabilities for a particle to traverse one path or the other.

Here we show that the interpretation of this path distinguishability as information about the path of an individual particle is inconsistent. In particular, we show an experimental situation involving interference between three alternative paths, for which the above interpretation leads to a contradiction.

We apply the duality relations to experiments in which interference is observed between photon pair emissions from different sources, as in the previous chapter. We show that in the case of three indistinguishable sources of a photon pair, an experimental situation exists, in which it is impossible to ascribe a definite origin to a photon pair (i.e. full path information), although full

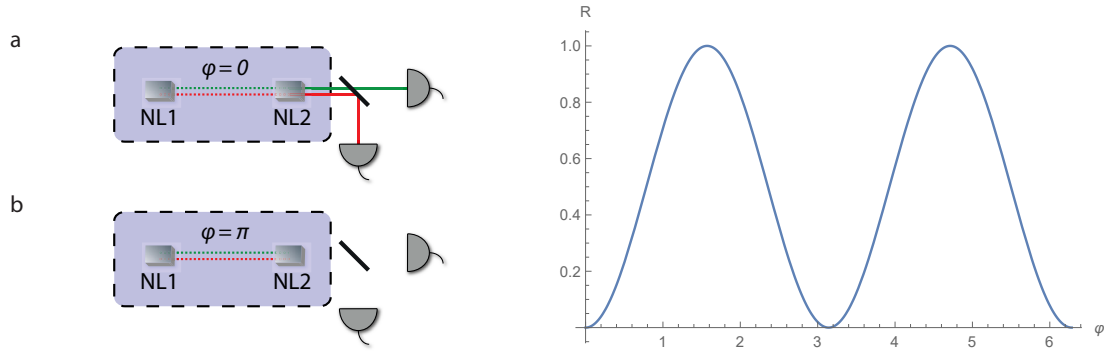


**Figure 6.1:** Frustrated down conversion. If a photon pair can be emitted by either one of two nonlinear crystals NL1 or NL2 in an indistinguishable way, the two SPDC processes interfere. This results in an enhanced (a), or in a suppressed (b) rate of photon pair emission. The dependence of the total pair emission rate on the relative phase between the two individual photon pair emissions follows an interference law.

“path distinguishability” is available and no interference is observed.

This apparent paradox does not have an equivalent in two dimensions, i.e. if only two sources are used. The results have implications on the precise meaning of the term “path information” and its connection to Feynman’s “first principles” (Sec. 2.1.1).

## 6.2 Duality Relations in Frustrated Down-Conversion with Two Sources

In the following, the complementarity between interference and “which-source” information in the case of frustrated down-conversion with two SPDC sources is analyzed. To this end, we consider the setup in Fig. 6.1 (see also Sec. 2.4.3).

As shown in Sec. 2.4.3, the rate of emitted photon pairs from two indistinguishable sources depends on the relative phase between the probability amplitudes corresponding to the alternative emissions. This phase can be adjusted by varying the optical path of either pump, signal, or idler beams of one source with respect to the other.

In the case of perfect indistinguishability (zero path information) of the two possible pair emission events, the interference attains ideally 100 % visibility. If complete path information is introduced by blocking or misaligning the path from one of the two sources, no interference occurs.

The intermediate case of partial path information and partial visibility can be analyzed using the relations discussed in Sec. 2.2.2. In particular, the inequality Eq. 2.8,

$$V^2 + \mathcal{P}^2 \leq 1, \quad (6.1)$$

can be applied to two-source frustrated down-conversion, as the rate of photon pair emission is described by the an interference law analogous to the description of a particle in a two path interferometer (cf. Sec. 2.4.3),

$$R \propto |a + e^{i\varphi}b|^2 = a^2 + b^2 + 2ab \cos \varphi, \quad (6.2)$$

where perfect alignment and transmission of the beams have been assumed. The probability amplitudes  $a$  and  $e^{i\varphi}b$  in this case correspond to photon pair emissions from the first and from the second source, respectively. The visibility  $V$  is obtained using the minimum and maximum photon pair emission rates in a way analogous to traditional interferometry (Eq. 2.6). In the case of frustrated down-conversion, it quantifies the amount of suppression and enhancement

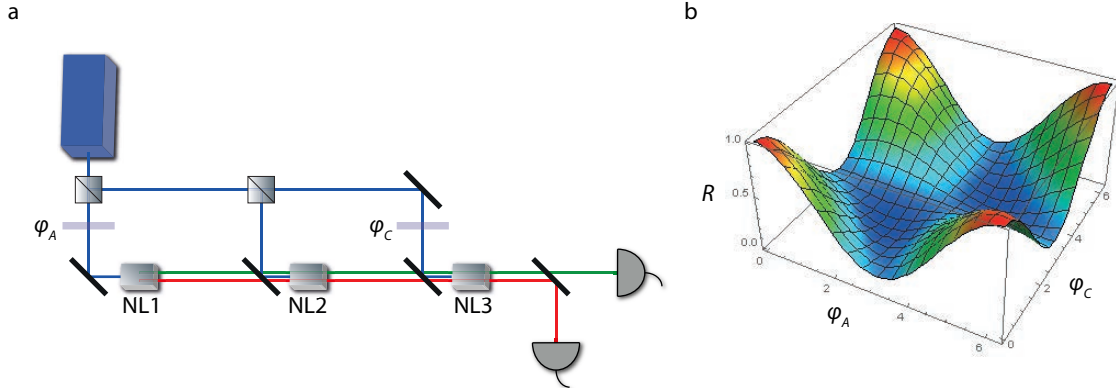


**Figure 6.2:** Emission of a photon pair from three indistinguishable sources. Schematic of the setup (a). Three nonlinear crystals NL1, NL2, and NL3 are pumped coherently. A photon pair can be emitted by each of them into identical signal and idler modes, and is subsequently detected. The rate of detected photon pairs depends on the relative phase settings between the individual sources. The predicted count rates on varying  $\varphi_A$  and  $\varphi_C$  are shown in (b). Equal emission probabilities  $a, b, c$  are assumed. Of particular relevance for the discussion here is the point  $\varphi_A = \varphi_C = \pi$ , which results in a non-zero photon pair emission rate.

of the photon pair emission rate. Path distinguishability  $\mathcal{P}$  in this case corresponds to the distinguishability of “which-source” produced a photon, and can be quantified according to Eq. 2.7.

If one of the two sources emits photon pairs with a higher probability than the other (if e.g. the crystals are pumped with different powers), it is possible to bet on the outcome of a “which-source” measurement and win in the majority of cases. In this sense, partial “which-source” information is present and inequality Eq. 6.1 accurately describes the relation between the achievable visibility and the amount of “which-source” information.

### 6.3 Indistinguishable Photon Pair Emission from Three Sources

In the case of three nonlinear crystals emitting photon pairs into identical modes (Fig. 6.2), the quantum state of the system can be written as (cf. the treatment in [15])

$$|\psi\rangle = ae^{i\varphi_A}|s\rangle|i\rangle + b|s\rangle|i\rangle + ce^{i\varphi_C}|s\rangle|i\rangle, \quad (6.3)$$

where  $ae^{i\varphi_A}, b, ce^{i\varphi_C}$  represent the probability amplitudes of pair creation at the respective crystal, and  $|s\rangle|i\rangle$  represents a signal and idler photon pair in the overlapped modes that can be detected. The rate of emitted photon pairs obeys the interference law

$$R(\varphi_A, \varphi_C) \propto |e^{i\varphi_A}a + b + e^{i\varphi_C}c|^2. \quad (6.4)$$

Equation 6.4 is represented graphically in Fig. 6.2b.

### 6.4 Inconsistent Which-Path Information

The duality relation between path information and interference has been generalized to multi-path interference (e.g. [168–172]), particularly in the case of three dimensional path information. Here, we analyze the situation in a different way. Instead of explicitly considering all three possible “paths”, we regard two of the three sources as one single source. The validity of this approach is discussed in Sec. 6.5.2. In any case, it is frequently used, e.g. by regarding a

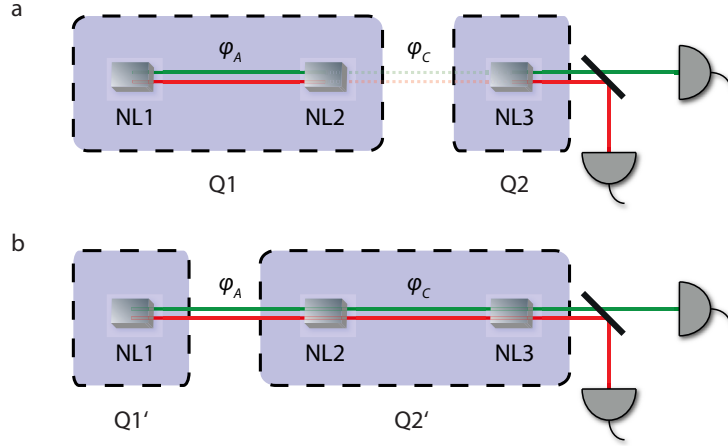


**Figure 6.3:** Contradicting path information in three crystal frustrated down-conversion. In (a), the combination of NL1 and NL2 is considered a single photon pair source (Q1), which emits indistinguishable to the second source (Q2), consisting only of NL3. The relative phase  $\varphi_A$  between NL1 and NL2 changes the emission probability of Q1. If it is set to  $\varphi_A = \pi$ , photon pair emission from Q1 is completely suppressed. Accordingly, a constant pair emission rate from the combined setup is observed, regardless of whether Q1 is blocked or not. At the same time, no photons are detected if Q2 is removed. No visibility of the total emission rate is observed upon varying the relative phase  $\varphi_C$  between Q1 and Q2. These observations are consistent with the assertion that we have full “path predictability” as to all photons must have been emitted by NL3. In (b), NL1 corresponds to source Q1', whereas NL2 and NL3 are considered a single source Q2'. Using the same arguments, we arrive at the conclusion that if  $\varphi_C = \pi$ , Q2' does not emit and all photons must have been originated from NL1. The two contradicting situations can be realized in the same experiment, if the intensities are balanced and  $\varphi_A = \varphi_C = \pi$ .

periodically poled crystal as a single source, although it is actually an interfering system of many different coherent pair emission processes.

Below, we show that the analysis of the amount of “which-source” information and visibility from this point of view leads to a contradiction between two possible interpretations of the same experiment.

Consider the first two nonlinear crystals (NL1 and NL2) constitute one source labeled by Q1, whereas NL3 constitutes a second source Q2 (Fig. 6.3a). The quantum state of a photon pair is written as

$$|\psi\rangle = [\alpha + ce^{i\varphi_C}] |s\rangle|i\rangle, \quad (6.5)$$

where  $\alpha = ae^{i\varphi_A} + b$  is the probability amplitude corresponding to photon pair emission by Q1 and  $ce^{i\varphi_C}$  corresponds to an emission by Q2. The rate of emitted photons is given by

$$R(\varphi_C) \propto |\alpha + e^{i\varphi_C} c|^2. \quad (6.6)$$

Eq. 6.1 can be consistently applied to relate the observed visibility upon varying  $\varphi_C$  to the amount of available “source information”, i.e. to the balance of probability amplitudes  $\alpha$  and  $c$ . Consider an experimental situation, in which  $a = b$  and  $\varphi_A = \pi$ . It follows that  $\alpha = 0$ . In other words, the probability amplitude corresponding to a photon pair emission by Q1 (the combination of NL1 and NL2) is equal to zero. This is consistent with the observation that Q1 corresponds to a frustrated down-conversion-experiment tuned to completely destructive interference. Consequently, if Q2 is removed, in principle no photon pairs are emitted from the system. On the other hand, if instead the first “double” source (Q1) is blocked or removed, the photon pair emission rate is unchanged compared to the unblocked case. By varying the relative phase  $\varphi_C$  between Q1 and Q2, zero interference visibility is observed. These observations are consistent with Eq. 2.8, as the sources Q1 and Q2 are unbalanced and “which-source”

information is available. One might conclude that in this system, all photon pairs are created in the source Q2, i.e. in NL3. However, this interpretation leads to a contradiction as is shown below.

Instead of the grouping of events into photon pair emission from either Q1 or Q2, consider the following alternative view on the experiment. Crystal NL1 is considered the first source (Q1') and the combination of NL2 and NL3 is considered to be the second source (Q2'), as indicated in Fig. 6.3b. The possible events are identified accordingly as photon pair emission either from Q1' or from Q2'. Using this partition, we arrive at the quantum state

$$|\psi\rangle = [ae^{i\varphi_A} + \beta] |s\rangle|i\rangle, \quad (6.7)$$

with the probability amplitude for an emission by Q1' being  $ae^{i\varphi_A}$  and the amplitude for Q2' is  $\beta = b + ce^{i\varphi_C}$ .

The rate of emitted photons is given by

$$R(\varphi_A) \propto |ae^{i\varphi_A} + \beta|^2. \quad (6.8)$$

If  $b = c$  and  $\varphi_C = \pi$ , it follows that  $\beta = 0$ . Again, Eq. 2.8 can be applied in a self-consistent way. Individual blocking of Q1' and Q2' shows that Q2' does not emit photon pairs. Consequently, no interferometric visibility is observed upon varying  $\varphi_A$ , corresponding to full “which-source” information. One arrives at the conclusion that all photons were emitted by Q1', that is, by NL1.

It is important to stress that the apparatus needs not to be modified in any way between these two cases. The situation  $a = b = c$  and  $\varphi_A = \varphi_C = \pi$  can be realized in one and the same experiment. It follows from Eq. 6.4, that the corresponding rate of detected photons is non-zero. The question arises, whether it is sensible to ask which crystal produced these photons.

Both above viewpoints are equally self-consistent and obey the duality relation Eq. 2.8. Nevertheless the interpretation provided by analyzing “which-source” information in two alternative ways of partitioning the system into two separate sources are incompatible with each other.

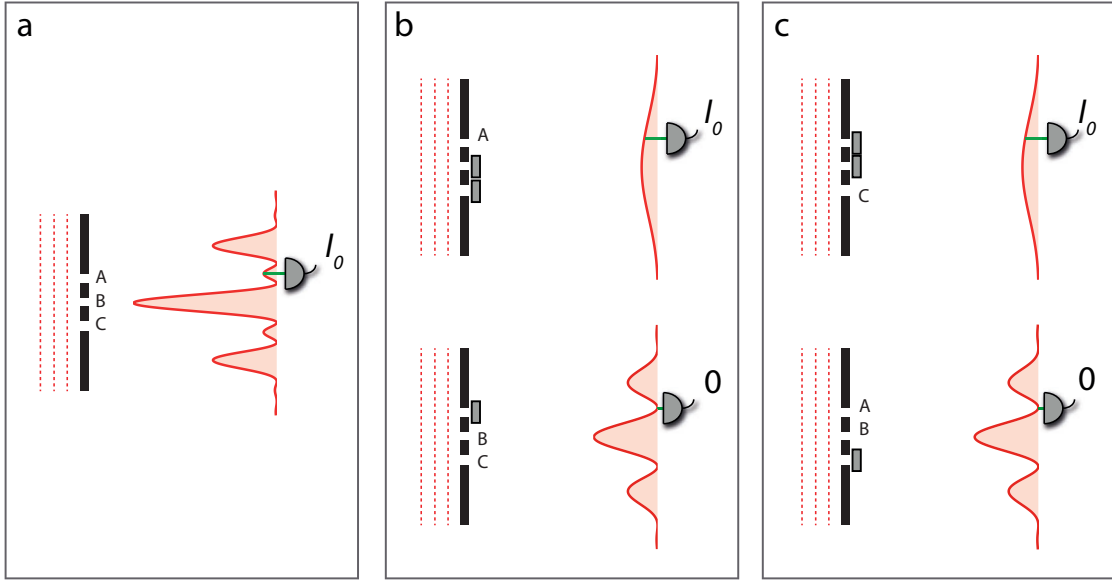


**Figure 6.4:** Inconsistency of interpreting path information as particle trajectory in a triple slit interference experiment. Light passing through three slits (A, B, C) produces the interference pattern indicated in (a) on a screen after propagating to the far field. A detector placed at a fixed point on the screen (corresponding to  $\varphi_A = \varphi_C = \pi$ ) records the intensity  $I_0$ . Under the assumption that every detected photon arrives through a definite one of the slits, the measurements indicated in (b) are performed. First, both slits B and C are blocked, which results in the same count rate  $I_0$  at the detector as in the unobstructed case. Second, slit A is blocked and the count rate at the detector drops to essentially zero. These observations may lead to the conclusion that every photon that arrives at the detector traveled via slit A, even in the case of three open slits. However, if the path measurements are performed as indicated in (c), we observe an unaffected count rate upon blocking A and B; but no detection events upon blocking slit C. The same arguments as before lead to the conclusion that photons arrive via slit C. The fact that the conclusions of (b) and (c) contradict each other shows the inconsistency of assigning definite path information to a photon while observing interference.

## 6.5 Discussion

### 6.5.1 Analogy to Three Slit Interference

The inconsistency is also present in other interference experiments. As an example, consider the case of three slit interference illustrated in Fig. 6.4a. The detection rate observed at a particular fixed point on the screen obeys Eq. 6.4, if  $ae^{i\varphi_A}$ ,  $b$ ,  $ce^{i\varphi_C}$  are regarded as probability amplitudes of the particle traveling via the respective individual slits.

Two different ways of grouping the three slits into two alternatives by which a particle can reach a point on the screen again lead to contradicting results as to which path the particle traveled through. In Fig. 6.4b, the question whether a detected photon came through slit A or through the other slits is addressed by subsequently blocking either slit A or the remaining two. The rate of detected photons is consistent with the conclusion that photons would always reach the detector via slit A. However, if instead the question is asked, whether a detected photon came via slit C or via the other two (6.4c), the results are consistent with the statement that all photons pass through slit C, which leads to a contradiction with the previous statement.

It should be noted that in the case of three slits, the measurement device plays a slightly different role than in the case of three crystals. Consider first the case when one of the slits is blocked and no photons arrive at the detector via the other two open slits. The fact that no photons arrive at the detector is due to destructive interference between the two remaining

paths. This destructive interference is observed when the detector is located at a dark fringe of the resulting double slit interference pattern. The location of the detector must ensure that the measurement projects onto a state with a relative phase of  $\pi$  between the two paths. If the detector is moved, photons are recorded. In the case of frustrated down-conversion from two nonlinear crystals, no change of the detector position would result in a possibility to “see” photons emitted by the system.

### 6.5.2 Remarks on Regarding Two Sources as One Combined Source

One might question the validity of grouping two slits in the three path interferometer together and assign a single probability amplitude to the possibility of traveling via either of them. But in fact, this is done frequently when applying the quantum mechanical formalism to real experiments. Individual paths are assigned probability amplitudes although one could always subdivide a single path into different sections and describe the path by adding the amplitudes corresponding to these sections.

In the case of nonlinear crystals, virtually all quantum optics experiments using SPDC omit the substructure of the crystals. This substructure is manipulated in order to achieve periodic poling, where the amplitudes of pair creation at different sections of the crystal are engineered to interfere constructively in order to increase the pair creation efficiency. Nevertheless, it is neglected in most experiments and a single probability amplitude is assigned to the photon pair emission by the entire crystal. One could even imagine a crystal with “anti”-periodic poling and produce efficiency zero SPDC. It sounds unreasonable to claim photons would come from there.

Similarly, in the experiment of frustrated down-conversion (i.e. complete destructive interference between two photon pair emission processes), ideally no photon pairs are detected. The above arguments show that nevertheless, the interpretation that no photon pairs are emitted by such a system holds only if the absence of photon pairs is actually detected. If a third nonlinear crystal would be inserted before the detectors, the situation described above can be realized and consequently, the possibility for a photon pair originating from frustrated down conversion cannot be ruled out.

Another interesting point is to realize a subtle difference in the meaning of “which-path information” depending on what measurement is performed. If the triple slit experiment is analyzed considering the three slits separately, “path information” refers to the question “which of the three slits” did a photon pass through before it arrived at the detector. If two of the slits are grouped together and assigned one common probability amplitude, the which-path measurement corresponds to the question “which of the *two* possible events happened, did a photon pass through the first slit, or through the combination of the other two”. Moreover, in order to determine the visibilities in the Q1-Q2 scenario compared to Q1'-Q2', different phases are varied.

Nevertheless, the amount of path information between two possible paths does not depend on the relative phase setting, but solely on the visibility (cf. the duality inequalities [45, 47, 48]). Therefore, in the situation of both phases set to  $\pi$ , all three pictures are equally valid and self-consistent although they lead to contradicting which path information.

## 6.6 Conclusion

We have analyzed the situation of frustrated down-conversion in a scenario involving three indistinguishable sources. We found that by regarding two of the three sources as a single source, two contradicting interpretations of path information are possible within the same experimental configuration.

Recalling Feynman’s “First Principles” of quantum mechanics (Sec. 2.1.1), the first crucial step in connecting the mathematical formalism to an experimental situation is to identify macroscopically distinguishable “events” and to assign probability amplitudes to them. However, this

identification of “events” is in general ambiguous. Nevertheless, either analysis of our scheme in terms of “which-path information” and visibility is self-consistent, as long as the assignment of events to probability amplitudes is not changed.

The assignment of a probability amplitude of zero to a particular event is commonly interpreted as zero probability of this event to happen. However, we have shown that this premise cannot hold in general. Any event could in principle be subdivided into sub-events of possibly non-zero probability amplitude, which lead to an apparent zero probability amplitude of the combined event. Therefore, a measured probability of zero for an isolated event does not allow the conclusion that this probability remains zero in the presence of other events, which could lead to indistinguishable experimental outcomes. An experimental realization of this situation is currently being implemented in the laboratory.

## Conclusions and Outlook

In summary, this thesis describes several experiments that explore the phenomenon of path indistinguishability in photon pair emission processes. The overall aim of this work is to contribute to the understanding of the resulting interference phenomena and of complementarity in novel situations that deserve to be studied in a deeper way.

The first two experiments investigated induced coherence without induced emission in a spatially multimode scenario. In the first experiment, we demonstrated that spatial interference fringes between two photon beams can be created by controlling a third beam that is not itself interfering and which remains undetected. We analyzed analogies and differences of these “induced” interference fringes to the spatial interference pattern encountered in traditional interferometry. In classical interferometry, manipulations in one of the interfering beams produce a qualitatively similar pattern as manipulations in the undetected beam in our case. We found that the fringe pattern is governed not merely by the wavelength of the interfering light, but by a combination of the involved wavelengths. This effect is attributed to the role of the momentum correlation between the employed photon pairs.

The momentum correlation between two photons is studied in more detail in the second experiment. There, the fringe pattern obtained by detecting single photons is used to access information about the correlation between the two photons of a pair. This possibility enables a novel method for measuring the momentum correlation between two photons without detecting one of them, which we demonstrated experimentally. The method shows that the complementarity principle is not merely a philosophical concept for the interpretation of quantum mechanics, but it can also lead to practical applications. Moreover, the results contribute to a deeper understanding of quantum imaging with undetected photons, particularly with respect to the achievable spatial resolution.

In a third experiment, we showed that the effect of induced coherence without induced emission can be used to control the degree of polarization of a light beam without directly interacting with it but by varying the transmission of another light beam. This demonstrates a situation, in which the polarization is manipulated merely by controlling what information about it is accessible in principle.

The fourth experiment explores the related phenomenon of suppressed down-conversion, in

which the alignment of both photon beams leads to the suppression of photon pair emission from the combined system. Using fast switching, we performed a delayed-choice experiment, which demonstrates that the emission of photons from individual SPDC processes can be observed, even before the switching could have affected the source. Note that this result does not lead to a causality paradox, but can be understood in terms of quantum complementarity. The analogy of this experiment to an excited atom in the vicinity of a mirror suggests that an atom needs not to be influenced locally, in order for its emission rate to change. In our interpretation, a measurement of the emission from the atom-mirror system is complementary to the measurement of the emission from the atom in vacuum and thus cannot be determined in the same experiment. It remains open to discussion, what are the limits to the above analogy.

The phenomenon of suppressed down-conversion is further analyzed in a scenario with three indistinguishable photon pair emission processes. We present a situation, in which two self-consistent interpretations in terms of path information and visibility lead to contradicting conclusions. This result raises the question to what extent interferometric path information can be interpreted.

By performing these experiments, I hope to have made a contribution to the understanding of the remarkable quantum effect of induced coherence without induced emission. The results of the presented experiments stimulated a lot of follow-up questions, many of which motivate further study. Below, I outline some of them, which are either currently being investigated or which I hope to be able to investigate in the near future.

## 7.1 Questions For Future Research

- **Momentum Correlation and Which-Path Information** [173]

The momentum correlation between two photons in multimode induced coherence without induced emission allows transferring spatial information from the undetected beam to the interfering beams. We have shown that the visibility and the spatial resolution of the observed interference fringes increase with a sharper momentum correlation. On the other hand, a sharp momentum correlation can make it easier to distinguish which source a photon pair was emitted from. In the theoretical case of perfect momentum correlation, an ever so slight misalignment of the beams would already result in the possibility to partially distinguish between the two sources, as the sharp momentum correlation could in principle be used to determine the origin of a photon pair (e.g. by momentum resolved coincidence detection). The question arises, whether this fact leads to any fundamental limit on the achievable visibility or spatial resolution of quantum imaging with undetected photons.

- **Spatial Resolution of Quantum Imaging with Undetected Photons** [174]

The understanding of the role of the momentum correlation in induced coherence without induced emission developed in Ch. 3 can directly be applied to the experiment of quantum imaging with undetected photons. It follows that a higher momentum correlation allows for an improved spatial resolution. Given the analogy of this problem to our results holds, an interesting prediction is implied: the achievable resolution in quantum imaging with undetected photons is governed by the wavelength that illuminates the object, even when it is shorter than the wavelength of the detected light. This could in principle lead to promising high resolution imaging applications if the object is illuminated with light of a very short wavelength that is hard to detect directly. An experiment to test this prediction is currently being implemented in our laboratory.

- **Determining Correlations in Other Systems than SPDC by Measurements on One Particle**

Can our method of determining momentum correlations without coincidence measurement

be applied to other systems than SPDC? The scheme is expected to be applicable to any source of pairs of quantum particles, which can in principle be arranged to emit a pair in two indistinguishable ways. In situations, in which coincidence detection is technically difficult (e.g. detecting certain types of atoms), it might be a feasible approach to perform correlation measurements with a single detector.

- **Multimode Induced Coherence Exploiting Different Correlations [173]**

In the implementation to observe multimode induced coherence without induced emission, we used the far-field correlation of photon pairs to map spatial modes of the undetected beam to spatial modes of the observed superposed beam. This was done by lens systems that map a plane wave mode at the sources to a point on the camera. It remains open, whether it is possible to observe the same effect if near-field correlations were used instead, i.e. by imaging the photon pair sources on the camera and possibly onto an object in the case of quantum imaging.

The question arises, whether the spatial resolution is governed by the strength of the near-field correlations in a photon pair, in analogy to the far-field (momentum) correlations in the current experiments? The product of the spatial “sharpnesses” in the two cases might not be achievable classically. Based on this, is it possible to find a real qualitative “quantum advantage” of quantum imaging with undetected photons as opposed to its high-gain counterparts?

A related question is, whether it is possible to extend the method of measuring momentum correlations between two particles by detecting one of them to a measurement of near-field (“transverse position”) correlations in SPDC. In this case, is it possible to demonstrate spatial entanglement by measurements on only one particle, without employing coincidence detection?

- **Measurements of Correlations on One Particle and the Fundamental Understanding of a Measurement in Quantum Mechanics**

We demonstrated that the momentum correlation of a photon pair can be determined by measurements on only one of the photons. This shows that in principle, it is possible to determine a property that is encoded in the second order (in intensity) correlation of the light by a measurement in first order. A question that immediately connects to this fact is how far this technique can be generalized, i.e. to what extent can general two particle properties be measured by detecting only one of the particles. From an even more fundamental perspective, how does the two-photon state “collapse” by performing this type of measurement?

- **Frustrated Down-Conversion and Atom/Mirror Analogy [175]**

Next steps following the experiment in Ch. 5 could be to employ space-like separated random setting choices and more efficient detection in order to provide stronger restrictions for local realistic explanations of the experiment.

Another approach is to explore different scenarios in the optical experiment to investigate the limits of the analogy to the atom and mirror case further. Such scenarios could be the suppression of SPDC in different cavity geometries, or to increase the coherence length of the emitted photon pairs beyond the distance between crystal and mirror.

Another interesting avenue of research concerns the pump photon in experiments of frustrated down-conversion. Qualitatively different behavior might be observed if the pump photon is in a single photon Fock state as opposed to a coherent state. It remains to be tested, whether this is the case.

- **Three Crystal Suppressed Down-Conversion [176]**

It will be interesting to test the situation described in Ch. 6 experimentally and to clarify

its conceptual implications. For instance, it might be possible to connect this phenomenon to the non-contextuality of quantum systems, which also does not have an equivalent in two dimensions. Moreover, the question arises whether “path information” has a meaning outside the mathematical formalism. Inconsistencies seem to arise as soon as the connection between observable events and the formalism (i.e. the assignment of probability amplitudes) is altered. It will be interesting to analyze precisely to what extent the way of applying the quantum mechanical formalism to observations in the laboratory is ambiguous and thus to what extent observer independent interpretations of the phenomena can be produced.



# Appendix

## A.1 Experimental Details on Interference Fringes in Induced Coherence Without Induced Emission

### A.1.1 Initial Alignment of the Idler Beam Lens System

A key step in our experiment is the alignment of the setup to an initial position, in which the observed interference pattern is spatially uniform. Positioning the lens  $L_{I1}$  in Fig. 3.2 on page 50 exactly at the corresponding position is experimentally challenging, as it cannot be done precisely by mere visual inspection of the pattern. As soon as the first minimum is further away from the beam center than the beam radius, the lens position at which a flat “phase-front” is achieved is hard to determine.

In order to accurately find this “zero” position, the following procedure was used. Instead of aligning the transverse degree of freedom and eliminating any straight fringes before aligning the focus, straight fringes are purposefully introduced by a transverse shift of the lens. This has the effect of inclining the idler beam of the first crystal with respect to the idler beam emerging from the second crystal. In this configuration, a small change of the focus position has a recognizable effect on the curvature of the observed fringes.

By successive “tilting” and focusing, it is possible to reach a lens position at which the fringes appear straight. The final step is to align the inclinations of the two beams by undoing the transverse shift of the lens.

### A.1.2 Phase-Shift of a Defocused $4f$ System

In the following, the spatially dependent phase shift produced by defocusing a  $4f$  imaging system is computed in a Fourier Optics calculation [58]. We compare the result with the approximation made in Chapter 3 (Eqs. 3.1 and 3.16).

Consider an optical field propagating from the plane P1 (spatial coordinate  $\xi$ ) to the plane P2 (spatial coordinate  $x$ ) in Fig. A.1. Initially, the lenses are positioned at focal distance from the

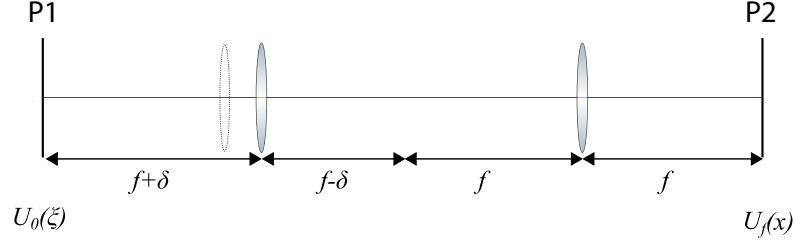


**Figure A.1:** Defocused  $4f$  system. An optical field  $U_0(\xi)$  propagates from the plane P1 to the plane P2. The first lens of the  $4f$  system is shifted a distance  $\delta$ . This results in the field  $U_f(x)$  at P2. The effect of the defocused lens system on the spatially dependent phase can be approximated by the phase shift obtained in free-space propagation about a distance  $d = f^2\delta/(f^2 + \delta^2)$ .

input and output planes with a distance between the two lenses of  $2f$ . In this configuration, the optical field at P2 is an inverted copy of the optical field at P1. In the experiment, we depart from this initial alignment by shifting the first lens a distance  $\delta$  closer towards the second lens. In this case, the field at P2 is given by the following expression [58],

$$U_f(x) \propto \int_{-\infty}^{\infty} d\xi U_0(\xi) \exp\left(\frac{ik}{2} \left[ x^2 \left( \frac{1}{\delta} + \frac{\delta}{f^2} \right) - 2x\xi \frac{1}{\delta} + \xi^2 \frac{1}{\delta} \right]\right). \quad (\text{A.1})$$

If we compare Eq. A.1 with the effect of free-space propagation (without any lens) over a distance  $d = f^2\delta/(f^2 + \delta^2)$  [58],

$$U_{prop}(x) \propto \int_{-\infty}^{\infty} d\xi U_0(\xi) \exp\left(\frac{ik}{2} \left[ x^2 \left( \frac{1}{\delta} + \frac{\delta}{f^2} \right) - 2x\xi \left( \frac{1}{\delta} + \frac{\delta}{f^2} \right) + \xi^2 \left( \frac{1}{\delta} + \frac{\delta}{f^2} \right) \right]\right), \quad (\text{A.2})$$

we find that the two expressions become identical in the limit  $\delta^2/f^2 \ll 1$ . In our experiment, the largest value of  $\delta^2/f^2$  is smaller than 0.06. Note that we have neglected a spatially independent phase factors, as in this context we are only concerned with the spatial phase variation.

Thus we can approximate the phase shift produced by the  $\delta$  lens shift by that of free space propagation by a distance  $d$  [145, 146] (Fig. A.2),

$$\varphi(\mathbf{q}) = \frac{d\lambda}{4\pi} |\mathbf{q}|^2. \quad (\text{A.3})$$

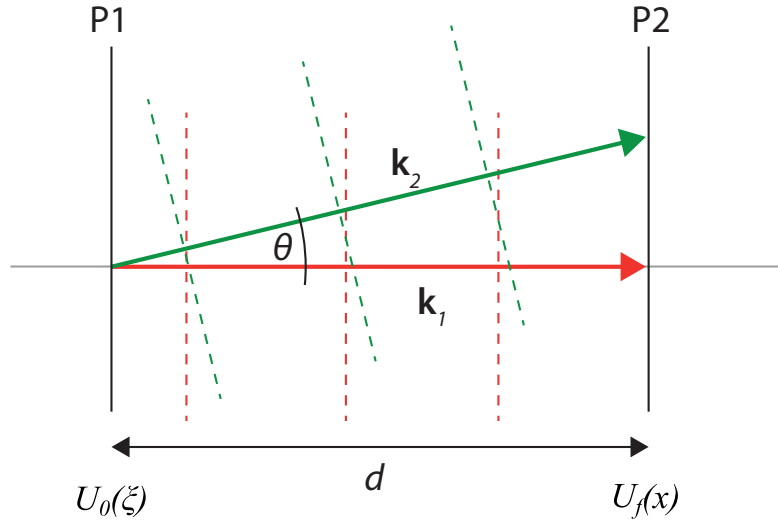


**Figure A.2:** Phase shift due to free space propagation about a distance  $d$ . Light in the plane wave mode propagating along the the optical axis  $\mathbf{k}_1$  acquires the phase  $\varphi_1 = d2\pi/\lambda$ . A plane wave traveling at an angle  $\theta$  with respect to the optical axis propagates a longer path  $d'=d/\cos\theta$ . The consequent phase shift  $\varphi_2 = d2\pi/\lambda \cos\theta$  can be approximated as  $\varphi_2 = d2\pi/\lambda(1 - \theta^2/2)$ . With  $\theta = |\mathbf{q}|\lambda/2\pi$ , this leads to  $\varphi(\mathbf{q}) = A - |\mathbf{q}|^2 d\lambda/4\pi$ , with a negligible constant  $A$ .

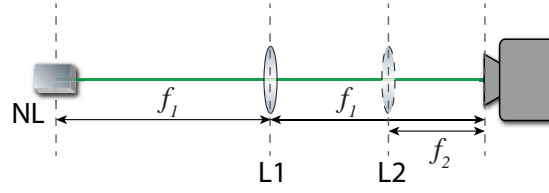


**Figure A.3:** Imaging of the down-converted beams for alignment. Without L2 in place, the lens L1 maps the Fourier plane of the crystal onto the camera plane i.e. one transverse  $k$ -vector at the crystal corresponds to one point on the camera. If additionally, the lens L2 is inserted, the two lenses constitute an imaging system producing an image of the crystal at the camera.

## A.2 Experimental Details on Delayed-Choice Frustration of Down-Conversion

### A.2.1 Auxiliary Alignment Imaging System for Obtaining High-Visibility Frustration of SPDC

The alignment of the setup is performed in a similar fashion as in the experiments described in Chapters 3 and 4. The crucial point is to ensure both spectral and spatial indistinguishability of the respective beams. The fact that only one SPDC crystal is used in the experiment to observe frustrated down-conversion rendered the balancing of the photon pair frequency spectra by scanning the crystal temperatures unnecessary. The temperature was only scanned to maximize the transmission through our bandpass filters.

A crucial part of the alignment procedure is to accomplish a good spatial overlap of the beams created in the first SPDC process with the beams from the second SPDC process. To facilitate this, we implemented an additional lens system in place of the detectors  $D_S$  and  $D_I$  (see Fig. 5.3 on page 84). This lens system allows to successively image signal and idler beams originating from both SPDC processes at the crystal and at its Fourier plane (Fig. A.3). Using an EMCCD camera, the photon beams from the two SPDC processes are aligned to overlap in both planes, which ensures their indistinguishability in any plane. After this alignment, the lens system and the camera are removed from the beam using a flip mirror.

### A.2.2 Electronics and Detection

In the experiment, the signals from each detector and the electronic trigger signal for the EOM are recorded using a time tagging unit (TTM). A schematic representation of the electronic signal routing is depicted in Fig. A.4.

A function generator outputs an electronic signal consisting of pulses at 100 kHz. This signal is fed to a so-called “splitter-box” (see e.g. [177] for details), which converts each received pulse to a sequence of pulses with constant time-offsets, two of which are used to trigger the switching of the EOM on and off (“EOM switching signals”). The high-voltage applied to the EOM is provided by a separate HV power supply. The timings are set to 50 ns between the on and the off pulse. The splitter-box generates an additional signal pulse (“EOM trigger signal”) at the beginning of each switching sequence, which is recorded with the time-tagging module. This signal is used to mark the time, at which the “clock” to measure the arrival times of photons at all detectors is set to zero. The time-delays between photon detections and the last recorded EOM trigger signal result in the histograms presented in Chapter 5. The absolute value of this delay includes the time it takes the signals to travel through cables, the time it takes photons to reach the detectors through optical fibers, the response time of the detectors, and other electronic delays. However, the time differences between the electronic signals is constant up to a small electronic

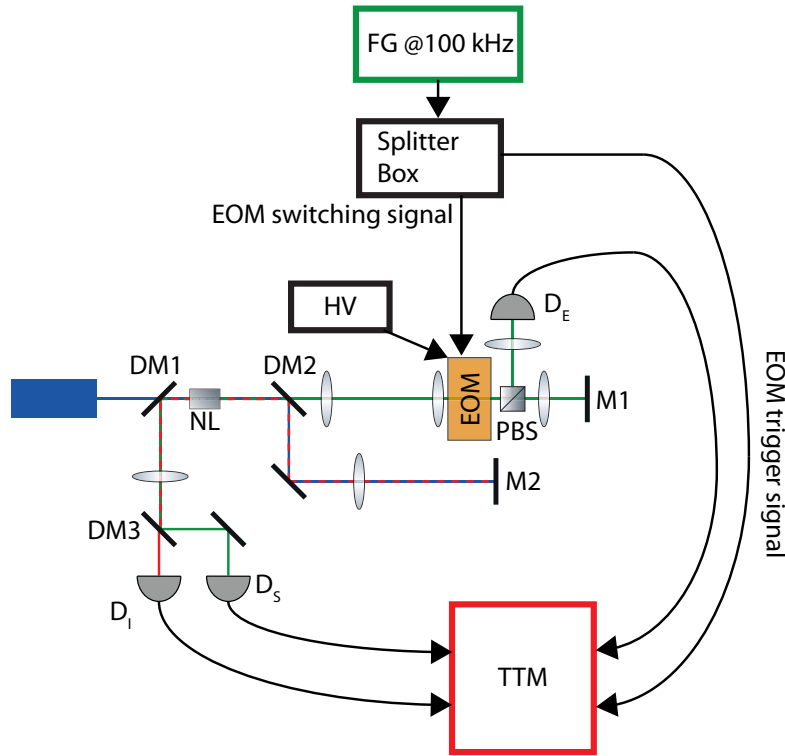


**Figure A.4:** Schematic of the electronic signal routing in the experiment of delayed-choice frustration of down-conversion. See text for details.

jitter. The jitter introduced by the detectors was characterized (Fig. A.6) and included in the error calculation.

## A.2.3 Electro Optical Modulator

### A.2.3.1 Principle of Operation

Our EOM is a Pockels cell consisting of two rubidium titanyl phosphate (RTP) crystals oriented perpendicularly to each other (Leysop RTP-X-4-20). The characteristic property of this material is the change of its refractive index for a particular polarization direction if a voltage is applied on the crystal (see e.g. [177, 178]). Our EOM was selected considering the trade-off between fast switching time and the possibility of a high repetition rate. A high repetition rate is important as the photon detection times are assigned to 660 ps long time bins<sup>30</sup>. Although the rate of produced photon pairs is in the order of  $10^5$  pairs per second, only a small number of photons is detected per time bin within a reasonable running time of the experiment. In order to collect good statistics of the arrival times, a large number of measurements and thus a high repetition rate was necessary.

### A.2.3.2 Alignment

The alignment of the EOM was performed as follows. First, the tilt of the cell is adjusted such that the beam aligns with one of the crystal axes. In this case, light polarized in any direction experiences the same refractive index and thus equal optical paths as long as no voltage is applied. Consequently, the polarization of a beam passing through the cell is ideally unaffected.

<sup>30</sup>This time bin width was chosen considering the trade-off between timing accuracy and required run-time of the experiment in order to collect a statistically significant amount of data in each bin.

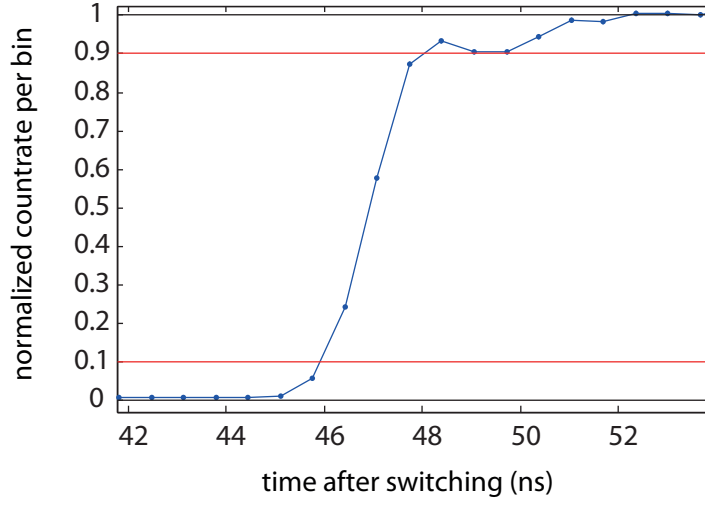


**Figure A.5:** Switching Profile of the EOM. The blue curve show the normalized detection rate per time bin at  $D_E$ . The black lines are the average count rates during the off time and on time. The red lines show the thresholds of 10% and 90% during the transient switching period. The 10-90% rise-time was evaluated as the time between the crossings of the two thresholds to  $1.9 \pm 0.1$  ns.

If a voltage is applied, the refractive indices along the two axes (perpendicular to the beam) are changed relative to each other. As a result, the polarization along one of the axes is delayed with respect to the other. The aim of the alignment procedure is to align the two perpendicular crystal axes with the diagonal and anti-diagonal polarization directions and to set the value of the applied voltage such that it corresponds to a delay of half the wavelength. In this way, the EOM acts as a half-wave plate oriented at  $45^\circ$  when switched on and transmits the beam without altering its polarization when switched off.

The standard alignment procedure for these devices consists of placing the EOM between two crossed polarizers with no voltage applied. Subsequently, the tilt is adjusted until a minimum in transmission is found, ensuring that the cell does not alter the polarization. If done correctly, the beam is aligned with one of the crystal axes and the cell can be rotated around this axis without altering the polarization. Voltage and tilt are optimized iteratively to achieve half-wave rotation of the polarization with the voltage applied.

The procedure is performed in a slightly different way in our setup. First, the tilt of the cell is aligned while maintaining the maximum possible visibility. For this, we also need to compensate the path length to account for the passage through the  $\approx 4$  cm RTP material. Maximizing the interferometric visibility accounts for both misalignment and minimizing the polarization rotation of with no voltage applied. This is due to a polarization rotation on the initially horizontally polarized beam introduces distinguishability between the two pair creation processes and reduces the interferometric visibility. Successively, the amount of photons switched towards  $D_E$  with voltage applied is maximized by rotating the cell and selecting the voltage. The ratio of switched to unaltered photons is optimized by evaluating coincidences between the EOM switching signal and detectors  $D_E$  and  $D_S$ , respectively.

#### A.2.3.3 Rise Time Measurement

The switching time of the EOM between its on and off state was determined as follows. The histogram of photon detections at detector  $D_E$  obtained in the reference measurement (Sec. 5.4) was analyzed during the transient time. The time between the rise of the count rate from 10% to 90% of its maximum value was evaluated to  $1.9 \pm 0.1$  ns (see Fig. A.5). The curve features a

characteristic peak followed by a small dip just before the count rate reaches its maximum level. This is expected due to piezoelectric ringing in the Pockels cell (see e.g. [177]).

### A.2.4 Timing Resolution in the Experiment

The time tagging electronics (TTM) has a nominal resolution of 82.3 ps [179]. However, the employed detectors exhibit a jitter in the order of 1 ns, which further limits the achievable timing resolution. In order to experimentally quantify the detector jitter as well as the individual detector's electronic delays, coincidence delay histograms of the idler detector ( $D_I$ ) with each of the two signal detectors were recorded (Fig. A.6). The widths of the coincidence peaks are determined using a Gaussian fit to  $\sigma < 0.8$  ns. They represent a convolution of the timing uncertainties of the two respective detectors. A conservative  $\sigma$  of 1 ns was taken into account to estimate the jitter of each single detector in the error calculation.

#### A.2.4.1 Analysis and Stability

Detection events at all detectors are assigned to time-bins representing the time difference between the detection and the last recorded electronic signal to switch the EOM. In order to allow for the necessary timing resolution, these time bins were set to 660 ps. Therefore, at a pair production rate in the order of  $10^5$  per second, measurement times of several hours are necessary to collect significant statistics of photon arrival times in each time-bin. This in turn requires the setup to be interferometrically stable for that time.

As a first step, the setup was covered in a plexiglass container to minimize airflow. A computer algorithm was implemented to periodically monitor the interferometric visibility and reset the interferometric phase. About one hour after closing the container, the stability of the interferometric phase was experimentally found to be enough to conduct the measurements without the need of a permanent active stabilization (see Fig. 5.7 on page 89).

A second issue was the stability of the frequency mode of the pump laser, which was strongly dependent on the temperature in the laboratory. The electrical current of the laser diode needed to be optimized to ensure stable single mode operation before each experimental run. This was done using a wave meter based on a Fizeau interferometer (Toptica WS1).

#### A.2.4.2 Normalization and Compensation of Electronic Delays

Due to electronic delays in the single-photon detectors as well as in cables and optical fibers, it is not possible to directly compare the raw time-tags of photon detections between different detectors. For this reason, the arrival times at  $D_S$  and  $D_I$  are corrected using the following compensation routine.

In the unblocked setup, for every signal photon that is detected at  $D_E$ , a partner idler photon can be detected at  $D_I$ . The electronic delay between these detections was determined using the peak in coincidence detection (Fig. A.6) and compensated for. Similarly, a coincidence peak is observed between  $D_I$  and  $D_S$ , which was used to compensate electronic delays in  $D_S$ . Using this method, the necessity of evaluating individual optical and electronic delays in the respective connections is avoided.

As a result of this compensation, the rise in count rate at  $D_E$  appears simultaneous to the reduction of counts at  $D_S$  (Fig. 5.6). In fact, after photons are detected at  $D_E$ , it takes the traveling time from the EOM through the setup to  $D_S$  (about 6.7 ns) before the switching can affect the detection rate at  $D_S$ .

It should be noted that only the detection times at  $D_E$  with respect to the EOM switching signal are used for further evaluation of a possible delay between the two measurement choices. No delay compensation was applied for this detector.

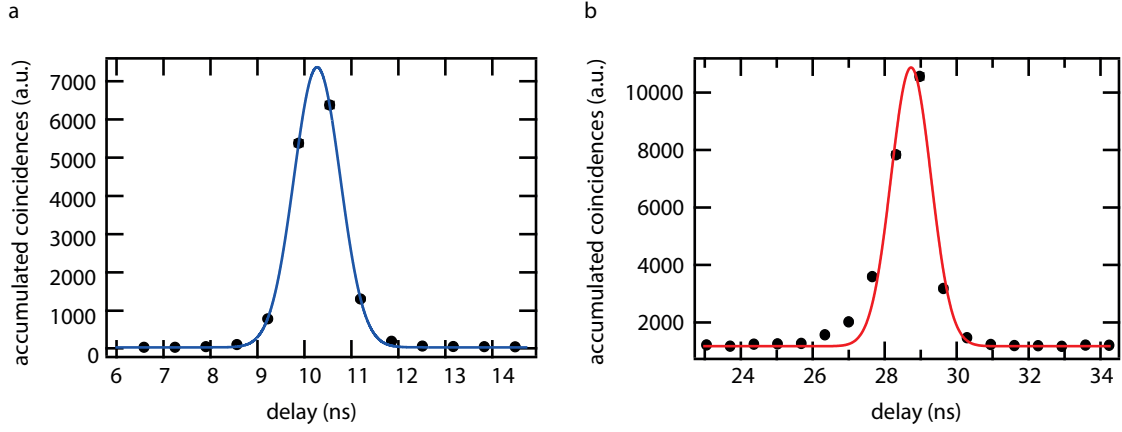


**Figure A.6:** Jitter measurements. Plot (a) shows the coincident counts between detectors  $D_E$  and  $D_I$ , whereas (b) shows the coincidences between  $D_I$  and  $D_S$ . The results were used to quantify the detector jitter, as well as electronic and optical relative delays between the individual detectors.

The normalization of the intensities was performed as follows. From the coincidences to singles ratios, the coupling and detection efficiencies of the respective detectors was determined and corrected for after subtracting individual dark count rates. A drift in the intensity of the pump laser was compensated by normalizing additionally by the count rates at  $D_E$  averaged over each second.

In this way, the count rate corresponding to an individual SPDC process is represented as 1 on the scale. Two non-interfering SPDC Processes add up to 2, whereas constructive interference from two sources corresponds to an intensity value of up to 4 in our normalization.

# References

- [1] Einstein, A., Podolsky, B. & Rosen, N. Can quantum-mechanical description of physical reality be considered complete? *Physical review* **47**, 777 (1935).
- [2] Schrödinger, E. Discussion of probability relations between separated systems. *Mathematical Proceedings of the Cambridge Philosophical Society* **31**, 555–563 (1935).
- [3] Feynman, R. P., Leighton, R. B. & Sands, M. *Quantum Mechanics, The Feynman Lectures on Physics, Vol. 3* (Reading, MA: Addison-Wesley, 1965).
- [4] Kalckar, J. (ed.) *Foundations of Quantum Physics II (1933-1958)*. Niels Bohr - Collected Works (Elsevier Science, 1996).
- [5] Bell, J. S. On the einstein podolsky rosen paradox. *Physics* **1**, 195 (1964).
- [6] Freedman, S. J. & Clauser, J. F. Experimental test of local hidden-variable theories. *Physical Review Letters* **28**, 938 (1972).
- [7] Burnham, D. C. & Weinberg, D. L. Observation of simultaneity in parametric production of optical photon pairs. *Physical Review Letters* **25**, 84 (1970).
- [8] Bohr, N. Das Quantenpostulat und die neuere Entwicklung der Atomistik. *Naturwissenschaften* **16**, 245–257 (1928).
- [9] Bohr, N. Discussion with Einstein on epistemological problems in atomic physics. *Albert Einstein: Philosopher-Scientist*, P. A. Schilpp, ed., pp. 200-41 *The Library of Living Philosophers*, Evanston (1949).
- [10] Shih, Y. & Alley, C. O. New type of Einstein-Podolsky-Rosen-Bohm experiment using pairs of light quanta produced by optical parametric down conversion. *Physical Review Letters* **61**, 2921 (1988).
- [11] Ou, Z. & Mandel, L. Violation of Bell's inequality and classical probability in a two-photon correlation experiment. *Physical Review Letters* **61**, 50 (1988).
- [12] Kwiat, P. G., Waks, E., White, A. G., Appelbaum, I. & Eberhard, P. H. Ultrabright source of polarization-entangled photons. *Physical Review A* **60**, R773 (1999).

- [13] Zou, X. Y., Wang, L. J. & Mandel, L. Induced coherence and indistinguishability in optical interference. *Physical review letters* **67**, 318 (1991).
- [14] Wang, L. J., Zou, X. Y. & Mandel, L. Induced coherence without induced emission. *Physical Review A* **44**, 4614 (1991).
- [15] Herzog, T., Rarity, J., Weinfurter, H. & Zeilinger, A. Frustrated two-photon creation via interference. *Physical review letters* **72**, 629 (1994).
- [16] Lemos, G. B., Borish, V., Cole, G. D. , Ramelow, S., Lapkiewicz, R. & Zeilinger, A. Quantum imaging with undetected photons. *Nature* **512**, 409–412 (2014).
- [17] Young, T. II. the Bakerian lecture. On the theory of light and colours. *Philosophical transactions of the Royal Society of London* **92**, 12–48 (1802).
- [18] Davisson, C. & Germer, L. H. Diffraction of electrons by a crystal of nickel. *Physical review* **30**, 705 (1927).
- [19] Rauch, H., Treimer, W. & Bonse, U. Test of a single crystal neutron interferometer. *Physics Letters A* **47**, 369–371 (1974).
- [20] Estermann, I. & Stern, O. Beugung von Molekularstrahlen. *Zeitschrift für Physik* **61**, 95–125 (1930).
- [21] Carnal, O. & Mlynek, J. Young’s double-slit experiment with atoms: A simple atom interferometer. *Physical review letters* **66**, 2689 (1991).
- [22] Keith, D. W., Ekstrom, C. R., Turchette, Q. A. & Pritchard, D. E. An interferometer for atoms. *Physical review letters* **66**, 2693 (1991).
- [23] Arndt, M. , Nairz, O., Vos-Andrae, J. , Keller, C., van der Zouw, G. & Zeilinger, A. Wave–particle duality of c 60 molecules. *Nature* **401**, 680 (1999).
- [24] Bohr, N. Causality and complementarity. *Philosophy of Science* **4**, 289–298 (1937).
- [25] Ma, X.-s., Kofler, J. & Zeilinger, A. Delayed-choice gedanken experiments and their realizations. *Reviews of Modern Physics* **88**, 015005 (2016).
- [26] Heisenberg, W. Über den anschaulichen Inhalt der quantentheoretischen Kinematik und Mechanik. *Zeitschrift für Physik* **43**, 172–198 (1927).
- [27] von Weizsäcker, C. Ortsbestimmung eines Elektrons durch ein Mikroskop. *Zeitschrift für Physik* **70**, 114–130 (1931).
- [28] Hermann, G. Die naturphilosophischen Grundlagen der Quantenmechanik. *Naturwissenschaften* **23**, 718–721 (1935).
- [29] von Weizsäcker, C. Zur Deutung der Quantenmechanik. *Zeitschrift für Physik* **118**, 489–509 (1941).
- [30] Wheeler, J. A. Law without law. *Quantum Theory and Measurement, Princeton Univ. Press, J.A Wheeler and W.H.Zurek eds* 182–213 (1983).
- [31] Hellmuth, T., Walther, H., Zajonc, A. & Schleich, W. Delayed-choice experiments in quantum interference. *Physical Review A* **35**, 2532 (1987).
- [32] Alley, C. O., Jakubowicz, O. G. & Wickes, W. C. Results of the delayed-random-choice quantum mechanics experiment with light quanta. In *Proceedings of the 2nd International Symposium on Foundations of Quantum Mechanics, Tokyo*, 36 (1986).

- [33] Balduhn, J., Mohler, E. & Martienssen, W. A wave-particle delayed-choice experiment with a single-photon state. *Zeitschrift für Physik B Condensed Matter* **77**, 347–352 (1989).
- [34] Lawson-Daku, B. , Asimov, R., Gorceix, O. , Miniatura, C., Robert, J. & Baudon, J. Delayed choices in atom Stern-Gerlach interferometry. *Physical review A* **54**, 5042 (1996).
- [35] Kawai, T. , Ebisawa, T., Tasaki, S., Hino, M., Yamazaki, D., Akiyoshi, T. , Matsumoto, Y., Achiwa, N. & Otake, Y. Realization of a delayed choice experiment using a multilayer cold neutron pulser. *Nuclear Instruments and Methods in Physics Research Section A: Accelerators, Spectrometers, Detectors and Associated Equipment* **410**, 259–263 (1998).
- [36] Kim, Y.-H., Yu, R., Kulik, S. P., Shih, Y. & Scully, M. O. Delayed “choice” quantum eraser. *Physical Review Letters* **84**, 1 (2000).
- [37] Chaves, R., Lemos, G. B. & Pienaar, J. Causal modeling the delayed-choice experiment. *Physical Review Letters* **120**, 190401 (2018).
- [38] Huang, H.-L., Luo, Y., Bai, B., Deng, Y., Wang, H., Zhao, Q. , Zhong, H. S., Nie, Y., Jiang, W., Wang, X. L. & Zhang, J. Compatibility of causal hidden-variable theories with a delayed-choice experiment. *Physical Review A* **100**, 012114 (2019).
- [39] Scully, M. O. & Drühl, K. Quantum eraser: A proposed photon correlation experiment concerning observation and” delayed choice” in quantum mechanics. *Physical Review A* **25**, 2208 (1982).
- [40] Scully, M. O., Englert, B. G. & Walther, H. Quantum optical tests of complementarity. *Nature* **351**, 111–116 (1991).
- [41] Peres, A. Delayed choice for entanglement swapping. *Journal of Modern Optics* **47**, 139–143 (2000).
- [42] Ma, X.-S., Zotter, S., Kofler, J., Ursin, R., Jennewein, T., Brukner, C. & Zeilinger, A. Experimental delayed-choice entanglement swapping. *Nature Physics* **8**, 479 (2012).
- [43] Wootters, W. K. & Zurek, W. H. Complementarity in the double-slit experiment: Quantum nonseparability and a quantitative statement of Bohr’s principle. *Physical Review D* **19**, 473 (1979).
- [44] Bartell, L. Complementarity in the double-slit experiment: On simple realizable systems for observing intermediate particle-wave behavior. *Physical Review D* **21**, 1698 (1980).
- [45] Greenberger, D. M. & Yasin, A. Simultaneous wave and particle knowledge in a neutron interferometer. *Physics Letters A* **128**, 391–394 (1988).
- [46] Mandel, L. Coherence and indistinguishability. *Optics letters* **16**, 1882–1883 (1991).
- [47] Jaeger, G., Shimony, A. & Vaidman, L. Two interferometric complementarities. *Physical Review A* **51**, 54 (1995).
- [48] Englert, B. G. Fringe visibility and which-way information: An inequality. *Physical review letters* **77**, 2154 (1996).
- [49] Klyshko, D. N. Scattering of light in a medium with nonlinear polarizability. *Sov. Phys. JETP* **28**, 522 (1969).
- [50] Boyd, R. W. *Nonlinear optics* (Elsevier, 2007).
- [51] Kwiat, P. G., Steinberg, A. M. & Chiao, R. Y. High-visibility interference in a Bell-inequality experiment for energy and time. *Physical Review A* **47**, R2472 (1993).

- [52] Mosley, P. J. *et al.* Heralded generation of ultrafast single photons in pure quantum states. *Physical Review Letters* **100**, 133601 (2008).
- [53] Laiho, K., Cassemiro, K. & Silberhorn, C. Producing high fidelity single photons with optimal brightness via waveguided parametric down-conversion. *Optics express* **17**, 22823–22837 (2009).
- [54] Ramelow, S., Ratschbacher, L., Fedrizzi, A., Langford, N. & Zeilinger, A. Discrete tunable color entanglement. *Physical review letters* **103**, 253601 (2009).
- [55] Monken, C. H., Ribeiro, P. H. S. & Pádua, S. Transfer of angular spectrum and image formation in spontaneous parametric down-conversion. *Physical Review A* **57**, 3123 (1998).
- [56] Walborn, S. P., Monken, C. H., Pádua, S. & Ribeiro, P. S. Spatial correlations in parametric down-conversion. *Physics Reports* **495**, 87–139 (2010).
- [57] Grice, W. P., Bennink, R. S., Goodman, D. S. & Ryan, A. T. Spatial entanglement and optimal single-mode coupling. *Physical Review A* **83**, 023810 (2011).
- [58] Goodman, J. W. *Introduction to Fourier optics* (Roberts and Company Publishers, 2005).
- [59] Howell, J. C., Bennink, R. S., Bentley, S. J. & Boyd, R. W. Realization of the Einstein-Podolsky-Rosen paradox using momentum-and position-entangled photons from spontaneous parametric down conversion. *Physical review letters* **92**, 210403 (2004).
- [60] Hor-Meyll, M., de Almeida, J. O., Lemos, G. B., Ribeiro, P. H. S. & Walborn, S. P. Ancilla-assisted measurement of photonic spatial correlations and entanglement. *Physical review letters* **112**, 053602 (2014).
- [61] O’Sullivan-Hale, M. N., Khan, I. A., Boyd, R. W. & Howell, J. C. Pixel entanglement: experimental realization of optically entangled  $d=3$  and  $d=6$  qudits. *Physical review letters* **94**, 220501 (2005).
- [62] Edgar, M. P. *et al.* Imaging high-dimensional spatial entanglement with a camera. *Nature communications* **3**, 984 (2012).
- [63] Schneeloch, J. & Howell, J. C. Introduction to the transverse spatial correlations in spontaneous parametric down-conversion through the biphoton birth zone. *Journal of Optics* **18**, 053501 (2016).
- [64] Reid, M. & Drummond, P. Quantum correlations of phase in nondegenerate parametric oscillation. *Physical review letters* **60**, 2731 (1988).
- [65] Mancini, S., Giovannetti, V., Vitali, D. & Tombesi, P. Entangling macroscopic oscillators exploiting radiation pressure. *Physical review letters* **88**, 120401 (2002).
- [66] Ou, Z., Pereira, S. F., Kimble, H. & Peng, K. Realization of the einstein-podolsky-rosen paradox for continuous variables. *Physical Review Letters* **68**, 3663 (1992).
- [67] Pittman, T. B., Shih, Y. H., Strekalov, D. V. & Sergienko, A. V. Optical imaging by means of two-photon quantum entanglement. *Physical Review A* **52**, R3429 (1995).
- [68] Rubin, M. H., Klyshko, D. N., Shih, Y. & Sergienko, A. Theory of two-photon entanglement in type-II optical parametric down-conversion. *Physical Review A* **50**, 5122 (1994).
- [69] Strekalov, D. V., Sergienko, A. V., Klyshko, D. N. & Shih, Y. H. Observation of two-photon “ghost” interference and diffraction. *Physical review letters* **74**, 3600 (1995).

- [70] Ribeiro, P. S., Pádua, S., Da Silva, J. M. & Barbosa, G. Controlling the degree of visibility of Young's fringes with photon coincidence measurements. *Physical Review A* **49**, 4176 (1994).
- [71] Ou, Z., Wang, L., Zou, X. & Mandel, L. Evidence for phase memory in two-photon down conversion through entanglement with the vacuum. *Physical Review A* **41**, 566 (1990).
- [72] Ghosh, R. & Mandel, L. Observation of nonclassical effects in the interference of two photons. *Physical Review Letters* **59**, 1903 (1987).
- [73] Ou, Z. & Mandel, L. Observation of spatial quantum beating with separated photodetectors. *Physical review letters* **61**, 54 (1988).
- [74] Ou, Z., Zou, X., Wang, L. & Mandel, L. Observation of nonlocal interference in separated photon channels. *Physical review letters* **65**, 321 (1990).
- [75] Kwiat, P., Vreken, W., Hong, C., Nathel, H. & Chiao, R. Correlated two-photon interference in a dual-beam Michelson interferometer. *Physical Review A* **41**, 2910 (1990).
- [76] Klyshko, D. Combine EPR and two-slit experiments: Interference of advanced waves. *Physics Letters A* **132**, 299–304 (1988).
- [77] Horne, M. A., Shimony, A. & Zeilinger, A. Two-particle interferometry. *Physical Review Letters* **62**, 2209 (1989).
- [78] Zou, X. Y., Grayson, T., Barbosa, G. A. & Mandel, L. Control of visibility in the interference of signal photons by delays imposed on the idler photons. *Physical Review A* **47**, 2293 (1993).
- [79] Barbosa, G. A. Degree of visibility in experiments of induced coherence without induced emission: A heuristic approach. *Physical Review A* **48**, 4730 (1993).
- [80] Grayson, T. P. & Barbosa, G. A. Spatial properties of spontaneous parametric down-conversion and their effect on induced coherence without induced emission. *Physical Review A* **49**, 2948 (1994).
- [81] Zajonc, A., Wang, L., Zou, X. & Mandel, L. Quantum eraser. *Nature* **353**, 507 (1991).
- [82] Wang, L. & Rhee, J.-K. Propagation of transient quantum coherence. *Physical Review A* **59**, 1654 (1999).
- [83] Herzog, T. J., Kwiat, P. G., Weinfurter, H. & Zeilinger, A. Complementarity and the quantum eraser. *Physical Review Letters* **75**, 3034 (1995).
- [84] Milonni, P., Fearn, H. & Zeilinger, A. Theory of two-photon down-conversion in the presence of mirrors. *Physical Review A* **53**, 4556 (1996).
- [85] Yurke, B., McCall, S. L. & Klauder, J. R. SU (2) and SU (1, 1) interferometers. *Physical Review A* **33**, 4033 (1986).
- [86] Stern, A., Aharonov, Y. & Imry, Y. Phase uncertainty and loss of interference: A general picture. *Physical Review A* **41**, 3436 (1990).
- [87] Ribeiro, P. S. & Barbosa, G. Mirror effects and induced coherence in parametric down-conversion. *Optics communications* **139**, 139–147 (1997).
- [88] Jha, A. K., O'Sullivan, M. N., Chan, K. W. C. & Boyd, R. W. Temporal coherence and indistinguishability in two-photon interference effects. *Physical Review A* **77**, 021801 (2008).

- [89] Kalashnikov, D. A., Paterova, A. V., Kulik, S. P. & Krivitsky, L. A. Infrared spectroscopy with visible light. *Nature Photonics* (2016).
- [90] Chekhova, M. & Ou, Z. Nonlinear interferometers in quantum optics. *Advances in Optics and Photonics* **8**, 104–155 (2016).
- [91] Hochrainer, A., Lahiri, M., Lapkiewicz, R., Lemos, G. B. & Zeilinger, A. Quantifying the momentum correlation between two light beams by detecting one. *Proceedings of the National Academy of Sciences* **114**, 1508–1511 (2017).
- [92] Lahiri, M., Hochrainer, A., Lapkiewicz, R., Lemos, G. B. & Zeilinger, A. Partial polarization by quantum distinguishability. *Physical Review A* **95**, 033816 (2017).
- [93] Paterova, A., Yang, H., An, C., Kalashnikov, D. & Krivitsky, L. Measurement of infrared optical constants with visible photons. *New Journal of Physics* **20**, 043015 (2018).
- [94] Paterova, A., Yang, H., An, C., Kalashnikov, D. & Krivitsky, L. Polarization effects in nonlinear interference of down-converted photons. *Optics express* **27**, 2589–2603 (2019).
- [95] Paterova, A. V., Yang, H., An, C., Kalashnikov, D. A. & Krivitsky, L. A. Tunable optical coherence tomography in the infrared range using visible photons. *Quantum Science and Technology* **3**, 025008 (2018).
- [96] Vallés, A., Jiménez, G., Salazar-Serrano, L. J. & Torres, J. P. Optical sectioning in induced coherence tomography with frequency-entangled photons. *Physical Review A* **97**, 023824 (2018).
- [97] Lahiri, M., Lapkiewicz, R., Lemos, G. B. & Zeilinger, A. Theory of quantum imaging with undetected photons. *Physical Review A* **92**, 013832 (2015).
- [98] Zou, X., Grayson, T. & Mandel, L. Observation of quantum interference effects in the frequency domain. *Physical review letters* **69**, 3041 (1992).
- [99] Burlakov, A., Kulik, S., Penin, A. & Chekhova, M. Three-photon interference: Spectroscopy of linear and nonlinear media. *Journal of Experimental and Theoretical Physics* **86**, 1090–1097 (1998).
- [100] Korystov, D. Y., Kulik, S. P. & Penin, A. N. Rozhdestvenski hooks in two-photon parametric light scattering. *Journal of Experimental and Theoretical Physics Letters* **73**, 214–218 (2001).
- [101] Kulik, S. P., Maslennikov, G. A., Merkulova, S. P., Penin, L. K., Radchenko, L. K. & Krasheninnikov, V. N. Two-photon interference in the presence of absorption. *Journal of Experimental and Theoretical Physics* **98**, 31–38 (2004).
- [102] Krenn, M., Hochrainer, A., Lahiri, M. & Zeilinger, A. Entanglement by path identity. *Physical review letters* **118**, 080401 (2017).
- [103] Kim, Y.-H., Chekhova, M. V., Kulik, S. P., Shih, Y. & Rubin, M. H. First-order interference of nonclassical light emitted spontaneously at different times. *Physical Review A* **61**, 051803 (2000).
- [104] Lähteenmäki, P., Paraoanu, G. S., Hassel, J. & Hakonen, P. J. Coherence and multimode correlations from vacuum fluctuations in a microwave superconducting cavity. *Nature communications* **7**, 12548 (2016).
- [105] Ou, Z., Wang, L., Zou, X. & Mandel, L. Coherence in two-photon down-conversion induced by a laser. *Physical Review A* **41**, 1597 (1990).

- [106] Wang, L., Zou, X. & Mandel, L. Observation of induced coherence in two-photon down-conversion. *JOSA B* **8**, 978–980 (1991).
- [107] Belinsky, A. & Klyshko, D. Interference of classical and non-classical light. *Physics Letters A* **166**, 303–307 (1992).
- [108] Wiseman, H. M. & Mølmer, K. Induced coherence with and without induced emission. *Physics Letters A* **270**, 245–248 (2000).
- [109] Shapiro, J. H., Venkatraman, D. & Wong, F. N. Classical imaging with undetected photons. *Scientific reports* **5**, 10329 (2015).
- [110] Cardoso, A. *et al.* Classical imaging with undetected light. *Physical Review A* **97**, 033827 (2018).
- [111] Lahiri, M., Hochrainer, A., Lapkiewicz, R., Lemos, G. B. & Zeilinger, A. Nonclassicality of induced coherence without induced emission. *Physical Review A* **100**, 053839 (2019).
- [112] Senitzky, I. Classical interpretation of “frustrated two-photon creation via interference”. *Physical review letters* **73**, 3040 (1994).
- [113] Herzog, T., Rarity, J., Weinfurter, H. & Zeilinger, A. Herzog *et al.* reply. *Physical review letters* **73**, 3041 (1994).
- [114] Herzog, T. J. *An Optical Test of Complementarity*. Ph.D. thesis, Leopold Franzens Universität Innsbruck (2000).
- [115] Kolobov, M. I., Giese, E., Lemieux, S., Fickler, R. & Boyd, R. W. Controlling induced coherence for quantum imaging. *Journal of Optics* **19**, 054003 (2017).
- [116] Giese, E., Lemieux, S., Manceau, M., Fickler, R. & Boyd, R. W. Phase sensitivity of gain-unbalanced nonlinear interferometers. *Physical Review A* **96**, 053863 (2017).
- [117] Purcell, E. M. Spontaneous emission probabilities at radio frequencies. *Physical Review* **69**, 681 (1946).
- [118] Drexhage, K. H. Interaction of light with monomolecular dye lasers. *in Progress in optics, Emil Wolf ed.* **12**, 163–232 (1974).
- [119] Kleppner, D. Inhibited spontaneous emission. *Physical Review Letters* **47**, 233 (1981).
- [120] Goy, P., Raimond, J., Gross, M. & Haroche, S. Observation of cavity-enhanced single-atom spontaneous emission. *Physical review letters* **50**, 1903 (1983).
- [121] Hulet, R. G., Hilfer, E. S. & Kleppner, D. Inhibited spontaneous emission by a rydberg atom. *Physical review letters* **55**, 2137 (1985).
- [122] Heinzen, D., Childs, J., Thomas, J. & Feld, M. Enhanced and inhibited visible spontaneous emission by atoms in a confocal resonator. *Physical review letters* **58**, 1320 (1987).
- [123] Jhe, W. *et al.* Suppression of spontaneous decay at optical frequencies: Test of vacuum-field anisotropy in confined space. *Physical review letters* **58**, 666 (1987).
- [124] Yablonovitch, E. Inhibited spontaneous emission in solid-state physics and electronics. *Physical review letters* **58**, 2059 (1987).
- [125] Deppe, D., Campbell, J., Kuchibhotla, R., Rogers, T. & Streetman, B. Optically-coupled mirror-quantum well ingaas-gaas light emitting diode. *Electronics Letters* **26**, 1665–1666 (1990).

- [126] Hoi, I.-C. *et al.* Probing the quantum vacuum with an artificial atom in front of a mirror. *Nature Physics* **11**, 1045 (2015).
- [127] Eschner, J., Raab, C., Schmidt-Kaler, F. & Blatt, R. Light interference from single atoms and their mirror images. *Nature* **413**, 495 (2001).
- [128] Dorner, U. & Zoller, P. Laser-driven atoms in half-cavities. *Physical Review A* **66**, 023816 (2002).
- [129] Milonni, P. W., Ackerhalt, J. R. & Smith, W. A. Interpretation of radiative corrections in spontaneous emission. *Physical Review Letters* **31**, 958 (1973).
- [130] Ackerhalt, J. R., Knight, P. L. & Eberly, J. H. Radiation reaction and radiative frequency shifts. *Physical Review Letters* **30**, 456 (1973).
- [131] Milonni, P. W. *The quantum vacuum: an introduction to quantum electrodynamics* (Academic press, 1993).
- [132] Milonni, P. & Knight, P. Spontaneous emission between mirrors. *Optics Communications* **9**, 119–122 (1973).
- [133] Parker, J. & Stroud Jr, C. Transient theory of cavity-modified spontaneous emission. *Physical Review A* **35**, 4226 (1987).
- [134] Gießen, H. *et al.* Cavity-modified spontaneous emission: From rabi oscillations to exponential decay. *Physical Review A* **53**, 2816 (1996).
- [135] Jedrkiewicz, O. & Loudon, R. Theory of transient spontaneous emission by an atom in a planar microcavity. *Physical Review A* **60**, 4951 (1999).
- [136] Fearn, H., Cook, R. J. & Milonni, P. W. Sudden replacement of a mirror by a detector in cavity qed: Are photons counted immediately? *Physical review letters* **74**, 1327 (1995).
- [137] Milonni, P. W. Spontaneous emission between mirrors. *Journal of Modern Optics* **54**, 2115–2120 (2007).
- [138] Morawitz, H. Self-coupling of a two-level system by a mirror. *Physical Review* **187**, 1792 (1969).
- [139] Weinfurter, H. *et al.* Frustrated downconversion: Virtual or real photons? a. *Annals of the New York Academy of Sciences* **755**, 61–72 (1995).
- [140] Branning, D., Migdall, A. L. & Kwiat, P. G. Experimental detection of photons emitted during inhibited spontaneous emission. In *Optical Engineering+ Applications*, 66640E–66640E (International Society for Optics and Photonics, 2007).
- [141] Wu, L.-A. & Kimble, H. J. Interference effects in second-harmonic generation within an optical cavity. *JOSA B* **2**, 697–703 (1985).
- [142] Kauranen, M., Van Rompaey, Y., Maki, J. J. & Persoons, A. Nonvanishing field between a dipole oscillator and a reflecting boundary during suppression of dipole radiation. *Physical review letters* **80**, 952 (1998).
- [143] Hochrainer, A., Lahiri, M., Lapkiewicz, R., Lemos, G. B. & Zeilinger, A. Interference fringes controlled by noninterfering photons. *Optica* **4**, 341–344 (2017).
- [144] Hecht, E. *Optics* (Pearson Education, 2012).

- [145] Born, M. & Wolf, E. *Principles of optics: electromagnetic theory of propagation, interference and diffraction of light* (Cambridge university press, 1999).
- [146] Lahiri, M., Hochrainer, A., Lapkiewicz, R., Lemos, G. B. & Zeilinger, A. Twin-photon correlations in single-photon interference. *Physical Review A* **96**, 013822 (2017).
- [147] Mandel, L. & Wolf, E. *Optical coherence and quantum optics* (Cambridge university press, 1995).
- [148] Abouraddy, A. F., Nasr, M. B., Saleh, B. E. A., Sergienko, A. V. & Teich, M. C. Demonstration of the complementarity of one-and two-photon interference. *Physical Review A* **63**, 063803 (2001).
- [149] Walborn, S., Ribeiro, P. S., Davidovich, L., Mintert, F. & Buchleitner, A. Experimental determination of entanglement with a single measurement. *Nature* **440**, 1022–1024 (2006).
- [150] Romero, G., López, C., Lastra, F., Solano, E. & Retamal, J. Direct measurement of concurrence for atomic two-qubit pure states. *Physical Review A* **75**, 032303 (2007).
- [151] Pires, H. D. L., Monken, C. H. & van Exter, M. P. Direct measurement of transverse-mode entanglement in two-photon states. *Physical Review A* **80**, 022307 (2009).
- [152] Just, F., Cavanna, A., Chekhova, M. V. & Leuchs, G. Transverse entanglement of biphotons. *New Journal of Physics* **15**, 083015 (2013).
- [153] Sharapova, P., Pérez, A. M., Tikhonova, O. V. & Chekhova, M. V. Schmidt modes in the angular spectrum of bright squeezed vacuum. *Physical Review A* **91**, 043816 (2015).
- [154] Lahiri, M. Wave-particle duality and polarization properties of light in single-photon interference experiments. *Physical Review A* **83**, 045803 (2011).
- [155] Al-Qasimi, A., Korotkova, O., James, D. & Wolf, E. Definitions of the degree of polarization of a light beam. *Optics letters* **32**, 1015–1016 (2007).
- [156] James, D. F., Kwiat, P. G., Munro, W. J. & White, A. G. On the measurement of qubits. In *Asymptotic Theory Of Quantum Statistical Inference: Selected Papers*, 509–538 (World Scientific, 2005).
- [157] Jacques, V. *et al.* Experimental realization of wheeler’s delayed-choice gedanken experiment. *Science* **315**, 966–968 (2007).
- [158] Jacques, V. *et al.* Delayed-choice test of quantum complementarity with interfering single photons. *Physical review letters* **100**, 220402 (2008).
- [159] Albota, M. A. & Wong, F. N. Efficient single-photon counting at 1.55  $\mu\text{m}$  by means of frequency upconversion. *Optics letters* **29**, 1449–1451 (2004).
- [160] VanDevender, A. P. & Kwiat, P. G. Quantum transduction via frequency upconversion. *JOSA B* **24**, 295–299 (2007).
- [161] O’Donnell, K. A. & U’Ren, A. B. Time-resolved up-conversion of entangled photon pairs. *Physical review letters* **103**, 123602 (2009).
- [162] Pe’Er, A., Dayan, B., Friesem, A. A. & Silberberg, Y. Temporal shaping of entangled photons. *Physical review letters* **94**, 073601 (2005).
- [163] Ghosh, R., Hong, C., Ou, Z. & Mandel, L. Interference of two photons in parametric down conversion. *Physical Review A* **34**, 3962 (1986).

- [164] Heuer, A., Menzel, R. & Milonni, P. W. Complementarity in biphoton generation with stimulated or induced coherence. *Physical Review A* **92**, 033834 (2015).
- [165] Heuer, A., Menzel, R. & Milonni, P. W. Induced Coherence, Vacuum Fields, and Complementarity in Biphoton Generation. *Physical review letters* **114**, 053601 (2015).
- [166] Ataman, S. An example of quantum imaging: rendering an object undetectable. *The European Physical Journal D* **70**, 127 (2016).
- [167] Lee, S. K., Yoon, T. H. & Cho, M. Quantum optical measurements with undetected photons through vacuum field indistinguishability. *Scientific Reports* **7**, 6558 (2017).
- [168] Dürr, S. Quantitative wave-particle duality in multibeam interferometers. *Physical Review A* **64**, 042113 (2001).
- [169] Zawisky, M., Baron, M. & Loidl, R. Three-beam interference and which-way information in neutron interferometry. *Physical Review A* **66**, 063608 (2002).
- [170] Bimonte, G. & Musto, R. On interferometric duality in multibeam experiments. *Journal of Physics A: Mathematical and General* **36**, 11481 (2003).
- [171] Englert, B.-G., Kaszlikowski, D., Kwek, L. C. & Chee, W. H. Wave-particle duality in multi-path interferometers: general concepts and three-path interferometers. *International Journal of Quantum Information* **6**, 129–157 (2008).
- [172] Asad Siddiqui, M. & Qureshi, T. Three-slit interference: A duality relation. *Progress of Theoretical and Experimental Physics* **2015** (2015).
- [173] Gilaberte, M. *et al.* in preparation.
- [174] Fuenzalida, J. *et al.* in preparation.
- [175] Hochrainer, A. *et al.* in preparation.
- [176] Hochrainer, A. *et al.* in preparation.
- [177] Scheidl, T. *A fundamental test and an application of quantum entanglement*. Ph.D. thesis, University of Vienna (2009).
- [178] LeysopLTD. 100khz rtp pockels cell q-switch system. [http://www.leysop.com/100khz\\_rtp\\_q-switch.htm](http://www.leysop.com/100khz_rtp_q-switch.htm). Accessed: 12.12.2018.
- [179] RoithnerLasertechnik. Ttm8000 manual. [http://www.roithner-laser.at/datasheets/accessories/ttm8000\\_manual.pdf](http://www.roithner-laser.at/datasheets/accessories/ttm8000_manual.pdf). Accessed: 12.12.2018.

# Acknowledgements

I would like to thank my supervisor Anton Zeilinger for giving me the opportunity to work in his group in which I started as a project student already in 2012. It was a unique opportunity to participate in great research and it taught me a lot about physics and about life in general. I am very grateful for the freedom to pursue and discuss own ideas with many talented and interesting people. Thanks to the highly motivating environment that has been created here, I very much enjoyed the time both in and outside the lab.

Special thanks go to the Mandel team: Gabi, Radek, Mayukh, and Jorge for uncountable discussions and arguments about physics and all kinds of topics. I learned a lot from you guys and it was a privilege to work closely with good friends and very skilled physicists.

I would like to thank all other current and former colleagues at IQOQI for the fun time and interesting discussions I had with you. Mario the ghetto-chessmaster and reincarnation of Arnold Schwarzenegger, Manuel the fancy wine sommelier, Robert and Christoph and their little brothers Jonas. Johnny, Scheidl, Dominik, Sebi, Lukas, and Bo for being a great company while watching quasars on a mountaintop in the middle of nowhere. Michi and Kahan for patiently listening to countless enthusiastic and loud arguments between me and Mayukh in the office. Johannes, Sebastian, Dominik, Kristian, Manuel, Lukas, Jorge for being the Rapid Wien of physics. Marissa, Sven, Sören, Bernhard, and Marijn for maintaining a royal atmosphere in the Hofburg basement. Rupi, Mateusz, Jarda, Matthias, Amir, Mei, Ya, Xiaoqin, Krishna, Mehul, Fabian, Markus, Marta, everyone in the admin team and all CoQuS students and organizers for the great time, for the discussions and for all their help.

A significant part of this thesis was written on trains, so I acknowledge the railway companies of Bulgaria (BDZ) and Turkey (TCDD) for providing an environment in which this was possible.

The work was supported by the Austrian Academy of Sciences Institute for Quantum Optics and Quantum Information Vienna, the Austrian Science Fund (FWF) Special Research Programme SFB F40 (FoQuS) and W1210-2 (CoQuS), the University of Vienna via the project QUESS, and the European Research Council (SIQS Grant No. 600645 EU-FP7-ICT).

Last but not least, this thesis would never have been finished without a lot of support from my family. I would like to express a big thank you to all of them, in particular to Amalia and Elias for their support and understanding over the years.

---

# CURRICULUM VITAE

Armin Hochrainer

---

## Education

4/2014 - present

**University of Vienna:** PhD Studies in Physics

- Dissertation: Experiments on Quantum Complementarity in Induced Coherence Without Induced Emission
- Fellow of the Vienna Doctoral Program of Complex Quantum Science CoQuS (10/2015 - present)
- Visiting Scholar in the group of Robert Boyd, University of Ottawa, Canada (2/2017 – 3/2017)

9/2007 – Apr 2014

**Vienna University of Technology:** Technical Physics

- Degrees awarded: MSc (30/4/2014, with distinction), BSc (14/7/2011)
- Master's thesis: "Low-loss optical elements for a loophole-free Bell Test"
- Teaching Assistance: Physics for students of electronics and electrical engineering (2013-2014)
- Participation in the TUtheTOP high potential program of the Technical University of Vienna (2013)
- ERASMUS scholarship at Loughborough University, UK (10/2009 – 2/2010)

3/2004 – 4/2008

**University of Vienna:** Mass Media and Communication Science

- Degree awarded: Bakk. phil. (23/4/2008)
- 

## Professional Experience

1/2019 – present

**Quantum Technology Laboratories GmbH, 1040 Vienna**

2/2013 – 12/2019

**Institute of Quantum Optics and Quantum Information (IQOQI) Vienna, Austrian Academy of Sciences, 1090 Vienna**

- Graduate researcher in the group of Anton Zeilinger
- Organization of group seminars (2018-2019)
- Various outreach activities

3/2007 – 8/2009

**forum moztartplatz raum für wirtschaft und kultur, 1040 Vienna**

- Event engineering
- Prepared and conducted technical trainings

8/2001

**Internship: com\_unit – Agentur für Kommunikation, 1080 Vienna**

- Graphics processing
  - PR assistance
- 

## Language Skills

- German (native), English (fluent), French (advanced), Italian (advanced), Japanese (basic), Indonesian (basic)
- 

## Computer Skills

- Proficient in C/C++ , LabView, Matlab, Mathematica, CAD (Fusion 360), ZEMAX
-

# List of Publications

9. **Can Induced Coherence without Induced Emission be Non-Quantum?**  
Mayukh Lahiri, [Armin Hochrainer](#), Radek Lapkiewicz, Gabriela Barreto Lemos, Anton Zeilinger. *Physical Review A* **100** (5), 053839 (2019).
8. **Experimental High-Dimensional Entanglement by Path Identity**  
Jaroslav Kysela, Manuel Erhard, [Armin Hochrainer](#), Mario Krenn, Anton Zeilinger. *arxiv:1904.07851* (2019).
7. **Cosmic Bell Test Using Random Measurement Settings from High-Redshift Quasars**  
Dominik Rauch, Johannes Handsteiner, [Armin Hochrainer](#), Jason Gallicchio, Andrew S. Friedman, Calvin Leung, Bo Liu, Lukas Bulla, Sebastian Ecker, Fabian Steinlechner, Rupert Ursin, Beili Hu, David Leon, Chris Benn, Adriano Ghedina, Massimo Cecconi, Alan H. Guth, David I. Kaiser, Thomas Scheidl, Anton Zeilinger. *Physical Review Letters* **121** (8), 080403 (2018).
6. **Entanglement by Path Identity**  
Mario Krenn, [Armin Hochrainer](#), Mayukh Lahiri, Anton Zeilinger. *Physical Review Letters* **118** (8), 080401 (2017).
5. **Twin-photon correlations in single-photon interference**  
Mayukh Lahiri, [Armin Hochrainer](#), Radek Lapkiewicz, Gabriela Barreto Lemos, Anton Zeilinger. *Physical Review A* **96** (1), 013822 (2017).
4. **Interference fringes controlled by noninterfering photons**  
[Armin Hochrainer](#), Mayukh Lahiri, Radek Lapkiewicz, Gabriela Barreto Lemos, Anton Zeilinger. *Optica* **4** (3), 341–344 (2017).
3. **Quantifying the momentum correlation between two light beams by detecting one**  
[Armin Hochrainer](#), Mayukh Lahiri, Radek Lapkiewicz, Gabriela Barreto Lemos, Anton Zeilinger. *Proceedings of the National Academy of Sciences* **114** (7), 1508–1511 (2017).
2. **Partial polarization by quantum distinguishability**  
Mayukh Lahiri, [Armin Hochrainer](#), Radek Lapkiewicz, Gabriela Barreto Lemos, Anton Zeilinger. *Physical Review A* **95** (3), 033816 (2017).

1. **Significant-loophole-free test of Bell's theorem with entangled photons**

Marissa Giustina, Marijn Versteegh, Sören Wengerowsky, Johannes Handsteiner, Armin Hochrainer, Kevin Phelan, Fabian Steinlechner, Johannes Kofler, Jan-Åke Larsson, Carlos Abellan, Waldimar Amaya, Valerio Pruneri, Morgan W. Mitchell, Jörn Beyer, Thomas Gerrits, Adriana E. Lita, Lynden K. Shalm, Sae Woo Nam, Thomas Scheidl, Rupert Ursin, Bernhard Wittmann, and Anton Zeilinger. *Physical Review Letters* **115** (25), 250401 (2015).